LEABHARLANN CHOLÁISTE NA TRÍONÓIDE, BAILE ÁTHA CLIATH | TRINITY COLLEGE LIBRARY DUBLIN
Ollscoil Átha Cliath | The University of Dublin

Terms and Conditions of Use of Digitised Theses from Trinity College Library Dublin

Copyright statement

All material supplied by Trinity College Library is protected by copyright (under the Copyright and Related Rights Act, 2000 as amended) and other relevant Intellectual Property Rights. By accessing and using a Digitised Thesis from Trinity College Library you acknowledge that all Intellectual Property Rights in any Works supplied are the sole and exclusive property of the copyright and/or other IPR holder. Specific copyright holders may not be explicitly identified. Use of materials from other sources within a thesis should not be construed as a claim over them.

A non-exclusive, non-transferable licence is hereby granted to those using or reproducing, in whole or in part, the material for valid purposes, providing the copyright owners are acknowledged using the normal conventions. Where specific permission to use material is required, this is identified and such permission must be sought from the copyright holder or agency cited.

Liability statement

By using a Digitised Thesis, I accept that Trinity College Dublin bears no legal responsibility for the accuracy, legality or comprehensiveness of materials contained within the thesis, and that Trinity College Dublin accepts no liability for indirect, consequential, or incidental, damages or losses arising from use of the thesis for whatever reason. Information located in a thesis may be subject to specific use constraints, details of which may not be explicitly described. It is the responsibility of potential and actual users to be aware of such constraints and to abide by them. By making use of material from a digitised thesis, you accept these copyright and disclaimer provisions. Where it is brought to the attention of Trinity College Library that there may be a breach of copyright or other restraint, it is the policy to withdraw or take down access to a thesis while the issue is being resolved.

Access Agreement

By using a Digitised Thesis from Trinity College Library you are bound by the following Terms & Conditions. Please read them carefully.

I have read and I understand the following statement: All material supplied via a Digitised Thesis from Trinity College Library is protected by copyright and other intellectual property rights, and duplication or sale of all or part of any of a thesis is not permitted, except that material may be duplicated by you for your research use or for educational purposes in electronic or print form providing the copyright owners are acknowledged using the normal conventions. You must obtain permission for any other use. Electronic or print copies may not be offered, whether for sale or otherwise to anyone. This copy has been supplied on the understanding that it is copyright material and that no quotation from the thesis may be published without proper acknowledgement.

Engineering tissues with a zonal structure and composition mimicking native articular cartilage

Lu Luo BSc, MSc

A thesis submitted to the University of Dublin in partial fulfilment of the requirements for the degree of

Doctor in Philosophy

Trinity College Dublin

November 2014

Supervisor
Dr Daniel J. Kelly

External Examiner
Dr Frederik Claeyssens
University of Sheffield

Internal Examiner
Dr Bruce P. Murphy

TRINITY COLLEGE
2 9 JUL 2015
LIBRARY DUBLIN

Thesis 10667

Declaration

I declare that this thesis has not been submitted as an exercise for a degree at this or any other university and it is entirely my own work.

I agree to deposit this thesis in the University's open access institutional repository or allow the library to do so on my behalf, subject to Irish Copyright Legislation and Trinity College Library conditions of use and acknowledgement.

Lu Luo

Lu Luo

November 2014

Summary

Engineering cartilage grafts with comparable functionality to the native tissue remains a major challenge in the field of regenerative medicine. The overall goal of this thesis was to engineer a cartilage graft with depth-dependent structure, composition and mechanical properties mimicking the native tissue. It has been previously shown that cartilage grafts mimicking certain aspects of the zonal composition of articular cartilage can be engineered by regulating the oxygen and mechanical environment through the depth of bone marrow derived mesenchymal stem cells (BM-MSCs) seeded hydrogels (Thorpe et al., 2013). Such strategies were however limited by hypertrophy and the poor mechanical properties of the engineered grafts, motivating the use of infrapatellar fat pad derived mesenchymal stem cells (IFP-MSCs) for zonal cartilage tissue engineering. As a prerequisite to achieving this goal, I first sought to explore how IFP-MSCs would response to joint specific mechanical stimuli. To this end, I examined and compared the effects of dynamic compression on chondrogenesis of BM-MSCs and IFP-MSCs. Both cell types demonstrated the capacity to facilitate the development of cartilage grafts with glycosaminoglycan (GAG) content and bulk compressive mechanical properties approaching those observed in skeletally immature articular cartilage. Although dynamic compression had no significant effect on chondrogenesis of IFP-MSCs, cartilage grafts engineered using IFP-MSCs showed no evidence of hypertrophy or endochondral ossification, unlike those engineered using BM-MSCs.

Having identified that IFP-MSCs represent a promising cell source to engineer phenotypically stable cartilage grafts, I next sought to explore if these cells could be used to engineer cartilage grafts with a zonal composition mimicking that of native articular cartilage. This was attempted by regulating the oxygen and mechanical environment through the depth of cell-laden hydrogels. IFP-MSCs were encapsulated in agarose hydrogel to make constructs of either 2 mm or 4 mm in height. Constructs were confined to half of their height and subjected to dynamic compression, in an attempt to mimic the spatial oxygen and mechanical environment within articular cartilage. The size of cell seeded constructs clearly impacted upon spatial nutrient

availability and subsequent matrix deposition within the engineered tissues. Furthermore, partial confinement coupled with dynamic compression promoted the development of a superficial region that stained strongly for type II collagen and weakly for GAG in both 2 mm and 4 mm high constructs, with proteoglycan 4 (PRG4) deposition further observed in 4 mm high samples, hence mimicking aspects of the zonal composition of normal articular cartilage.

While this strategy was able to recapitulate certain aspects of the zonal composition of articular cartilage, the benninghoff collagen architecture of mature articular cartilage was not reestablished in the engineered tissues. Furthermore, the bulk mechanical properties of the engineered grafts were still much lower than those of the native tissue. Therefore, I next explored the use of decellularized cartilage ECM-derived scaffolds, where the collagen structure of the native tissue was maintained, for engineering functional grafts. It was hypothesized that re-populating such scaffolds with IFP-MSCs would lead to the development of cartilage grafts with structure, composition and mechanical properties mimicking the native tissue. Skeletally immature and mature articular cartilage were decellularized using a protocol, which demonstrated to significantly reduce the DNA content and completely remove the GAG content while maintain the collagen content and architecture of the tissue. These decellularized cartilage scaffolds were then seeded with IFP-MSCs and cultured for 4 weeks. Both scaffold types supported cellular attachment, proliferation and chondrogenic differentiation of IFP-MSCs. In addition, they provided a natural template for the seeded IFP-MSCs to align and orient their synthesized matrix in a manner mimicking the underlying collagen architecture of the decellularized tissue. Most importantly, re-populating decellularized mature cartilage scaffolds with IFP-MSCs led to the development of grafts with a collagen structure and content, depth-dependent compressive properties and characteristic strain softening behavior mimicking native mature articular cartilage. In summary, this thesis highlights the importance of environmental factors and scaffold architecture on engineering zonal cartilage grafts. The findings also have important implications for the design of novel scaffolds for use in orthopedic medicine.

Acknowledgments

First, I want to thank God for all the grace, peace, strength and helps he has provided for me during these four years of study. I have experienced many difficulties and tough times. I would not have finished this thesis unless through his wonderful provisions. Secondly, I would like to give special thanks to Alanna Gannon and Gillian Stephenson, who helped and supported me during the most difficult time of this PhD study. I genuinely appreciated their helps, love and care for me.

Also, I would like to thank my supervisor Dr. Daniel Kelly. He is a very easy-going and friendly supervisor, which makes it very easy and lovely for me to communicate with him. Particularly, I would like to thank him for respecting and supporting me to test the idea of decellularized cartilage scaffolds in the last year of my PhD, which was a very challenging task. I appreciated all the kind helps he provided in correcting and proof-reading of all the papers and this thesis.

I would like to give special thanks to my colleagues Adam O'Reilly, Simon Carroll and Johnnie Chu for offering kind helps on the studies in chapter 4 and 5 in this thesis. They are such talented engineers. It was a pleasure to work with them within a cross-discipline environment.

In these four years of study, I have received so many laughter, cares, supports and faithful prayers from my colleagues and friends from my church. I would like to give genuine thanks to all of them! I can't list all of them but only a few here. Thanks very much, Raja, Grainne, Amy, Henrique, Linda, Gillian, and Lorraine. You are wonderful and precious friends! It is a blessing to have you in my life.

Finally, I would like to thanks my parents who supported me through all these years of study and loved me regardless of failure or success.

Table of Content

Declaration i

Summary ii

Acknowledgments iv

Table of Content v

List of Figures x

List of Tables xix

Nomendature xx

Conferences and Publications i

Chapter I 1

Introduction 1

1.1. Current Approaches to Articular Cartilage Repair 2

1.2. Engineering Zonal Cartilage Tissues 3

1.3 Objectives of the thesis 5

Chapter II 7

Literature review on zonal cartilage tissue engineering 7

2.1. The zonal structure of articular cartilage 8

2.1.1. Zonal variation at cellular level 8

2.1.2. Zonal variation at ECM level 9

2.1.3. Zonal variation at mechanical level 11

2.2. Why do we need to engineer zonal cartilage? 12

2.3. Classical zonal cartilage tissue engineering strategies 14

2.3.1. Utilizing zonal chondrocytes 14

2.3.2. Varying biomaterial properties 15

2.3.3. Combined approach 17

2.4. Recent advance in zonal cartilage tissue engineering 18

2.4.1. Bioprinting 18

2.4.2. Electrospinning 19

2.4.3. Bioreactors 20
2.5. Potential application of decellularized cartilage scaffolds in zonal cartilage tissue engineering 22
2.5.1. Decellularized tissue ECM derived scaffolds for tissue engineering applications 22
2.5.2. Decellularized cartilage ECM for cartilage tissue engineering 24
2.6. Summary 27
Chapter III 28
Effects of dynamic compression on chondrogenesis of bone marrow and infrapatellar fat pad derived mesenchymal stem cells 28
3.1. Introduction 29
3.2. Materials and Methods 32
3.2.1. Cell Isolation and Expansion 32
3.2.2. Hydrogel construct fabrication and culturing 32
3.2.3. Experimental design 33
3.2.4. Assessment of mechanical properties 33
3.2.5. Quantitative biochemical analysis 34
3.2.6. Histology and immunohistochemistry 35
3.2.7. Micro-computed tomography analysis 35
3.2.8. Statistical analysis 36
3.3. Results 37
3.3.1. Temporal and spatial development of cartilage grafts engineered in free swelling culture using different sources of MSCs 37
3.3.2. The influence of dynamic compression on the functional properties of cartilage grafts engineered using different sources of MSCs 42
3.3.3. The influence of DC on the spatial development of engineered cartilage 51
3.3.4. The influence of DC on hypertrophy of chondrogenically primed BM-MSCs 54
3.4. Discussion 56
Chapter IV 61

Engineering zonal cartilaginous tissue using infrapatellar fat pad derived mesenchymal stem cells by modulating the spatial environment within the developing construct 61

4.1. Introduction 62

4.2. Materials and Methods 65

4.2.1. Cell Isolation and Expansion 65

4.2.2. Hydrogel construct fabrication and culturing 65

4.2.3. Experimental design 66

4.2.4. Computational modelling of oxygen, glucose and mechanical environment within developing constructs 67

4.2.5. Assessment of mechanical properties 70

4.2.6. Quantitative biochemical analysis 70

4.2.7. Histology and immunohistochemistry 71

4.2.8. Statistical analysis 72

4.3. Results 73

4.3.1. Construct height determines the spatial development of tissue engineered cartilage 73

4.3.2. Modulating spatial oxygen and glucose availability within stem cell seeded hydrogels by partially confining the constructs alters matrix synthesis and the spatial development of the engineered tissue 77

4.3.3. The development of tissue engineered cartilage subjected to dynamic compression depends on the height of the construct 82

4.3.4. Coupling partial confinement and dynamic compression can lead to the development of engineered cartilage with zonal features mimicking certain aspects of the native tissue 87

4.4. Discussion 91

Chapter V 96

Engineering tissues that mimic the zonal characteristics of articular cartilage using decellularized cartilage scaffolds seeded with infrapatellar fat pad derived mesenchymal stem cells 96

5.1. Introduction 97
5.2. Materials and methods 100
5.2.1. Tissue retrieval 100
5.2.2. Decellularization 100
5.2.3. Cell Isolation and Expansion 102
5.2.4. Cell seeding and construct culture 102
5.2.5. Live/dead assay 103
5.2.6. DAPI and actin staining 104
5.2.7. Mechanical test 104
5.2.8. Quantitative biochemical analysis 106
5.2.9. Histology and PLM 106
5.2.10. Statistical analysis 107
5.3. Results 108
5.3.1. Effective decellularization of articular cartilage is accompanied by a complete loss in sGAG while maintaining tissue collagen content 108
5.3.2. The depth-dependent collagen architecture of skeletally mature and immature cartilage is maintained post- decellularization 111
5.3.3. Decellularized cartilage scaffolds support stem cell attachment, viability and proliferation 114
5.3.4. IFP-MSCs secreted comparable amounts of sGAG but higher levels of collagen in skeletally mature compared to immature cartilage scaffolds 116
5.3.5. Cellular and neo-matrix alignment in decellularized cartilage is driven by the underlying collagen architecture of the scaffold 120
5.3.6. Re-population of decellularized skeletally mature cartilage scaffolds with IFP-MSCs leads to the development of engineered cartilage with mechanical properties mimicking the native tissue 124
5.4. Discussion 127
Chapter VI 133
Discussion 133

6.1. Overview 134
6.2. Is there an ideal approach to engineering zonal cartilage grafts? 136
6.3. Implications for the design of novel scaffolds for zonal cartilage tissue engineering 139
Chapter VII 141
Conclusions and Future Directions 141
7.1. Main findings and conclusions 142
7.2. Future directions 144
Chapter VIII 145
Bibliography 145

List of Figures

Figure 2.1. A schematic diagram of cell and collagen fiber orientation in the superficial, middle and deep zone of articular cartilage. Adapted from (Mow and Guo, 2002). 9

Figure 2.2. Concept for bioprinting zonal cartilage constructs where chondrocytes subpopulations from the deep, middle and superficial zones are suspended in different biomaterials and printed using rapid-prototyping technologies in defined geometries. Adapted from (Klein et al., 2009b). 18

Figure 2.3. (A) Schematic diagram of confinement, in which constructs were press-fitted into custom made PTFE wells such that the bottom half of the construct were confined. (B) An axisymmetric computational model predicting the oxygen tension within the unconfined and confined constructs. Results showed reduced oxygen tension in the bottom half of the confined constructs compared to the unconfined controls. (C) An axisymmetric computational model predicting the maximum principle strain of the unconfined and confined constructs subjected to dynamic compression. Results showed increased maximum principle strain across the top of the confined constructs compared to the unconfined controls. Adapted from (Thorpe et al., 2013)..... 21

Figure 2.4. Decellularization of whole organs and characterization of intact vascular structures in the decellularized organ scaffolds. Original solid organs (a) can be decellularized using different decellularization methods to prepare acellular organ scaffolds (b). Various characterization methods for demonstrating intact vascular structures in each of decellularized organ matrices (c). 23

Figure 3.1. Biochemical content of FS BM and IFP constructs from donor 1 (left column) and donor 2 (right column) at day 21 and 42. (A) DNA content (ng/mg w/w); (B) GAG content (%w/w); (C) collagen content (%w/w). a: $p<0.05$ vs. same construct type at day 21; *: $p<0.05$, **: $p<0.01$; ***: $p<0.001$. 38

Figure 3.2. Histological and immunohistological staining of FS BM and IFP constructs from donor 1 (left) and donor 2 (right) at day 42. (A) Alcian blue staining for proteoglycan; (B) Picrosirius red staining for collagen; (C) Immunohistological staining for collagen type II; scale bar in A, B and C: 500 μm. (D) Immunohistological staining for collagen type I. Low magnification images (inserted) show staining at a bulk construct level; high magnification images show staining at the peripheral region of the samples. Box region in low magnification image indicates area from where high magnification images were taken. Scale bar in low magnification images: 500 μm; scale bar in high magnifications images: 50 μm. 40

Figure 3.3. Biochemical content of the top and bottom halves of FS BM and IFP constructs from donor 1 (left column) and donor 2 (right column) at day 42. (A) DNA content (ng/mg w/w); (B) GAG content (%w/w); (C) collagen content (%w/w). a: $p<0.05$ vs. BM constructs from the same region; *: $p<0.05$, **: $p<0.01$; ***: $p<0.001$. 41

Figure 3.4. Biochemical content of FS and DC BM (left) and IFP constructs (right) from donor 1 at day 42. (A, H) DNA content (ng/mg w/w); (B, I) GAG content (μg/sample); (C, J) GAG content (% w/w); (D, K) GAG/DNA (μg/μg); (E, L) collagen content (μg/sample); (F, M) collagen content (% w/w); (G, N) collagen/DNA (μg/μg).*:$p<0.05$. 43

Figure 3.5. Mechanical properties of FS and DC BM (left column) and IFP constructs (right column) from donor 1 (A, B, C, D) and donor 2 (E, F, G, H) at day 42. (A, C, E, G) equilibrium modulus (kPa); (B, D, F, H) 1Hz dynamic modulus (kPa). ***: $p<0.001$. 44

Figure 3.6. GAG and collagen content accumulated within the constructs, released into medium and the total synthesized (constructs + medium) from day 21 to day 42 in FS and DC BM (left column) and IFP constructs (right column) from donor 1 (upper) and donor 2 (lower). (A, C, E, G) GAG content (μg); (B, D, F, H) collagen content (μg). Medium samples from day 21 to day 42 were analyzed for GAG or collagen content released from the constructs (n=1 per group for donor 1, as medium from

each individual construct were pooled; n=4 per group for donor 2, as medium from each individual construct were kept separate). GAG or collagen content accumulated within constructs from day 21 to day 42 were calculated by subtracting the mean value of GAG or collagen content of day 21 samples from the value of GAG or collagen content of each individual day 42 samples (n=4 per group). Total amount of GAG or collagen synthesis from day 21 to day 42 was calculated by summing up the amount accumulated within constructs and the amount released into medium. *: $p<0.05$; **: $p<0.01$. 47

Figure 3.7. Histological staining of FS and DC BM and IFP constructs from donor 1 (left) and donor 2 (right) at day 42. Upper two rows: Alcian blue staining for proteoglycan; lower two rows: Picrosirius red for collagen. Scale bar: 500 μm. 49

Figure 3.8. Immunohistological staining of FS and DC BM and IFP constructs from donor 1 (left) and donor 2 (right) at day 42. Upper two rows: immunohistological staining for collagen type II, scale bar: 500 μm. Middle two rows: immunohistological staining for collagen type I, scale bar: 500 μm; Box region indicates area from where high magnification images (lower two rows) were taken. Lower two rows: immunohistological staining for collagen type I at the peripheral region of the samples (high magnification); L: ligament (positive control); C: cartilage (negative control). Scale bar: 50 μm. 50

Figure 3.9. Histological staining of FS and DC BM constructs from donor 1 at the peripheral and central region of the tissue at day 42. (A) Alcian blue staining for proteoglycan; (B) Picrosirius red staining for collagen. P: peripheral region; C: central region. Box region in low magnification images (side two columns) indicates area from where high magnification images (middle two columns) were taken. Asterisks and arrows in high magnification images indicate ECM and PCM respectively. Scale bar in low magnification images: 500 μm; scale bar in high magnification images: 50 μm. 53

Figure 3.10. Assessment of mineralization in FS and DC BM and IFP constructs from donor 1 and donor 2 at day 42. (A) Alizarin red staining of mineral deposition in FS

and DC BM and IFP constructs from donor 1 at day 42; scale bar: 500 μm. Images represent the main finding for both donors. (B) 3D images obtained with μCT scan of mineral deposition within FS and DC BM constructs from both donors. Scale bar: 1mm. (C) Volume of minerals in FS and DC BM constructs from both donors. Two constructs per group were scanned using μCT..... 55

Figure 4.1. Experimental design. Constructs were first cultured in unconfined free swelling (UFS) conditions until day 21, and care was taken to ensure constructs did not flip over during the whole culture period to maintain a stable oxygen and glucose gradient within them. Samples were then confined to half of their height and subjected to dynamic compress (CDC) until day 42 while samples remained in UFS conditions were used as controls. Constructs that were confined but still in free swelling (CFS) conditions and constructs that remained unconfined but subjected to dynamic compression (UDC) were also kept to study the effects of confinement alone and dynamic compression alone on the development of the tissue. 67

Figure 4.2. Oxygen and glucose environment and matrix distribution with 2mm and 4mm samples at day 42. (A) An axisymmetric computational model predicting oxygen environment and (B) an axisymmetric computational model predicting glucose environment within both 2mm and 4mm samples. The resulted oxygen/glucose concentration data was calculated from the regions within constructs which were indicated by grey boxes. (C) Alcian blue staining of GAG and (D) Picro-sirius red staining of collagen distribution within both samples at day 42. Histology images were taken at 2x magnification, and they represent approximately 2/3 of the whole sample..... 74

Figure 4.3. Biochemical content of the top and bottom halves of 2mm and 4mm unconfined free swelling (UFS) samples at day 42. (A) DNA content [ng/mg w/w]; (B) GAG content [% w/w]; (C) Collagen content [% w/w]; (D) GAG/DNA [ng/ng] and (E) Collagen/DNA [ng/ng]. +: trend, $p<0.1$; *: $p<0.05$; **: $p<0.01$; ***:$p<0.001$..... 76

Figure 4.4. An axisymmetric computational model predicting oxygen and glucose environment with unconfined and confined free swelling 2mm and 4mm samples

at day 42. The resulted oxygen/glucose data was calculated from regions within constructs which were indicated by grey boxes. Red circles highlight regions with lowered oxygen tension in the 2mm and 4mm confined samples.....78

Figure 4.5. (A) GAG content [μg] and (B) collagen content [μg] accumulated within constructs, released into media and total synthesized (accumulated+released) in unconfined free swelling (UFS) and confined free swelling (CFS) 2mm and 4mm constructs at day 42. Total GAG/DNA [μg/μg] and total collagen/DNA [μg/μg] value were also plotted on the right Y axis within each graph. (C) DNA content [ng/mg w/w], (D) GAG content [%w/w] and (E) collagen content [%w/w] of the top and bottom halves of the UFS and CFS 2mm and 4mm samples at day 42. #: $p<0.05$ vs. UFS; *: $p<0.05$; **: $p<0.01$; ***: $p<0.001$. 79

Figure 4.6. Histological staining of matrix deposition within UFS and CFS 2mm and 4mm constructs at day 42. (A) Alcian blue staining for GAG, (C) picro-sirius red staining for collagen and (D) Immunohistochemical staining for collagen type II accumulation within samples. All images were taken at 2x magnification, showing 2/3 of the whole construct. (B) Alcian blue staining for GAG deposition at the bottom periphery of the samples (indicated by box regions in (A)) and images were taken at 20x magnification. 81

Figure 4.7. An axisymmetric computational model predicting the mechanical environment of fluid pressure [MPa], tension strain [%, positive] and compression strain [%, negative] within (A) unconfined dynamically compressed (UDC) and (B) confined dynamically compressed (CDC) 2mm and 4mm constructs at day 21. The mechanical environment data were calculated from regions within constructs, which were indicated by grey boxes.....83

Figure 4.8. (A) GAG content [μg] and (B) collagen content [μg] accumulated within constructs, released into media and total synthesised (accumulated+released) in unconfined free swelling (UFS) and unconfined dynamically compressed (UDC) 2mm and 4mm constructs at day 42. Total GAG/DNA [μg/μg] and total collagen/DNA [μg/μg] value were also plotted on the right Y axis within each graph.

(C) DNA content [ng/mg w/w], (D) GAG content [%w/w] and (E) collagen content [%w/w] of the top and bottom halves of the UFS and UDC 2mm and 4mm samples at day 42. α: trend, p<0.1 vs. UFS; #: p<0.05 vs. UFS; *: p<0.05; ***: p<0.001. 84

Figure 4.9. Histological staining of matrix deposition within UFS and UDC 2mm and 4mm constructs at day 42. (A) Alcian blue staining for GAG, (B) picro-sirius red staining for collagen and (C) Immunohistochemical staining for collagen type II accumulation within samples. Arrow indicates the enhanced staining for collagen type II at the superficial region of 2mm UDC constructs. All images were taken at 2x magnification, showing 2/3 of the whole construct. 86

Figure 4.10. (A) DNA content [ng/mg w/w], (B) GAG content [%w/w] and (C) collagen content [%w/w] of the top and bottom halves of the unconfined free swelling (UFS) and confined dynamically compressed (CDC) 2mm and 4mm samples at day 42. α: trend, p<0.1 vs. UFS; #: p<0.05 vs. UFS; +: trend, p<0.1; *: p<0.05; **: p<0.01; ***: p<0.001. 88

Figure 4.11. GAG, collagen type II and PRG 4 distribution within UFS and CDC 2mm and 4mm constructs at day 42. (A) Alcian blue staining for GAG and (B) Immunohistochemical staining for collagen type II accumulation in the top and bottom halves of the sample. T: top; B: bottom. Arrows indicate the enhanced collagen type II deposition in the superficial region of both 2mm and 4mm CDC constructs. (C) Immunohistochemical staining for PRG4 expression at the top surface of the sample. Images were taken at 10x magnification. All inserted images were taken at 2x magnification, and box regions indicate area where 10x magnification images were taken. 90

Figure 5.1. Transverse and cross section of channeled cartilage disks. In total 7 channels were introduced to each cartilage disk. 101

Figure 5.2. H&E, Alcian blue and Picrosirius red staining of the 4 month old native and decellularized articular cartilage. Images for H&E were taken at 40x, with inserted images taken at 2x. Images for Alcian blue and Picrosirius red were all taken at 2x. 109

Figure 5.3. A: DNA, GAG and collagen content of the 4 month old native and decellularized articular cartilage. B: DNA/dry weight (ng/mg), GAG %dry weight and collagen %dry weight level of the 4 month old native and decellularized articular cartilage. ***: p≤0.001.....110

Figure 5.4. H&E, Alcian blue and Picrosirius red staining and PLM images of collagen architecture of decellularized skeletally immature and mature cartilage ECM-derived scaffolds. H&E images were taken at 10x, showing cell removal through the depth of the decellularized tissue, with images shown by box region taken at 40x. Images for Alcian blue and Picrosirius red were all taken at 10x. Regions with bright color in PLM images indicate the existence of an organized collagen alignment (either horizontal or perpendicular) in these regions, leading to birefringence. Dark regions indicate the lack of collagen alignment in these areas. 113

Figure 5.5. A: viability of IFP-MSCs seeded in decellularized immature and mature cartilage scaffolds at day 1, 14 and 28. Live cells appear green and dead cells appear red. Arrows indicate magnified images shown in box regions (channels). B: DNA content of the cells seeded in decellularized immature and mature cartilage scaffolds at day 1 and 28. The DNA content of the cells is calculated by subtracting the residual DNA content of the scaffolds from the total DNA content of the constructs.*: p≤0.05; ***: p≤0.001. 115

Figure 5.6. GAG, collagen, collagen/GAG (μg/μg), GAG/DNA (ng/ng) and collagen/DNA (ng/ng) level of the matrix secreted by IFP-MSCs inside the cell seeded decellularized immature and mature cartilage scaffolds at day 28. The GAG or collagen or DNA level of matrix secreted by cells is calculated by subtracting the residual GAG or collagen or DNA level of the decellularized scaffolds from the total GAG or collagen or DNA level of the constructs. *: p≤0.05.....116

Figure 5.7. Alcian blue staining of cell seeded decellularized immature and mature cartilage scaffolds at day 14 and 28. Images from first and second row were taken at 2x. Images from third row were taken at 10x, showing cell morphology and GAG

distribution within the channels, with inserted images taken at 40x. Images from last row were taken at 20x, showing cell migration into the ECM of the decellularized scaffolds at sites shown in box regions in images from the second row. 118

Figure 5.8. Picrosirius red staining of cell seeded decellularized immature and mature cartilage scaffolds at day 14 and 28. All images were taken at 2x. 119

Figure 5.9. DAPI and F-actin staining showing cell alignment within the channels of cell seeded decellularized immature and mature cartilage scaffolds at day 14 and 28. Images in first and third column represent the highest degree of cell alignment observed in the two groups at corresponding time points, while images in second and fourth column represent the average degree of cell alignment observed in the two groups. Images from first to third row were all taken at 20x. Images from the fourth row show the magnified images of the box regions in third row. 121

Figure 5.10. PLM images of collagen alignment within the channels of the cell seeded decellularized immature and mature cartilage scaffolds at day 14 and 28. All images were taken at 10x. 123

Figure 5.11. A) Total GAG %wet weight level, B) total collagen %wet weight level, and C) 1Hz dynamic modulus (kPa) of the engineered immature and mature cartilage grafts at day 28. ***: $p \leqslant 0.001$. 124

Figure 5.12. A: The equilibrium modulus (for a global compressive strain of 5%) of the superficial zone (SZ), middle zone (MZ), upper deep zone (DZ-upper) and lower deep zone (DZ-lower) of the day 1 and 28 cell seeded decellularized immature and mature scaffolds. B: The equilibrium modulus of the upper deep zone of the day 1 and 28 cell seeded decellularized immature and mature scaffolds for 2.5%, 5% 7.5%, 10%, 12.5% and 15% global strain. *:$p \leqslant 0.05$; **: $p \leqslant 0.01$; #:$p \leqslant 0.05$ vs. day1; ##: $p \leqslant 0.01$ vs. day1. 126

Supplementary Figure 3. 1. Biochemical content of FS and DC BM (left) and IFP constructs (right) from donor 2 at day 42. (A, H) DNA content (ng/mg w/w); (B, I)

GAG content (μg/sample); (C, J) GAG content (% w/w); (D, K) GAG/DNA (μg/μg); (E, L) collagen content (μg/sample); (F, M) collagen content (% w/w); (G, N) collagen/DNA (μg/μg). 45

Supplementary Figure 3.2. Biochemical content of top and bottom halves of FS and DC BM (left) and IFP constructs (right) from donor 1 (A, B, C, D) and donor 2 (E, F, G, H) at day 42. (A, C, E, G) GAG content (%w/w); (B, D, F, H) collagen content (%w/w). +: $p<0.1$; *: $p<0.05$, **: $p<0.01$; ***: $p<0.001$. 52

Supplementary Figure 4.1. (A) GAG/DNA [ng/ng] and (B) collagen/DNA [ng/ng] value of the top and bottom halves of UFS and CFS 2mm and 4mm constructs at day 42. #: $p<0.05$ vs. UFS; +: trend, $p<0.1$; *: $p<0.05$. 80

Supplementary Figure 4.2. (A) GAG/DNA [ng/ng] and (B) collagen/DNA [ng/ng] value of the top and bottom halves of UFS and UDC 2mm and 4mm constructs at day 42. #: $p<0.05$ vs. UFS; *: $p<0.05$. 86

Supplementary Figure 4.3. (A) GAG/DNA [ng/ng] and (B) collagen/DNA [ng/ng] value of the top and bottom halves of UFS and CDC 2mm and 4mm constructs at day 42. α: trend, $p<0.1$ vs. UFS; #: $p<0.05$ vs. UFS; +: trend, $p<0.1$; *: $p<0.05$; **: $p<0.01$; ***: $p<0.001$. 89

List of Tables

Table 5.1. DNA, GAG and collagen content, dry and wet weight, and DNA/dry weight (ng/mg), collagen %dry weight, DNA/wet weight (ng/mg) and collagen %wet weight level of the decellularized skeletally immature and mature cartilage scaffolds. NS: not significant; *:p≤0.05; **: p≤0.01; ***: p≤0.001. 112

Nomendature

AC	Articular cartilage
ALP	Alkaline phosphatase
ANOVA	Analysis of variance
BM	Bone marrow
BM-MSCs	Bone marrow derived mesenchymal stem cells
BSA	Bovine serum albumin
CDC	Confined dynamically compressed
CFS	Confined free swelling
CS	Chondroitin sulfate
DAPI	4',6-diamidino-2-phenylindole
D	Diffusion coefficient
D_{ag}	Diffusion coefficient for agarose
D_{H2O}	Diffusion coefficient for water
DAB	Diaminobenzide
DC	Dynamic compression
DNA	Deoxyribonucleic acid
DNase	Deoxyribonuclease
DTT	Dithiothreitol
DZ	Deep zone
dsDNA	Double-stranded deoxyribonucleic acid
ε	Strain
ECM	Extracellular matrix
EDTA	Ethylenediaminetetraacetic acid
FBS	Fetal bovine serum
FE	Finite element
FGF-2	Basic fibroblast growth factor
FS	Free swelling

GAG	Glycosaminoglycan
H&E	Hematoxylin and eosin
HCl	Hydrochloric acid
Hz	Hertz
hgDMEM	High glucose dulbecco's modified eagle medium
IFP	Infrapatellar fat pad
Km	Concentration at half the maximum consumption rate
kPa	Kilo Pascal
M	Molar
$MgCl_2$	Magnesium chloride
MMP-pep	Matrix Metalloproteinases peptide
MPa	Mega Pascal
MSCs	Mesenchymal stem cells
MZ	Middle zone
mg	Milligram
min	Minute
ml	Milliliter
mm	Millimeter
mM	Millimolar
NaCl	Sodium chloride
NaOH	Sodium hydroxide
ng	Nanogram
OA	Osteoarthritis
P2	Passage two
PBS	Phosphate buffered saline
PCL	Polycaprolactone
PCM	Pericellular matrix
PDGF	Platelet-derived growth factor
PEG	Polyethylene glycol

PGA	Polyglycolic acid
PTFE	Polytetrafluoroethylene
PRG4	Proteoglycan 4
Q_m	Maximum consumption rate
RNase	Ribonuclease
AM	Additive manufacturing
RT	Room temperature
SD	Standard deviation
SDS	Sodium dodecyl sulfate
sGAG	Sulfated glycosaminoglycan
SZ	Superficial zone
s	Second
TGF-β	Transforming growth factor beta
t	time
UDC	Unconfined dynamically compressed
UFS	Unconfined free swelling
µCT	Micro-computed tomography
µM	Micromolar
µL	Microliter
VEGF	Vascular endothelial growth factor
v/v	Volume/volume
w/v	Weight/volume
2D	2-dimensional
3D	3-dimensional
% w/w	Percentage of wet weight
Ø	Diameter
∂	Partial derivative

Conferences and Publications

Conference Abstracts

Luo, L., Chu, J.Y., Eswaramoorthy, R., Kelly, D.J. Engineering tissues that mimic the zonal characteristics of articular cartilage using decellularized cartilage scaffolds seeded with infrapatellar fat pad derived mesenchymal stem cells. In 21st Annual Conference of the Section of Bioengineering, Royal Academy of Medicine in Ireland, January 2015, Maynooth, Ireland (Oral Presentation)

Luo, L., Eswaramoorthy, R., Buckley, C.T., Kelly, D.J. Development of a novel biomimetic scaffold for cartilage repair using decellularized cartilage matrix. In 20th Annual Conference of the Section of Bioengineering, Royal Academy of Medicine in Ireland, January 2014, limerick, Ireland (Oral Presentation)

Luo, L., O'Reilly, A., Thorpe, S.D., Buckley, C.T., Kelly, D.J. Engineering zonal cartilaginous tissue using infrapatellar fat pad derived stem cells by modulating the spatial environment within the developing construct. In Orthopaedic Research Society 2013 Annual Meeting, February 2013, San Antonio, Texas, USA (Oral Presentation)

Luo, L., O'Reilly, A., Thorpe, S.D., Buckley, C.T., Kelly, D.J. Engineering zonal cartilaginous tissue using infrapatellar fat pad derived stem cells by modulating the spatial environment within the developing construct. In 19th Annual Conference of the Section of Bioengineering, Royal Academy of Medicine in Ireland, January 2013, Co. Meath, Ireland (Oral Presentation)

Luo, L., Thorpe, S.D., Buckley, C.T., Kelly, D.J. Engineering zonal cartilaginous tissue using infrapatellar fat pad derived stem cells. In 3rd Tissue Engineering and

Regenerative Medicine World Congress, September 2012, Vienna, Austria (poster Presentation)

Luo, L., Thorpe, S.D., Buckley, C.T., Kelly, D.J. Effects of dynamic compression on chondrogenesis of bone marrow and infrapatellar fat pad derived stem cells. In 3rd Tissue Engineering and Regenerative Medicine World Congress, September 2012, Vienna, Austria (poster Presentation)

Luo, L., Thorpe, S.D., Kelly, D.J. A comparison of the response of bone marrow and infrapatellar fat pad derived mesenchymal stem cells to dynamic compression. In 18th Annual Conference of the Section of Bioengineering, Royal Academy of Medicine in Ireland, January 2012, Belfast, UK (Oral Presentation)

Research work to be submitted

Studies in chapter 3, 4 and 5 are to be submitted as papers.

Chapter I

Introduction

1.1. Current Approaches to Articular Cartilage Repair

Articular cartilage is a loading-bearing tissue that lines the ends of long bones, providing a low-friction and wear-resistant surface during normal joint movement (Bhosale and Richardson, 2008). Due to its avascular nature, once damaged the tissue does not spontaneously heal (Hunziker, 1999, Steadman et al., 2001). If left untreated, many cartilage injuries will progress into osteoarthritis (OA). This disease is characterized by a loss of the articular cartilage, typically progressing from superficial fibrillation to complete erosion to the subchondral bone (Horton et al., 2006). It is estimated that OA affects at least 27 million Americans (Lawrence et al., 2008) and also a comparable fraction of the populations in Europe and Asia (Zeng et al., 2008).

The majority of current medical treatments for damaged cartilage and OA mainly aim for pain relief (Hilaire, 2006), while surgical treatments including microfracture (Steadman et al., 1999), autologous osteochondral transplantation (Hangody et al., 2001) and autologous chondrocyte implantation (Brittberg et al., 1994, Brittberg et al., 2003) aim to improve joint function. However, limitations such as the formation of fibrocartilage repair tissue and the introduction of further damage to patients' healthy cartilage are often associated with these surgical treatments (Hunziker, 2002, Lee et al., 2000). Although joint replacement, the last choice for patients with advanced OA, allows for recovery of some function and reduction of pain (Creamer, 2000), the implanted joint prosthesis tend to loosen over time and revision surgeries are often required in younger patients.

Tissue engineering offers an attractive option for cartilage repair. Cartilage tissue engineering aims to regenerate a three-dimensional (3D) cartilage graft *in vitro*, through the combined application of chondrogenic cells, scaffolds and signaling factors, for subsequent implantation into the patients (Hunziker, 2002, Chung and Burdick, 2008). So far various cell sources have been tested. While chondrocytes

could be considered as a cell source for engineering cartilage tissue (Kisiday et al., 2004, Mesallati et al., 2012, Vinardell et al., 2011), their low proliferation potential and tendency to undergo dedifferentiation towards a more fibroblast-like phenotype during *in vitro* expansion hampers their clinical use (Benya and Shaffer, 1982, Homicz et al., 2002). In contrast, mesenchymal stem cells (MSCs), which can be obtained from various tissue types and have a high proliferative ability and multi-lineage differentiation potential (Caplan, 1991, Caplan, 2005), may represent a better cell source for cartilage tissue engineering. Successful chondrogenesis has been demonstrated in MSCs derived from various tissues, including bone marrow (BM) (Pittenger et al., 1999, Johnstone et al., 1998, Yoo et al., 1998), infrapatellar fat pad (IFP) (Dragoo et al., 2003, Buckley et al., 2010b, Vinardell et al., 2011) and synovium (Pei et al., 2008, Vinardell et al., 2012b). Particularly, MSCs can be isolated in a larger number from IFP compared to BM, with lower degree of invasiveness and patient morbidity (Dragoo et al., 2003). It remains unclear, however, if such cell types can be used to engineer functional cartilage grafts for joint regeneration.

1.2. Engineering Zonal Cartilage Tissues

Despise the numerous efforts made in identifying novel cell sources (Johnstone et al., 1998, Dragoo et al., 2003, Pei et al., 2008), scaffolds (Li et al., 2009, Thorpe et al., 2010, Kafienah et al., 2007) and signaling factors (Liu et al., 2013, Cals et al., 2012) in cartilage tissue engineering, generally most research result in a homogeneous engineered cartilage graft, which at best may mimic the bulk biochemical and mechanical properties of native cartilage. However, articular cartilage is an anisotropic and highly organized tissue with spatial-varying structure, composition and mechanical properties (Klein et al., 2009a). This depth-dependent structure and composition is critical to the biomechanical function of the tissue (Wilson et al., 2007). The acquisition of these depth-dependent properties in tissue engineered grafts is therefore highly desirable and may bring benefits such as better integration into the

surrounding native cartilage and long-term of mechanical stability, by providing a depth-dependent structure and composition that matches to the surrounding native environment (Klein et al., 2009a, Klein et al., 2009b). It therefore remains an ongoing challenge to engineer cartilage grafts with a depth-dependent structure, composition and mechanical properties mimicking native tissue.

To date, a small number of studies have attempted to engineer articular cartilage grafts mimicking aspects of the depth-dependent properties of the native tissue. Early efforts involved isolating chondrocytes from different zones of articular cartilage and incorporating them separately into specific regions of the construct in an attempt to engineer zonal cartilage tissue (Kim et al., 2003, Klein et al., 2003, Sharma et al., 2007). Challenges with this approach include the difficulty to distinguish different zones in diseased cartilage and the relatively low availability of zonal chondrocytes, which may limit the clinical translation of this approach. Other strategies include varying the stiffness (Ng et al., 2009, Ng et al., 2006, Ng et al., 2005) or composition (Nguyen et al., 2011b) through the depth of a scaffold. However, potential limitations associated with such approach include the development of a distinct boundary between gel layers, with potentially poor integration and mechanical discontinuity at the interface of layers.

An alternative approach to engineering zonal cartilage grafts is to recapitulate the key factors of the tissue micro-environment which may be responsible for the development of the depth-dependent properties of articular cartilage during development and skeletal maturation (Thorpe et al., 2013). Oxygen tension and mechanical signals are two key environmental factors that are believed to play an important role in articular cartilage development. A previous study from our lab demonstrated that the application of partial confinement (regulates oxygen tension through the depth of the engineered tissue) combined with dynamic compression to BM-MSCs seeded hydrogels led to the development of engineered grafts with a zonal composition mimicking aspects of the native tissue. However, calcification and

expression of type I and X collagen were also observed in the engineered grafts, indicating hypertrophy and endochondral ossification of the engineered tissue. Furthermore, the mechanical properties of these engineered tissues were still dramatically lower than that of native articular cartilage. These may be overcome by the use of an alternative cell source, such as IFP-MSCs, as studies have shown cartilage grafts engineered using such a cell source do not proceed along the endochondral pathway, and furthermore, is mechanically more robust than tissues engineered using BM-MSCs (Vinardell et al., 2012b). However, to engineer zonal grafts using IFP-MSCs will first require a proper understanding of how such cells will respond to the application of mechanical cues such as dynamic compression, and in particular its influence on matrix accumulation and the mechanical properties of tissues engineered using this promising cell source.

Another approach to engineering zonal cartilage grafts might be to decellularize native articular cartilage tissue, maintain the depth-dependent structure of the tissue, and re-populate these decellularized extra-cellular matrix (ECM) derived scaffolds with MSCs. Decellularization has been achieved for porcine osteo-chondral plugs with near-complete removal of genomic DNA from the decellularized tissues and a significant loss in GAG content (Kheir et al., 2011). However, limited cell infiltration into the decellularized scaffold was observed after subcutaneous implantation into nude mice. Moreover, it is still not clear if such a decellularized scaffold would support chondrogenesis of MSCs.

1.3 Objectives of the thesis

The overall objective of this thesis is to engineer cartilaginous tissue mimicking aspects of the depth-dependent properties of articular cartilage using infrapatellar fat pad derived MSCs. Two different strategies will be explored. This thesis will first investigate if the combined application of partial confinement and dynamic

compression to IFP-MSCs seeded hydrogels, in an attempt to mimic the oxygen and mechanical environment present within developing articular cartilage, will lead to the development of engineered tissues with a zonal composition similar to native tissue. It will then explore the use of decellularized cartilage ECM-derived scaffolds for zonal cartilage tissue engineering. The specific objectives of the thesis are:

- Firstly, to investigate the influence of dynamic compression on matrix accumulation and the subsequent mechanical properties of the cartilage tissue engineered using different sources of MSCs, specifically BM-MSCs and IFP-MSCs.

- Secondly, to explore if it is possible to engineer a cartilage construct with a zonal composition mimicking that of the native tissue using IFP-MSCs through the application of a bioreactor that modulates the oxygen levels and mechanical environment though the depth of cell laden hydrogels.

- Thirdly, to examine the possibility of using decellularized cartilage ECM-derived scaffolds seeded with IFP-MSCs to engineer cartilage tissues with structure, composition and depth-dependent mechanical properties equivalent to the native tissue.

Chapter II

Literature review on zonal cartilage tissue engineering

2.1. The zonal structure of articular cartilage

Articular cartilage is a highly organized heterogeneous tissue, with spatial-varying composition and organization through the depth of the tissue (Klein *et al.*, 2009a). It is typically divided into three zones: the superficial zone, middle zone and deep zone, with each zone displaying distinct physicochemical and biological properties and functions (Klein *et al.*, 2009b). Such a zonal structure is evident in numerous species (Klein *et al.*, 2009a). Also this zonal variation is very exquisite and complex, with variations displayed in multiple levels including cell, extracellular matrix (ECM) and mechanical levels, and it has a great impact on the mechanical, metabolic, and transport properties of the tissue (Hunziker, 2002, Poole, 2001).

2.1.1. Zonal variation at cellular level

Chondrocytes are the cell type within articular cartilage responsible for the turnover and maintenance of the tissue. A zonal variation in cell morphology, orientation, and protein expression has been found in native cartilage (Klein *et al.*, 2009a, Poole, 2001). In the superficial zone, chondrocytes display a flattened and ellipsoidal shape, lying parallel to the joint surface (Figure 2.1). Cells in this zone uniquely express proteoglycan 4 (PRG4), a protein that is important for boundary lubrication and provides the tissue with low-friction properties (Schumacher *et al.*, 1994). Recent researches have also suggested clusterin as another potential marker for cells in this zone, as it has been shown that this protein is uniquely expressed in the superficial layer of healthy cartilage and also in cultures of primary chondrocytes isolated from the superficial zone of articular cartilage (Malda *et al.*, 2010). In the middle zone, cells are more round and are randomly oriented. Whereas in the deep zone, cells are larger and often group in clusters and columns with an orientation perpendicular to the sub-chondral bone (Figure 2.1). The cartilage intermediate layer protein may be a potential marker for the middle-deep zones, as this protein has been seen uniquely

expressed in the middle and deep layers of human articular cartilage but not in the superficial layer (Lorenzo *et al.*, 1998). Furthermore, cells in the deepest layer near the calcified cartilage express collagen type X, a marker for chondrocyte hypertrophy and endochondral ossification (although the expression of this protein in the surface of adult canine articular cartilage has also been reported (Gannon *et al.*, 1991)). Overall, the cell density is highest in the superficial zone and gradually decreases in the middle and deep zone (Mitrovic *et al.*, 1983).

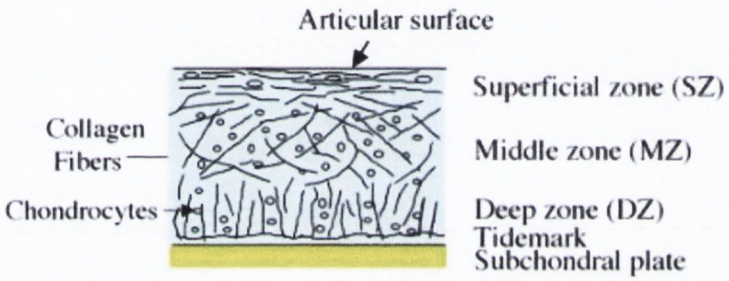

Figure 2.1. A schematic diagram of cell and collagen fiber orientation in the superficial, middle and deep zone of articular cartilage. Adapted from (Mow and Guo, 2002).

2.1.2. Zonal variation at ECM level

Collagen and proteoglycan are the main extracellular matrix components presented in articular cartilage, forming up to ~20% and ~10% wet weight of the tissue respectively (Poole, 2001). The zonal variation in the ECM of the tissue mainly displays in two aspects-the change in collagen network organization and the change in collagen and proteoglycan content through the depth of the tissue.

The change in collagen network organization

It has been demonstrated that the mature articular cartilage has a distinct collagen network organization with changes in collagen fiber orientation observed through the

depth of the tissue (Bhosale and Richardson, 2008, Klein *et al.*, 2009a, Poole, 2001) (Figure 2.1). In the superficial zone, collagen fibrils are densely packed and run parallel to the articular surface, providing the tissue with high tensile strength to withstand the tensile stresses associated with joint loading. In the middle zone, collagen fibrils are larger, less dense and arcade from a parallel to a perpendicular orientation resulting in a more random organization. In the deep zone, collagen fibrils are orientated perpendicular to the sub-chondral bone, thus anchoring the tissue to its bony bed. However it has also been reported that this collagen network organization is not present in skeletally immature tissue, leading to the suggestion that growth of the bone epiphysis with simultaneous adaptation of the cartilage in response to increased joint loading may be responsible for the maturation of the collagen network organization (Rieppo *et al.*, 2009).

The change in collagen and proteoglycan content

There are five main types of collagen in articular cartilage (collagen type II, VI, IX, X, and XI). Among them collagen type II is the major type. Collagen type IX and XI act together with collagen type II to form macrofibrils through crosslinking (Eyre, 2002). It has been demonstrated that in human adult articular cartilage the collagen content as a % of dry weight decreases with depth (Muir *et al.*, 1970). In contrast, the proteoglycan content increases with depth from the superficial to the deep zone (Muir *et al.*, 1970, Klein *et al.*, 2007). This change in proteoglycan content with depth may be partial due to the significant differences in metabolic properties of the chondrocytes from different zones (Kim et al., 2003, Klein et al., 2003, Sharma et al., 2007), and it may also be related to the decreased oxygen tension environment through the depth of the tissue (Zhou *et al.*, 2004, Malda *et al.*, 2004a).

2.1.3. Zonal variation at mechanical level

The mechanical properties of articular cartilage are dependent on the unique structure and biochemical composition of ECM (Wilson *et al.*, 2007). The tensile strength is the highest (Roth and Mow, 1980, Williamson *et al.*, 2003) while the hydraulic permeability is the lowest in the superficial zone, and this could be attributed to the high content and the compacted and paralleled organization of the collagen fibers (Maroudas *et al.*, 1968, Mansour and Mow, 1976). In contrast, the compressive modulus increases with depth from the superficial zone to the deep zone, and this correlates to the increase in proteoglycan content upon the depth (Chen *et al.*, 2001, Schinagl *et al.*, 1997, Wang *et al.*, 2002, Klein *et al.*, 2007).

2.2. Why do we need to engineer zonal cartilage?

Engineering the zonal structure of articular cartilage, especially the collagen organization in the superficial zone, may be of particular importance for clinical success in cartilage repair. Gannon *et al.* has demonstrated that the superficial zone played a key role in elevating the dynamic properties of articular cartilage and the removal of this zone led to a significant decrease in the dynamic properties of the remaining tissue (Gannon *et al.*, 2012). It is postulated that this decrease in the dynamic properties is due at least in part to the superficial zone acting as a low permeability barrier, where its removal decreased the ability of the tissue to maintain fluid load support. Furthermore, studies have also shown that once the articular surface is removed, the equilibrium deformation is reached sooner and the quantity of fluid exchange during loading is also increased (Torzilli *et al.*, 1983). This may cause excessive mechanical force being transferred into cells embedded in the ECM and a significant loss of important cartilage matrix components such as proteoglycans into the synovial fluid. It has been shown that the disruption of the superficial zone in articular cartilage is often associated with the initiation and/or progression of OA (Guilak *et al.*, 1994), thus highlighting the necessity of predesigning the zonal structure (particularly the collagen organization in the superficial zone) in tissue engineered cartilage.

There are two potential areas where tissue engineered cartilage with a zonal structure mimicking the native tissue can be applied. First, tissue engineered zonal cartilage can be used as a more accurate model to study cartilage development, disease onset and progression and relative pharmacological treatment (Klein *et al.*, 2009a). It has been increasingly clear that 3D tissue culture system provides a more accurate model to study cellular interaction over the standard monolayer culture (2D) system, as the 2D system does not mimic the native environment (i.e. 3D) and may produce misleading results (Lee *et al.*, 2008). Therefore based on the similar rationale, engineered cartilage with a zonal structure mimicking the native tissue may

represent a better model to study chondrocytes interactions and their response to external environmental cues, thus providing a key insight into cartilage development (e.g. what leads to the development of the zonal structure). For example, one study, which attempted to engineer zonal aspects of native cartilage by regulating the mechanical and oxygen environment through the depth of the construct, has provided a key insight into how external environment may contribute to the development of zonal structure in articular cartilage (Thorpe *et al.*, 2013). Furthermore, engineered zonal cartilage may also provide a more native-like *in vitro* model to study the impact of mechanical stimuli on OA disease onset and progression and the outcome of drugs on OA treatment.

Secondly, tissue engineered zonal cartilage can also be used for clinical cartilage transplantation. Zonal cartilage transplants can offer a few benefits over homogeneous transplants in cartilage repair. First of all, it has been demonstrated using computational models that a viable superficial zone is critical to achieve long term survival in repairing articular cartilage (Owen and Wayne, 2006, Owen and Wayne, 2011). Thus zonal constructs with a predesigned superficial zone may more likely withstand the *in vivo* loading environment and lead to more stable repair than homogeneous tissues. Also once implanted into the defects, both the zonal and homogeneous constructs will have to experience an *in vivo* remodeling process to achieve a native zonal structure and integrate with the surrounding tissue. The provision of zonal properties from the beginning may allow for less remodeling *in vivo* and quicker and better integration with the surrounding native tissue by matching the zonal construct mechanical properties to the surrounding tissues to reduce strain discontinuities at the interface. This may offer a shorter rehabilitation time and thus lower cost for patients (Klein *et al.*, 2009a).

2.3. Classical zonal cartilage tissue engineering strategies

Despite the great promises and advantages that a zonal cartilage construct can offer over a homogeneous construct, to date the field has predominately focused on engineering a homogeneous tissue with bulk biochemical and mechanical properties approaching those of the native cartilage. Few studies have explored the possibility of engineering a heterogeneous graft with a zonal structure mimicking the native tissue. Classic zonal cartilage tissue engineering strategies can be separated into three categories: 1) utilizing zonal chondrocytes (Kim et al., 2003, Klein et al., 2003, Sharma et al., 2007); 2) varying biomaterial properties (Ng *et al.*, 2005, Ng *et al.*, 2006, Woodfield *et al.*, 2005, Nguyen *et al.*, 2011a, Nguyen *et al.*, 2011b); and 3) a combination of both (Ng *et al.*, 2009).

2.3.1. Utilizing zonal chondrocytes

The biological rationale behind this approach is based on the differences in biosynthetic activity of chondrocytes isolated from different zones of articular cartilage (Kim et al., 2003, Klein et al., 2003, Sharma et al., 2007, Hwang et al., 2007). Both Kim *et al.* and Klein *et al.*, who isolated zonal chondrocytes and used them separately to engineer cartilage, have showed cells isolated from the deep or middle zone can produce constructs with significantly more GAG and collagen compared to those isolated from the superficial zone (Kim et al., 2003, Klein et al., 2003). Both of them demonstrated that it is possible to manipulate and encapsulate zonal chondrocytes into a multi-layered construct. Therefore the strategy for zonal cartilage tissue engineering using this approach is to embed these zonal chondrocytes in specific regions of the constructs with a native-like order, hoping these cells would maintain their phenotypic differences and produce a zonal specific ECM in appropriate regions of the engineered tissue. However in these two studies, the spatial matrix composition within the engineered tissue was not examined. Thus

it is not clear if the zonal composition was obtained in such constructs. Similarly, Sharma *et al.*, who embedded zonal chondrocytes (superficial and deep zone) into a bi-layered construct, have showed a significant higher proliferation and biosynthesis activity in deep zone cells compared to the superficial cells (Sharma *et al.*, 2007). Although increased GAG accumulation with depth through the tissue was observed in the bi-layered constructs, the collagen content was also significant higher in the bottom layer of tissues. Furthermore, the mechanical properties of the engineered constructs were significant lower than those of the native tissue.

Although this approach emphasizes and utilizes the significant differences in the biosynthesis of zonal chondrocytes, it should be also noted that researchers have demonstrated that cells expanded over several passages did not retain these differences (Hayes *et al.*, 2007). The potential limitations in this approach are that the isolated zonal chondrocytes are limited in number and that it is difficult to distinguish and isolate zonal chondrocytes in damaged and diseased human cartilage where the zonal differences are less distinct (Thorpe *et al.*, 2013).

2.3.2. Varying biomaterial properties

Another approach to engineer zonal cartilage is to vary the biomaterial properties such as stiffness (Ng *et al.*, 2005, Ng *et al.*, 2006) or composition (Nguyen *et al.*, 2011a, Nguyen *et al.*, 2011b) in different layers of the constructs and hope this difference in local environment would guide a single population of cells to differentiate in a zonal manner. Ng *et al.* has demonstrated that it is possible to manipulate and vary the stiffness through the depth of the construct by combining layers of 2% (at top) and 3% (at bottom) agarose, thus leading to zonal difference in the initial mechanical properties of the constructs (Ng *et al.*, 2005). Although this mechanical zonal difference was maintained at the end of culture, zonal differences in ECM composition was not examined in the study. Furthermore, results showed

that the chondrocytes matrix establishment in such bi-layered construct and the subsequent mechanical properties of the tissue was inferior to that of the uniform 2% agarose. Also, it should be noted that the biomaterial type has a great impact on the outcome of this strategy. For example, in previous studies that reported using increased hydrogel stiffness upon the depth of the construct to engineer zonal cartilage, different results were observed when different hydrogels were used, with a zonal-like GAG gradient achieved in study using polyethylene glycol (PEG) gels but not alginate gels (Klein *et al.*, 2009b).

Researches have also demonstrated that unique biomaterial compositions can direct BM-MSCs into specific chondrocytic phenotypes corresponding to the various zones of articular cartilage (Nguyen *et al.*, 2011a). Thus it is possible to engineer zonal cartilage by varying the biomaterial compositions within the construct. Nguyen *et al.* showed a three-layer PEG-based hydrogel, seeded with a single population of BM-MSCs and with chondroitin sulfate (CS) and matrix metalloproteinase-sensitive peptides (MMP-pep) incorporated into the top layer, CS incorporated into the middle layer and hyaluronic acid incorporated in the bottom layer, can create a construct with spatially-varying mechanical and biochemical properties similar to the native cartilage (Nguyen *et al.*, 2011b). In such a construct, a native-like collagen type II and GAG gradient was observed, however the fine zonal structure such as the collagen network organization has yet to be achieved. Also the key superficial zone functional protein PRG4 was not assessed in this study. Since MMP-a family of proteins which can degrade various types of ECM proteins including proteoglycan and collagen (Eisen *et al.*, 1968) was incorporated in the superficial layers, it is less likely to expect its expression in the superficial lay of such constructs.

Lastly, the potential limitation associated with the strategy of varying biomaterial properties is the development of a distinct boundary between gel layers, with potential poor integration and mechanical discontinuity at the interface of layers.

2.3.3. Combined approach

Researches have also used combined approaches such as varying both the cell source and biomaterial properties in the construct to engineer zonal cartilage. Using a hydrogel system, Ng *et al.* seeded zonal chondrocytes into a bi-layered hydrogel with initially prescribed depth-varying mechanical properties (3% agarose atop 2% agarose) to mimic the depth-depended cellular and compressive mechanical inhomogeneity of the native cartilage (Ng *et al.*, 2009). Although increased GAG and compressive mechanical properties was observed upon the depth of the tissue, the collagen gradient in the engineered tissue was non-zonal like.

2.4. Recent advance in zonal cartilage tissue engineering

The emergence of new technologies in biomedical engineering, such as bioprinting, electrospinning, and bioreactors, may bring advance in engineering zonal cartilage.

2.4.1. Bioprinting

The recent advance in additive manufacturing (AM) technology opens a new field for tissue engineering-bioprinting. This technique could be helpful in designing and engineering tissues with complex structures such as cartilage. It can bring unique advantages in engineering zonal cartilage especially through the combined approach, i.e. bioprinting of different cell populations (e.g. zonal chondrocyte subpopulations) suspended in biomaterials with different properties into a continuous construct (Mironov *et al.*, 2006, Klein *et al.*, 2009a, Klein *et al.*, 2009b) (Figure 2.2).

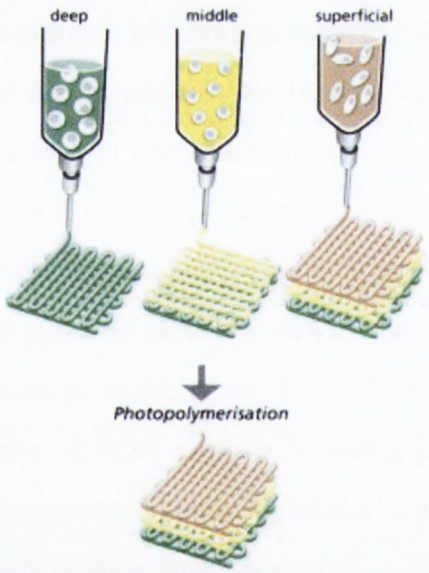

Figure 2.2. Concept for bioprinting zonal cartilage constructs where chondrocytes subpopulations from the deep, middle and superficial zones are suspended in different biomaterials and printed using rapid-prototyping technologies in defined geometries. Adapted from (Klein et al., 2009b).

With AM technology, bioprinting of 3D cell laden hydrogel with highly reproducible architecture, compositional and mechanical variation can be achieved, offering a fine control over pore size, geometry, and orientation as well as porosity and interconnectivity (Woodfield *et al.*, 2004). The ability to predesign the porosity and interconnectivity of the cell laden constructs can be beneficial toward nutrient transport and cell waste remove (Malda *et al.*, 2004b).

This technique also enables printing cell laden hydrogel at a desired orientation (Fedorovich *et al.*, 2012). If nozzle size could be small enough to produce a drop of suspension containing one single cell, then this technique could be of particular use to print the superficial zone of articular cartilage. However, this is yet to be achieved, as to the best of my knowledge current researches have only tested large strand size (Klein *et al.*, 2009a, Fedorovich *et al.*, 2012) (~300 μm). In this case, even the strand fiber can be printed with specific orientation and layers of strand fiber with different orientation can be printed and incorporated into a continuous scaffold, however, given the strand size is so large, cells inside the strand can be still randomly oriented.

2.4.2. Electrospinning

Unlike AM, electrospinning can produce scaffold fibers with a size at a nanometer scale (Klein *et al.*, 2009a). It has been shown that such nanofiber scaffolds more closely mimic the native ECM environment, where collagen fibers are also at a nanometer scale and can provide a 3D environment for cell attachment, thus promoting more robust chondrogenesis than the large fiber scaffolds (Li *et al.*, 2006).

Furthermore, this technique can be used to produce scaffolds with tunable fiber size, spacing and orientation (Mauck *et al.*, 2009). This can be very useful to fabricate scaffolds with aligned fiber orientation mimicking the superficial zone of articular cartilage. For example, McCullen *et al.* have used electrospinning to fabricate a

continuous scaffold that mimicked the structural organization of the collagen fibrillar network within cartilage (McCullen *et al.*, 2012). A three-layered-scaffold with parallel fiber orientation in the superficial layer and increasing fiber size from the superficial layer (1 μm) to the deep layer (5 μm) was created. Interestingly, chondrocytes assumed an aligned morphology and deposited collagen type II with an orientation similar to the fiber orientation in the aligned (superficial) layer of this scaffold. However, little matrix production was found in the middle layer, suggesting pool cell migration from the superficial layer. This could possibly be due to the small pore size in the aligned superficial layer, which is a common limitation in producing scaffolds with aligned fibers using this technique (Baker *et al.*, 2008).

2.4.3. Bioreactors

An alternative approach to engineer zonal cartilage is to attempt to recapitulate aspects of the tissue microenvironments which may be responsible for the formation of the zonal structure in articular cartilage during tissue development and maturation (Thorpe *et al.*, 2013). *In vivo* mechanical stimulus is one of these key microenvironments. Thus bioreactors which provide mechanical stimuli such as compression, tension and shear stress can be of particular use in zonal cartilage tissue engineering. For example, a hip simulator based bioreactor which can apply shear stress and dynamic compression has been shown to enhance the PRG-4 production in chondrocyte seeded scaffold (Grad *et al.*, 2005). Also it has been demonstrated that intermittent cyclic tensile strain can lead to an increase in collagen accumulation in MSC seeded constructs (Connelly *et al.*, 2010, Baker *et al.*, 2011).

A recent study from our lab has used confinement (modulating nutrient and oxygen transport) combined with dynamic compression to further mimic the oxygen tension (low at bottom) and mechanical environment (high strain at the surface) within

articular cartilage (see Fig. 2.3) (Thorpe et al., 2013). Results showed that a construct, with increased GAG but deceased collagen content through the depth of the tissue and with deposition of PRG4 on the tissue surface, can be engineered using BM-MSCs. While certain aspects of articular cartilage was obtained in the engineered tissue, the overall biochemical and mechanical properties of the constructs were still significantly lower than those of the native tissue. Furthermore, calcification and expression of type X collagen was also found in the constructs, indicating hypertrophy of the engineered tissue.

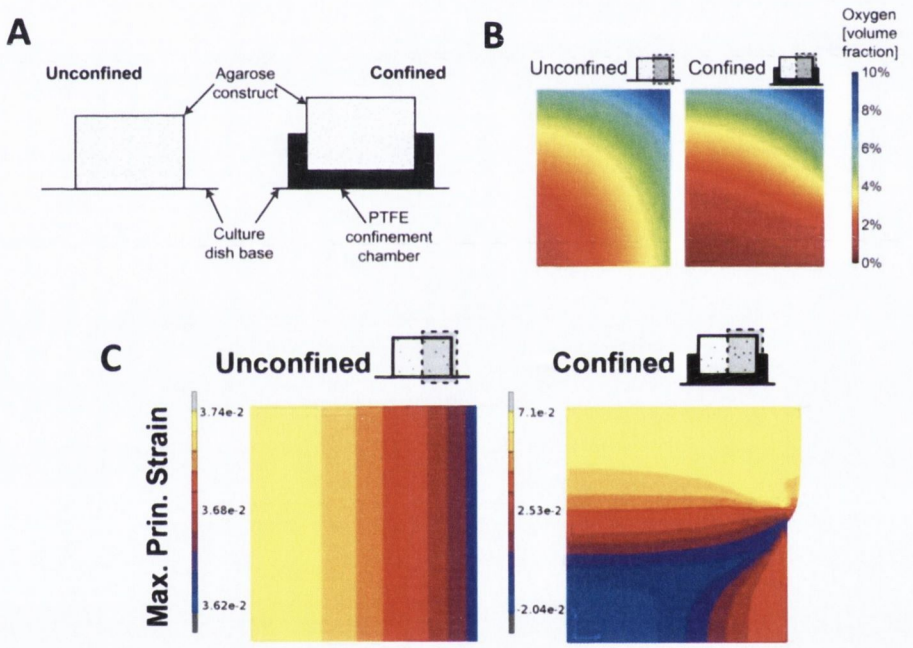

Figure 2.3. (A) Schematic diagram of confinement, in which constructs were press-fitted into custom made PTFE wells such that the bottom half of the construct were confined. (B) An axisymmetric computational model predicting the oxygen tension within the unconfined and confined constructs. Results showed reduced oxygen tension in the bottom half of the confined constructs compared to the unconfined controls. (C) An axisymmetric computational model predicting the maximum principle strain of the unconfined and confined constructs subjected to dynamic compression. Results showed increased maximum principle strain across the top of the confined constructs compared to the unconfined controls. Adapted from (Thorpe et al., 2013).

2.5. Potential application of decellularized cartilage scaffolds in zonal cartilage tissue engineering

Another approach to engineering zonal cartilage grafts using a 'bottom-up' tissue engineering strategy would be to repopulate a decellularized cartilage ECM-derived scaffold, which retains the structure of the tissue, with stem cells.

2.5.1. Decellularized tissue ECM derived scaffolds for tissue engineering applications

Tissue decellularization and regeneration of biological acellular scaffolds have been achieved for various tissue types such as dermis, urinary bladder, heart valves, liver, lung and kidney (see Fig 2.4) (Crapo et al., 2011, Arenas-Herrera et al., 2013). These decellularized tissue ECM derived scaffolds offer great promise for tissue engineering. Firstly, they are rich in natural ECM components such as collagen and GAG, offering many advantages over synthetic materials. Also it has been shown that decellularized tissue ECM contains various growth factors such as fibroblast growth factor-2 (FGF-2), vascular endothelial growth factor (VEGF), transforming growth factor-β (TGF-β) and platelet-derived growth factor (PDGF) (Benders et al., 2013, Arenas-Herrera et al., 2013). Furthermore decellularized tissue ECM has been demonstrated to support cell attachment and differentiation (Kang et al., 2012, Cheng et al., 2013, Gong et al., 2011) and induce a constructive host tissue remodeling response (Xu et al., 2010, Parekh et al., 2009, Valentin et al., 2010).

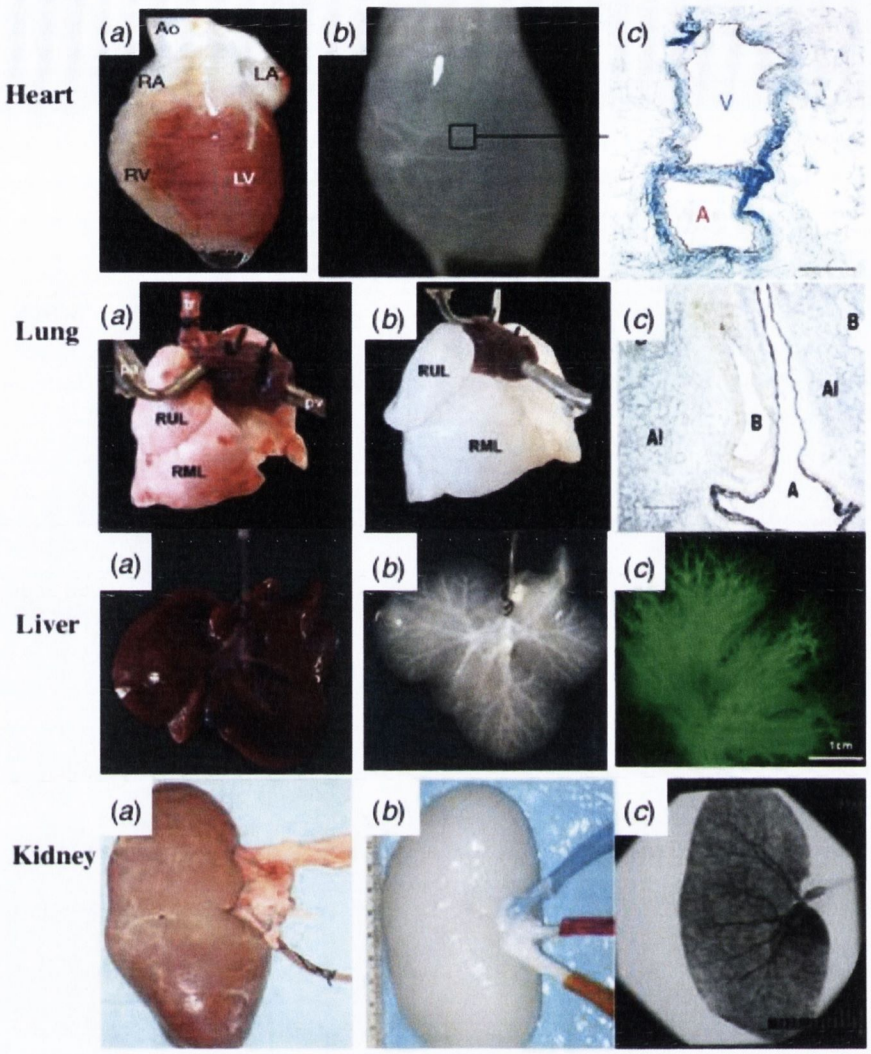

Figure 2.4. Decellularization of whole organs and characterization of intact vascular structures in the decellularized organ scaffolds. Original solid organs (a) can be decellularized using different decellularization methods to prepare acellular organ scaffolds (b). Various characterization methods for demonstrating intact vascular structures in each of decellularized organ matrices (c).

In the field of cartilage repair and tissue regeneration, decellularized cartilage ECM derived scaffolds may offer additional benefits. Due to the avascular nature of articular cartilage, it is believed that this tissue is immune-privileged to a large extent. This opens up many options in choosing the ECM source, including allergenic and xenogeneic sources, with a low risk of immune rejection (Benders et al., 2013). Furthermore, if the depth-dependent collagen architecture of articular cartilage can

be retained after decellularization, the resulting scaffold may then offer a 'golden' template to engineer zonal cartilage tissues, since to date no synthetic scaffolds can recapitulate this complex and highly organized structure.

2.5.2. Decellularized cartilage ECM for cartilage tissue engineering

Over the past decade, researchers have started to explore the potential of decellularized cartilage ECM as a scaffold for cartilage regeneration. Many studies have shown that decellularized cartilage ECM may support cellular attachment and chondrogenic differentiation of stem cells and chondrocytes (Kang et al., 2012, Yang et al., 2011, Gong et al., 2011), as well as promoting good quality repair in cartilage defects *in vivo* (Kang et al., 2012, Yang et al., 2011). Most of these studies used mincing or cyro-milling to particulate cartilage ECM prior to the fabrication of the scaffold, which aims to increase the porosity of the produced scaffolds. However such processes destroy the macroscopic structure of articular cartilage and overlook the potential of retaining a native-like tissue structure in decellularized cartilage ECM scaffolds for zonal cartilage tissue engineering. Only a few studies have explored decellularization on whole cartilage tissue and the potential of using this structurally intact decellularized cartilage scaffold for cartilage tissue engineering.

Elder and colleagues studied the effect of incubation time in decellularization solutions on cell removal, ECM components and subsequent mechanical properties of articular cartilage, with an aim to produce a decellularized cartilage replacement for facet joint cartilage repair (Elder et al., 2010). The study compared 2, 4 and 8 h treatment in 2% (w/v) Sodium dodecyl sulfate (SDS). Results showed while 2 h incubation in 2% SDS maintained the GAG and collagen content and mechanical properties of the tissue, it only led to a 4% decrease in DNA content. Cell removal increased with incubation time. Treatment for 8 h resulted in complete histological

decellularization and a 40% reduction in DNA content, meanwhile maintaining collagen content and tensile properties. However, a significant reduction in GAG content and compressive properties was observed. The concentration of SDS used in this study to decellularize articular cartilage was however considerably high. Other studies have suggested that a high concentration of SDS may result disruption of the ECM structure, and the residual SDS inside the decellularized scaffolds may lead to cell toxicity or hinder further recellularization (Crapo et al., 2011).

Kheir *et al.* attempted to decellularize articular cartilage-bone constructs, with a combination of 0.1% SDS and various other decellularization reagents, for tissue engineering applications (Kheir et al., 2011). Results showed a near-complete removal of genomic DNA from the decellularized tissue, while the collagen content and structure of the tissue was not significantly affected. However, decellularization was accompanied by a significant reduction in GAG content and compressive properties of the tissue. It was found that the decellularized tissue exhibited favorable biocompatibility in both *in vitro* and *in vivo* tests. However, the chondro-inductive capacity of this decellularized scaffold was not examined.

Recently, Schwarz *et al.* have also explored the potential of decellularized cartilage matrix for nasal septum cartilage reconstruction (Schwarz et al., 2012b). The study used a combination of various chemical decellularization reagents, including NaOH, GndHCl and H_2O_2, to decellularize porcine nasal septum cartilage. Decellularization was found to lead to complete removal of cells and α-gal epitope, significant reduction in GAG and mechanical properties of the tissue, while retaining collagen structure as well as increasing tissue porosity. *In vitro* cytotoxicity tests showed no growth inhibition or cytotoxic effects on the seeded fibroblasts. In a following up study, these decellularized scaffolds were seeded with human nasal septum chondrocytes and were cultured *in vitro* for 6 weeks (Schwarz et al., 2012a). Results demonstrated that decellularized cartilage scaffolds supported cell adhesion and migration, as well as chondrogenic differentiation, with the expression of type II

collagen and aggrecan. Furthermore, the engineered constructs exhibited near native levels of mechanical properties, with no significant difference found between constructs and native tissues. However, limited cell infiltration into the body of scaffolds (up to 200 μm after 6 weeks culture) was also reported.

In conclusion, these studies have demonstrated the capacity of decellularize whole cartilage scaffolds for cartilage regeneration. However, they all reported significant GAG loss during decellularization procedure, which subsequently compromised the mechanical properties of the decellularized scaffolds. Further improvement may be required in the decellularization procedure to retain some level of GAG in the decellularized tissue. Moreover, additional efforts need to be made in improving the recellularization in these scaffolds, since the dense nature of the tissue ECM may create a barrier for cell migration into the scaffolds.

2.6. Summary

Given the importance of the depth-dependent structure and composition of articular cartilage on the mechanical function of the tissue, this thesis aims to engineer a cartilage graft that mimics key aspects of the depth-dependent properties of articular cartilage. The bioreactor study proposed by Thorpe and colleagues (section 2.4) highlights the potential of spatially regulating oxygen and mechanical environment in stem cell laden hydrogels for zonal cartilage tissue engineering. The limitation associated with previous studies, such as hypertrophy and the low mechanical properties of the engineered constructs, motivated us towards the use of IFP-MSCs for zonal cartilage tissue engineering in this thesis. However, to engineer zonal grafts using IFP-MSCs will first require a proper understanding of how such cells will respond to the application of joint associated mechanical stimuli such as dynamic compression. This thesis will therefore try to address the following research questions in chapter 3, 4 and 5 respectively:

- What is the effect of dynamic compression on chondrogenesis of BM-MSCs and IFP-MSCs?
- Can cartilage constructs with a zonal composition mimicking that of the native tissue be engineered using IFP-MSCs by spatially regulating oxygen and mechanical environment within the developing constructs?
- Is it possible to engineer zonal cartilage tissues using decellularized whole cartilage ECM-derived scaffolds seeded with IFP-MSCs?

Chapter III

Effects of dynamic compression on chondrogenesis of bone marrow and infrapatellar fat pad derived mesenchymal stem cells

3.1. Introduction

Mesenchymal stem cells (MSCs) are a population of multipotent cells which are capable of differentiating along a number of mesenchymal lineages (Caplan, 1991, Pittenger et al., 1999). Due to their ability to rapidly self-renew and undergo chondrogenesis, MSCs represent a promising cell source for cartilage tissue engineering applications. They have been identified in various tissues, such as bone marrow (BM) (Pittenger et al., 1999, Johnstone et al., 1998, Yoo et al., 1998), infrapatellar fat pad (IFP) (Dragoo et al., 2003, Wickham et al., 2003, English et al., 2007) and synovium (Pei et al., 2008, Pei et al., 2009, Vinardell et al., 2012b), among which BM-MSCs are the most extensively studied cell type. Various studies have demonstrated successful chondrogenic induction of BM-MSCs in a number of different biomaterials, including naturally derived materials (e.g., alginate, agarose) (Li et al., 2009, Thorpe et al., 2010) and synthetic materials (e.g., polyglycolic acid (PGA) and polycaprolactone (PCL)) (Kafienah et al., 2007, Wise et al., 2009). In spite of their tremendous promise, there are a number of potential limitations associated with BM-MSCs based tissue engineering strategies for articular cartilage repair. Firstly, it has been demonstrated that cartilage engineered using BM-MSCs has inferior biochemical and biomechanical properties to that engineered using chondrocytes (Erickson et al., 2009, Mauck et al., 2006). Furthermore, studies have also shown cartilage tissues engineered using BM-MSCs have the potential to undergo hypertrophy and endochondral ossification (Kafienah et al., 2007, Pelttari et al., 2006). This has motivated the use of alternative stem cell sources for cartilage tissue engineering. Compared to BM-MSCs, MSCs isolated from the IFP of the knee are arguably easier to isolate, with lower degree of invasiveness and minimal patient morbidity (Dragoo et al., 2003). Successful chondrogenesis of IFP-MSCs has been reported by a number of studies (Buckley and Kelly, 2012, Buckley et al., 2010a, Buckley et al., 2010b, Liu et al., 2013, Liu et al., 2012), with tissues engineered using

IFP-MSCs demonstrating at least comparable functionality to those generated using BM-MSCs (Vinardell et al., 2011).

Physiologically articular cartilage exists in a complex biomechanical environment, experiencing a number of different types of mechanical stimuli such as compression and hydrostatic pressure during joint movement (Mow and Wang, 1999). It has been demonstrated mechanical loading plays an important role in the development (Mikic et al., 2000, Mikic et al., 2004), remodelling (Williamson et al., 2001) and repair of this tissue (Wakitani et al., 1994). For example, the mechanical properties of repair tissue formed following implantation of MSCs seeded hydrogels into cartilage defects has been shown to vary depending on the location of the defect site on the joint surface, which may be due to the different degrees of loading experienced at these different sites (Wakitani et al., 1994). More recently, dynamic compression has been explored as a potential stimulus to enhance chondrogenesis for cartilage tissue engineering. Numerous studies have demonstrated dynamic compression can increase cartilage-specific matrix synthesis in chondrocytes (Demarteau et al., 2003, Mauck et al., 2000, Buschmann et al., 1995). Moreover, dynamic compression has also been shown to regulate chondrogenesis of BM-MSCs at both gene and protein level (Huang et al., 2005, Haugh et al., 2011, Kelly and Jacobs, 2010, Thorpe et al., 2008, Thorpe et al., 2010), with increased glycosaminoglycan (GAG) accumulation observed in BM-MSCs seeded hydrogels following the application of loading (Mauck et al., 2007, Kisiday et al., 2009, Thorpe et al., 2013). Such mechanical stimulation protocols have also been shown to improve the mechanical properties of MSCs seeded constructs (Huang et al., 2010, Thorpe et al., 2013, Bian et al., 2012).

Understanding how cartilaginous tissues engineered using MSCs will respond to their local mechanical environment will be critical to successful clinical cartilage repair. While a number of studies have shown that dynamic compression can promote chondrogenesis of BM-MSCs, to the best of our knowledge no study to date has compared the response of MSCs isolated from different tissue sources to this

biophysical stimulus. Therefore, the objective of this study was to compare the effects of dynamic compression on chondrogenesis of BM-MSCs and IFP-MSCs that were embedded into agarose hydrogels. We hypothesized dynamic compression would enhance the chondrogenic potential of both BM-MSCs and IFP-MSCs. Specifically in this study, porcine BM-MSCs and IFP-MSCs were encapsulated into agarose hydrogels and cultured in the presence of TGF-β3 for 3 weeks before being subjected to dynamic compression of 10% strain (1Hz, 1 hour/day) for a further 3 weeks. We investigated the influence of dynamic compression on: 1) cartilage specific matrix accumulation (GAG and collagen) and the subsequent mechanical properties of the engineered cartilage; 2) the spatial distribution of matrix within the engineered tissue; and 3) the tendency of MSCs seeded cartilage constructs to undergo hypertrophy and mineralization.

3.2. Materials and Methods

3.2.1. Cell Isolation and Expansion

Porcine BM-MSCs and IFP-MSCs were isolated from the bone marrow of the femur and from the whole IFP of the animal respectively (n=2, 3-4 months old, ~50kg). BM-MSCs were isolated using an adapted protocol used for human BM-MSCs isolation (Lennon and Caplan, 2006); IFP-MSCs were isolated using a previously described protocol from our lab (Buckley and Kelly, 2012) after 4 hours digestion with collagenase type II (750 U/ml, 4 ml of collagenase containing medium was used for per gram of IFP tissue, Worthington Biochemical, LanganBach Services, Ireland) under constant rotation at 37 °C. After isolation, BM-MSCs and IFP-MSCs were seeded at a density of $5x10^3$ cell/cm^2 in high-glucose Dulbecco's modified Eagle's medium (hgDMEM) GlutaMAX™ supplemented with 10% fetal bovine serum and 1% penicillin (100 U/mL)-streptomycin (100 µg/mL) (all GIBCO, Biosciences, Dublin, Ireland) and expanded to passage two (P2) in a humidified atmosphere of 5% CO_2 @37 °C. For both BM-MSCs and IFP-MSCs, 5 ng/ml fibroblast-growth factor-2 (ProSpec-Tany TechnoGene Ltd, Israel) were added into the medium (from the beginning of P0 for IFP-MSCs; from the beginning of P1 for BM-MSCs) to promote the growth and chondrogenic potential of the MSCs (Buckley and Kelly, 2012).

3.2.2. Hydrogel construct fabrication and culturing

BM-MSCs and IFP-MSCs (both P2) were encapsulated respectively in agarose (Type VII) as previously described (Thorpe et al., 2010) to obtain a final gel concentration of 2% and a cell density of 30 x 10^6 cells/ml. The agarose-gel suspension was then casted into a stainless steel mold from which cylindrical constructs (Ø6 mm × 4 mm thickness) were removed using a biopsy punch. Constructs were then maintained

separately in 6-well-plates in 9 ml chondrogenic medium (per construct) consisting of hgDMEM GlutaMAX™ supplemented with penicillin (100 U/ml)-streptomycin (100 µg/ml), 100 µg/ml sodium pyruvate, 40 µg/ml L-proline, 4.7 µg/mL linoleic acid, 50 µg/ml L-ascorbic acid-2-phosphate, 1.5 mg/ml bovine serum albumin, 1 × insulin–transferrin–selenium, 100 nM dexamethasone (all from Sigma-Aldrich, Dublin, Ireland) and 10 ng/ml recombinant human transforming growth factor β3 (TGF-β3; ProSpec-Tany TechnoGene Ltd). The medium was changed twice every week with the old medium kept and frozen @-85°C for biochemical analysis.

3.2.3. Experimental design

Cell seeded hydrogels (generated using both BM-MSCs and IFP-MSCs) were first maintained in free swelling (FS) conditions in a chondrogenic medium for 21 days to allow chondrogenic phenotype and matrix establishment (Haugh et al., 2011). After that half of the samples were subjected to dynamic compression (DC) of 10% strain (1Hz, 1 hour/day, 5 days/week) for a further 21 days as previously described (Thorpe et al., 2010), while rest samples were still maintained in FS conditions as a control. Constructs (n=6 per group) were assessed at day 0, 21 and 42.

3.2.4. Assessment of mechanical properties

Construct mechanical properties were tested (n=4 per group) using a standard materials testing machine with a 5N load cell (Zwick Roell Z005, Herefordshire, UK) as previously described (Buckley et al., 2009). Briefly, constructs were immersed in phosphate buffered saline (PBS) bath (room temperature) and placed between two impermeable platens. A preload of 0.01 N was used to ensure direct contact between construct surface and platen surface. An unconfined stress-relaxation test was then performed, which consisted of a ramp compression up to 10% stain of the sample

thickness followed by a hold period of 30 minutes until equilibrium of the sample was reached. The equilibrium Young's modulus of the sample was calculated from the equilibrium force. A dynamic test consisting of cyclic strain amplitude of 1% at 1 Hz for 10 cycles was then performed directly after the equilibrium test to determine the dynamic modulus.

3.2.5. Quantitative biochemical analysis

Construct analysis

After mechanical testing constructs were maintained in PBS for 30 mins to allow them to recover to their initial thickness, after which constructs (n=3/4 per group) were transversely sliced into two halves for determination of the spatial distribution of matrix within the engineered tissue. The top and bottom halves of the samples were weighed (wet) and stored separately at -85 °C for later analysis. Samples were then digested with 125 μg/ml papain in 0.1 M sodium acetate, 5 mM L-cysteine HCl, 0.05 M EDTA, pH 6.0 (all Sigma-Aldrich) under constant rotation at 60 °C for 18 hours. The DNA content of the samples was measured using the Hoechst bisBenzimide H 33258 dye assay with calf thymus DNA as a standard as previously described (Kim et al., 1988). GAG content was quantified using the dimethylmethylene blue dye-binding assay (Blyscan, Biocolor Ltd., Northern Ireland), with a chondroitin sulfate standard. Collagen content was determined through measurement of the hydroxyproline content (Kafienah and Sims, 2004) and calculated using a hydroxyproline-to-collagen ratio of 1:7.69 (Ignat'eva et al., 2007). The level of the biochemical content (DNA, GAG, collagen) in the whole sample (before being sliced into two halves) was calculated by summing up the levels of content in the top and bottom halves. Matrix accumulation (GAG and collagen) were normalized to construct wet weight and to DNA.

Medium analysis

Samples of construct culture medium taken at each medium exchange from day 21 to day 42 were analyzed for total GAG or collagen content secreted from constructs into the medium during this period using the methods described above. Total medium volume was accounted for and data is presented as average GAG or collagen content released per construct into medium from day 21 to day 42. Medium samples from day 21 to day 42 were also analyzed for alkaline phosphatase (ALP) activity using a Sensolyte pNPP Alkaline Phosphatase assay kit (Cambridge Biosciences, UK) with a calf intestine ALP standard (Sheehy et al., 2012).

3.2.6. Histology and immunohistochemistry

Unsliced constructs (n=2 per group) were fixed with 4% paraformaldehyde (Sigma-Aldrich), wax embedded and sectioned perpendicularly to the disk surface at thickness of 5 μm. Sections were stained histologically with 1% Alcian blue 8GX in 0.1 M HCl for GAG distribution, Picrosirius red for collagen distribution and 1% Alizarin red for mineral deposition (all Sigma–Aldrich). Sections were also immunohistochemically stained for collagen type I and II using a mouse monoclonal collagen type I antibody (1:100; 1.4 mg/mL; Abcam, Cambridge, UK) and a mouse monoclonal collagen type II antibody (1:80; 1 mg/mL; Abcam) respectively as previously described (Thorpe et al., 2010). Sections of porcine cartilage and ligament were included in each batch as controls.

3.2.7. Micro-computed tomography analysis

Constructs (n=2 per group) were scanned using micro-computed tomography (μCT) in order to quantify the mineral content within the samples. Scans were performed using a Scanco Medical μCT 40 system (Scanco Medical, Bassersdorf, Switzerland) at a voltage of 70 kVp and a current of 114 μA. Data is presented as the volume of

minerals within each construct. A 3 dimensional (3D) image of the mineral deposition within the constructs was also obtained from the system.

3.2.8. Statistical analysis

Statistics were performed using MINITAB 15.1 software (Minitab Ltd., Coventry, UK). For data where two factors of comparison (day 21 vs. 42 and/or BM vs. IFP and/or top vs. bottom and/or FS vs. DC) is required, a general linear model for analysis of variance with Tukey's test for multiple comparison was used. For direct comparison between FS and DC group, a two-sample T-test was used. Significance was determined at $P<0.05$ and a trend towards significance was determined at $p<0.1$. All graphical results are presented as mean ± standard deviation.

3.3. Results

3.3.1. Temporal and spatial development of cartilage grafts engineered in free swelling culture using different sources of MSCs

We first investigated the temporal development of cartilaginous constructs engineered using both BM-MSCs and IFP-MSCs in free swelling (FS) culture. A significant increase in DNA content was observed in IFP constructs from day 21 to day 42 ($p<0.05$ for both donors), indicating cell proliferation, while the DNA content of BM constructs remained relatively constant over the 42 days of culture (Fig. 3.1A). A significant increase in GAG and collagen content from day 21 to day 42 was also seen in both BM constructs and IFP constructs from both donors ($p<0.05$; Figs. 3.1B, 3.1C). At day 42, the collagen content was significantly higher in BM constructs compared to IFP constructs ($p<0.05$ for both donors; Fig. 3.1C). GAG accumulation was observed to be donor dependent in BM constructs, ranging from ~2% (w/w) to ~4% (w/w) by day 42, whereas the GAG content in IFP constructs was relatively consistent at ~ 3% (w/w) for both donors (Fig, 3.1B).

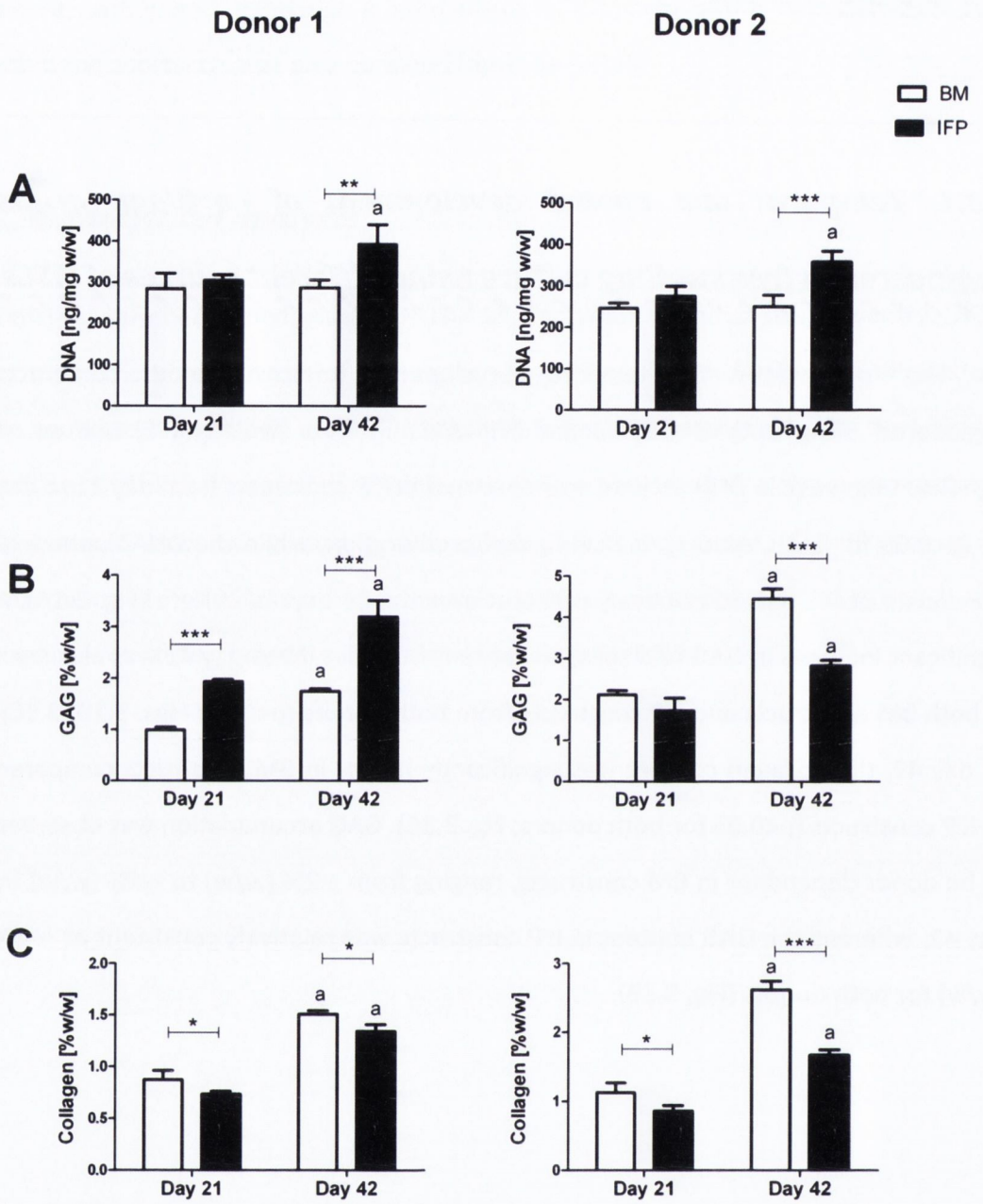

Figure 3.1. Biochemical content of FS BM and IFP constructs from donor 1 (left column) and donor 2 (right column) at day 21 and 42. (A) DNA content (ng/mg w/w); (B) GAG content (%w/w); (C) collagen content (%w/w). a: $p<0.05$ vs. same construct type at day 21; *: $p<0.05$, **: $p<0.01$; ***: $p<0.001$.

Histological staining was used to examine the spatial distribution of matrix within the FS constructs at day 42. A relatively homogeneous distribution of GAG and collagen was observed throughout the depth of BM constructs for both donors (Figs. 3.2A, 3.2B). This was further confirmed through biochemical quantification of the matrix content in the top and bottom halves of the constructs, showing similar levels of DNA, GAG and collagen content in the top and bottom of the BM constructs, although in donor 2 the top of the constructs had significantly more collagen content than the bottom ($p<0.01$; Fig. 3.3). In contrast, a more heterogeneous distribution of matrix was observed in IFP constructs (Figs. 3.2A, 3.2B). It was observed that both GAG and collagen accumulation decreased with depth through the engineered tissue (and also from periphery towards core). Biochemical data also confirmed a significantly higher level of GAG and collagen content in the top of IFP constructs from both donors compared to the bottom ($p<0.05$), although no significant difference in DNA content between top and bottom of the engineered tissue was observed (Fig. 3.3).

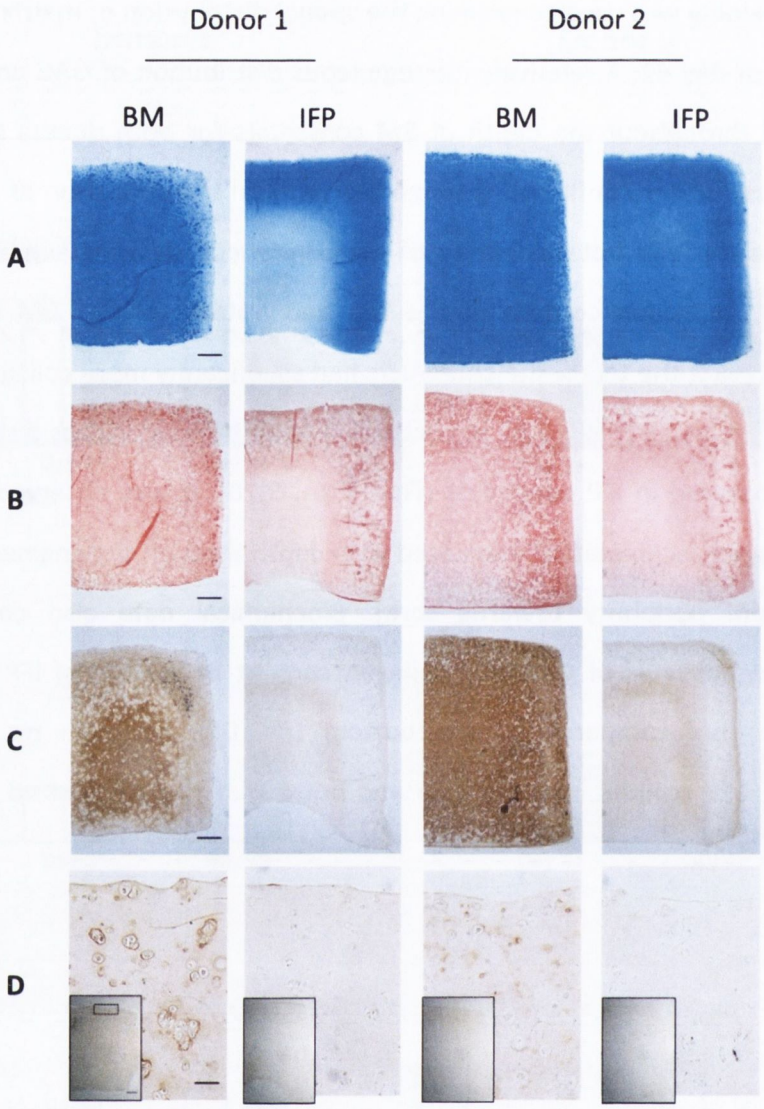

Figure 3.2. Histological and immunohistological staining of FS BM and IFP constructs from donor 1 (left) and donor 2 (right) at day 42. (A) Alcian blue staining for proteoglycan; (B) Picrosirius red staining for collagen; (C) Immunohistological staining for collagen type II; scale bar in A, B and C: 500 μm. (D) Immunohistological staining for collagen type I. Low magnification images (inserted) show staining at a bulk construct level; high magnification images show staining at the peripheral region of the samples. Box region in low magnification image indicates area from where high magnification images were taken. Scale bar in low magnification images: 500 μm; scale bar in high magnifications images: 50 μm.

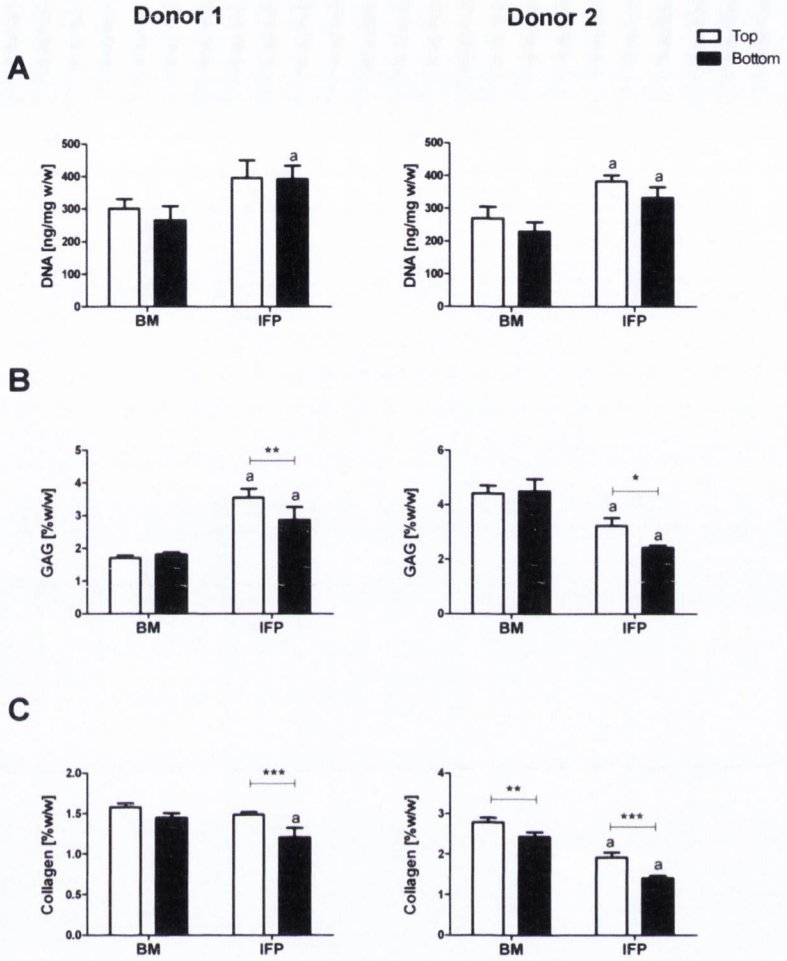

Figure 3.3. Biochemical content of the top and bottom halves of FS BM and IFP constructs from donor 1 (left column) and donor 2 (right column) at day 42. (A) DNA content (ng/mg w/w); (B) GAG content (%w/w); (C) collagen content (%w/w). a: $p<0.05$ vs. BM constructs from the same region; *: $p<0.05$, **: $p<0.01$; ***: $p<0.001$.

Immunohistochemical analysis showed a strong staining for collagen type II in BM constructs from both donors, with weaker staining found in IFP constructs (Fig. 3.2C). Positive staining for collagen type I was also observed in the peripheral region of the BM constructs from both donors (albeit less intensely than for collagen type II); while IFP constructs stained negatively for collagen type I (Fig. 3.2D).

3.3.2. The influence of dynamic compression on the functional properties of cartilage grafts engineered using different sources of MSCs

To access the effects of delayed dynamic compression (DC) on chondrogenesis of BM-MSCs and IFP-MSCs seeded constructs, samples were first cultured in a chondrogenic medium in FS conditions for 3 weeks (day 0-21) to allow matrix establishment, and were then subjected to DC for a further 3 weeks (day 21-42). DC significantly increased GAG ($p=0.023$; Fig. 3.4B) and collagen ($p=0.024$; Fig. 3.4E) content in BM constructs from donor 1. When normalized to construct wet weight, GAG content (% w/w) and collagen content (% w/w) were also significantly higher in loaded constructs ($p=0.042$ for GAG (%w/w) and $p=0.048$ for collagen (%w/w); Figs. 3.4C, 3.4F). However, when normalized to DNA content, these differences were no longer significant (Figs. 3.4A, 3.4D, 3.4G). For IFP constructs from donor 1, DC didn't significantly change any of the biochemical measurements of the engineered tissue (Figs. 3.4 H-N). At day 42, the equilibrium and dynamic modulus of FS BM constructs from donor 1 was ~70 kPa and ~700 kPa respectively (Figs. 3.5A, 3.5B); while the equilibrium and dynamic modulus of FS IFP constructs from donor 1 were notably higher at ~300 kPa and ~1400 kPa respectively (Figs. 3.5C, 3.5D). DC significantly enhanced the equilibrium and dynamic modulus of BM constructs from donor 1 ($p<0.001$) (Figs. 3.5A, 3.5B), however it had no significant effects on the mechanical properties of IFP constructs from donor 1 (Figs. 3.5C, 3.5D). DC had no significant effect on the bulk biochemical measurements or the mechanical properties of grafts engineered using either BM-MSCs or IFP-MSCs from donor 2 (Supplementary Fig. 3.1 and Figs. 3.5 E-H).

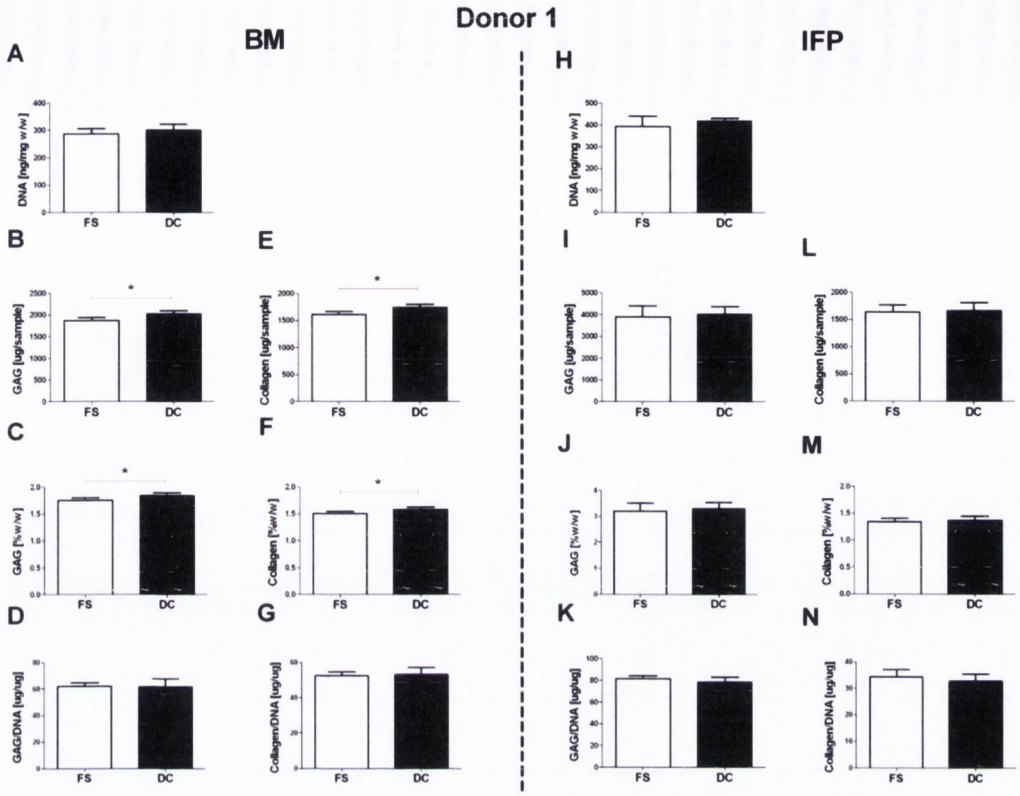

Figure 3.4. Biochemical content of FS and DC BM (left) and IFP constructs (right) from donor 1 at day 42. (A, H) DNA content (ng/mg w/w); (B, I) GAG content (μg/sample); (C, J) GAG content (% w/w); (D, K) GAG/DNA (μg/μg); (E, L) collagen content (μg/sample); (F, M) collagen content (% w/w); (G, N) collagen/DNA (μg/μg).*:$p<0.05$.

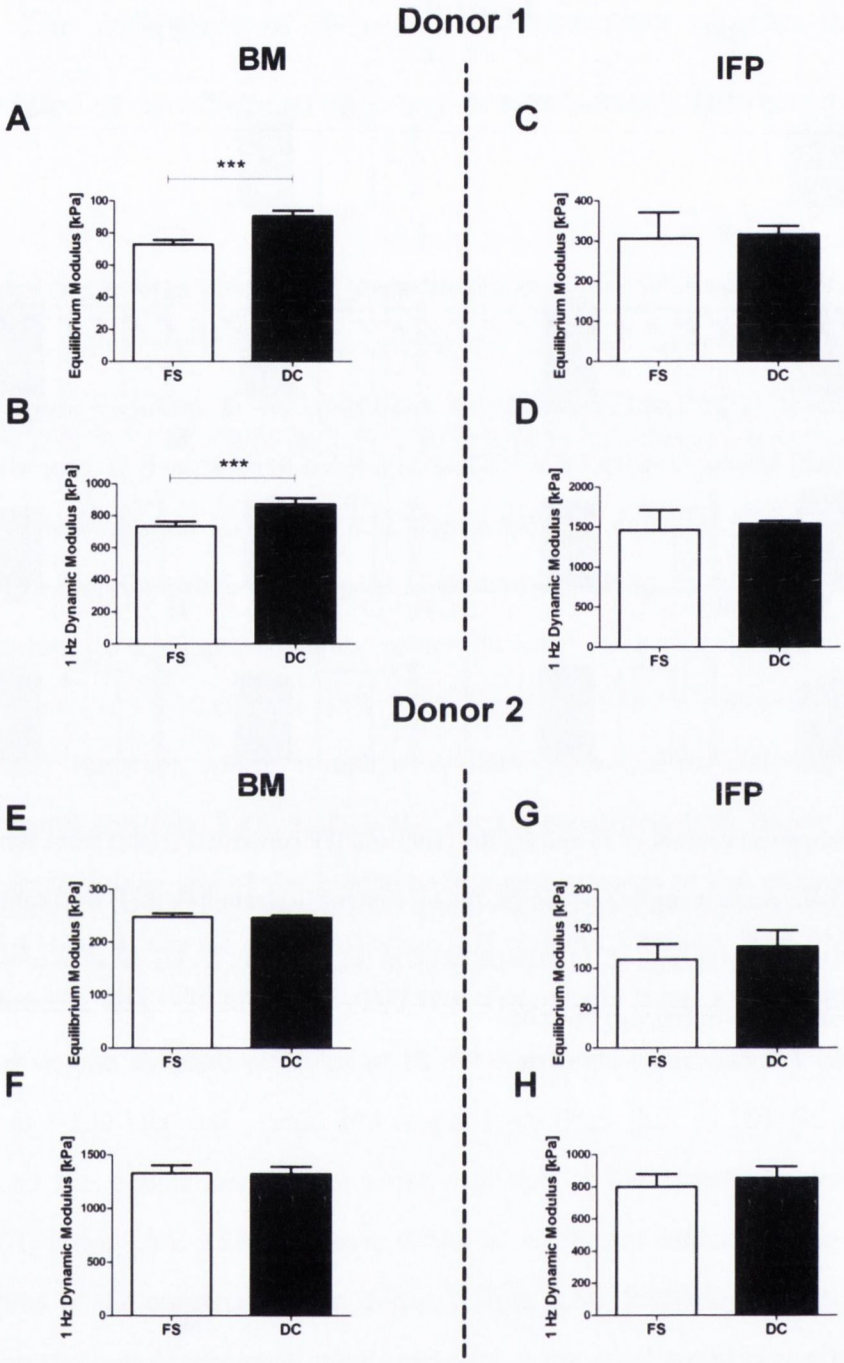

Figure 3.5. Mechanical properties of FS and DC BM (left column) and IFP constructs (right column) from donor 1 (A, B, C, D) and donor 2 (E, F, G, H) at day 42. (A, C, E, G) equilibrium modulus (kPa); (B, D, F, H) 1Hz dynamic modulus (kPa). ***: $p<0.001$.

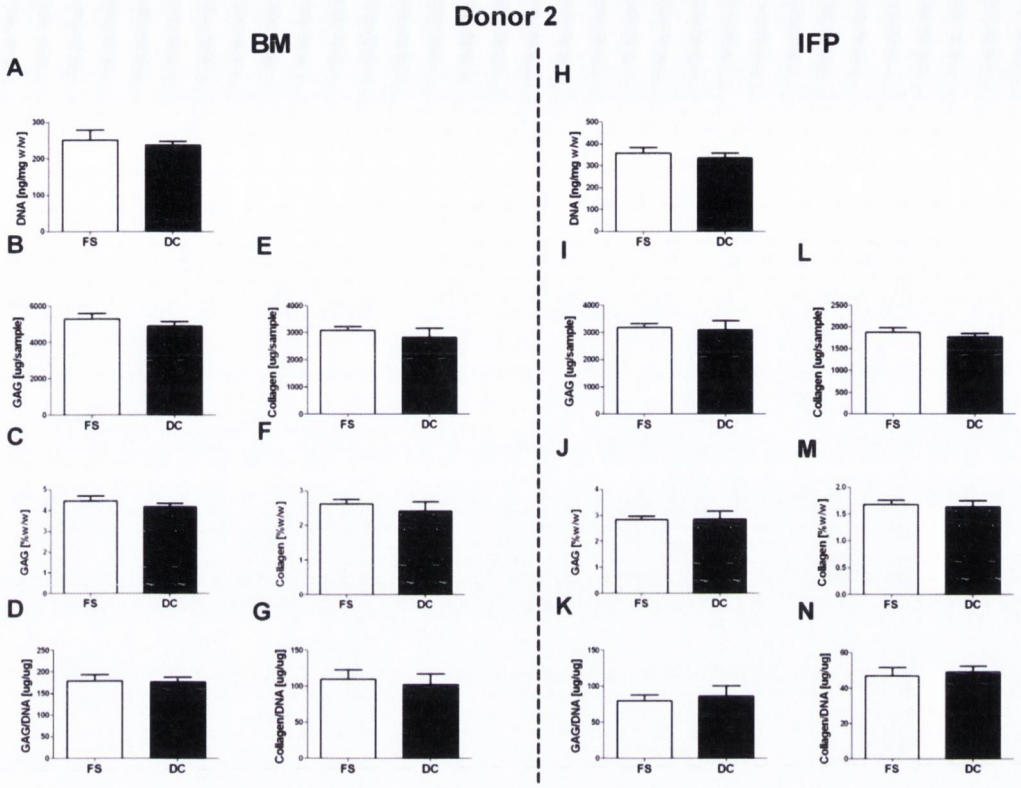

Supplementary Figure 3. 1. Biochemical content of FS and DC BM (left) and IFP constructs (right) from donor 2 at day 42. (A, H) DNA content (ng/mg w/w); (B, I) GAG content (μg/sample); (C, J) GAG content (% w/w); (D, K) GAG/DNA (μg/μg); (E, L) collagen content (μg/sample); (F, M) collagen content (% w/w); (G, N) collagen/DNA (μg/μg).

Extracellular matrix (ECM) accumulation within the hydrogels and release into medium during the loading period (day 21-42) was also assessed in order to examine the direct influence of DC on absolute levels of ECM synthesis. For donor 1, higher levels of GAG release into medium was observed in BM constructs with the application of loading, such that DC significantly enhanced total amount of GAG synthesis ($p<0.01$; Fig. 3.6A). The total amount of collagen synthesis in BM constructs from both donors was not affected by the application of DC (Figs. 3.6B, 3.6F). For IFP constructs from donor 1, no significant difference in GAG or collagen accumulation within constructs or release into the medium was observed between the FS and DC constructs (Figs. 3.6C, 3.6D). For IFP constructs from donor 2, although a significantly higher level of collagen release into medium was observed with the application of DC ($p<0.05$), there was no significant difference in total GAG or collagen synthesis from day 21 to day 42 between the FS and DC groups (Figs. 3.6G, 3.6H).

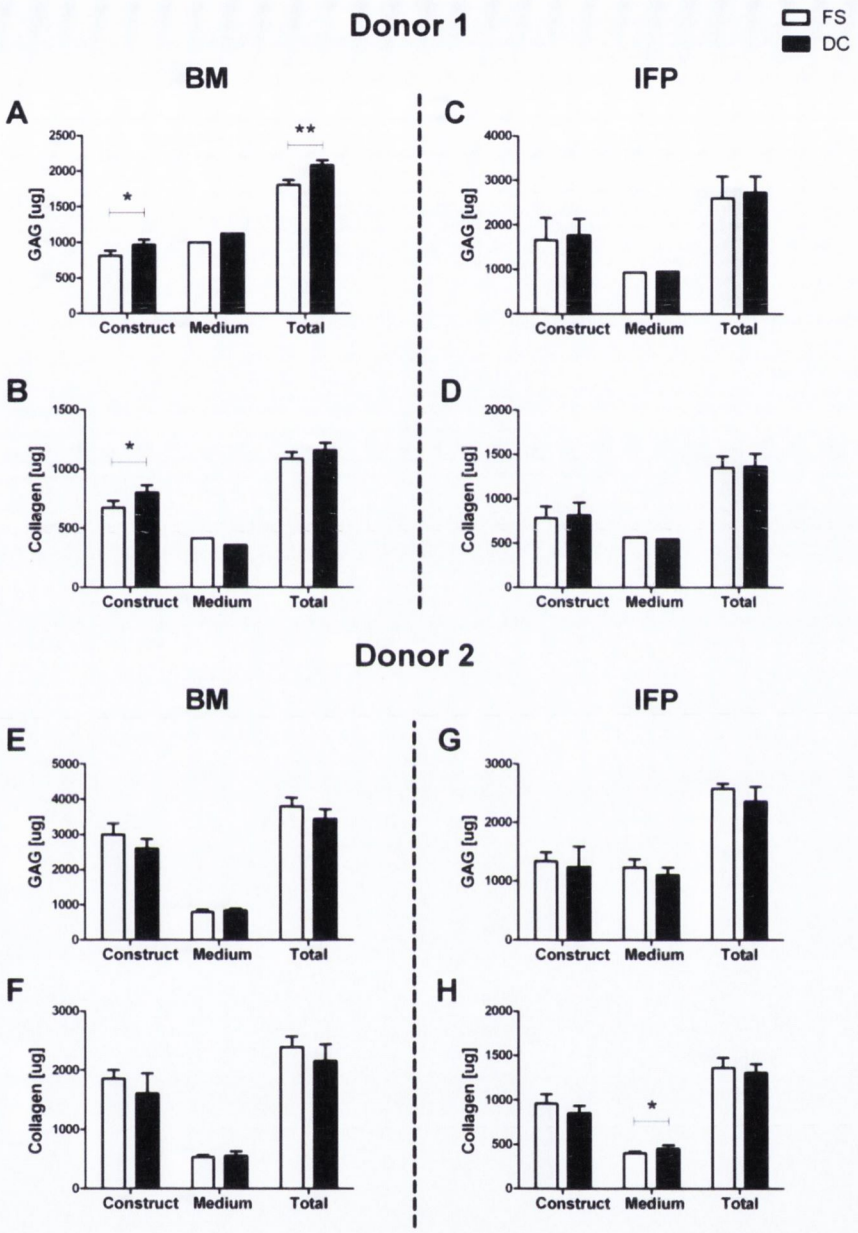

Figure 3.6. GAG and collagen content accumulated within the constructs, released into medium and the total synthesized (constructs + medium) from day 21 to day 42 in FS and DC BM (left column) and IFP constructs (right column) from donor 1 (upper) and donor 2 (lower). (A, C, E, G) GAG content (μg); (B, D, F, H) collagen content (μg). Medium samples from day 21 to day 42 were analyzed for GAG or collagen content released from the constructs (n=1 per group for donor 1, as medium from each individual construct were pooled; n=4 per group for donor 2, as medium from each individual construct were kept separate). GAG or collagen content accumulated within

constructs from day 21 to day 42 were calculated by subtracting the mean value of GAG or collagen content of day 21 samples from the value of GAG or collagen content of each individual day 42 samples (n=4 per group). Total amount of GAG or collagen synthesis from day 21 to day 42 was calculated by summing up the amount accumulated within constructs and the amount released into medium. *: $p<0.05$; **: $p<0.01$.

At the macroscopic level, there was no obvious difference in staining intensity for GAG or collagen between FS and DC samples for either BM or IFP constructs (Fig. 3.7). Similarly, DC did not appear to influence collagen type II accumulation (Fig. 3.8). Interestingly, moderate staining for collagen type I was found in the peripheral region of FS BM constructs from both donors; with less intense staining observed in constructs subjected to DC (Fig. 3.8). IFP constructs stained negatively for collagen type I regardless of the loading condition (Fig. 3.8).

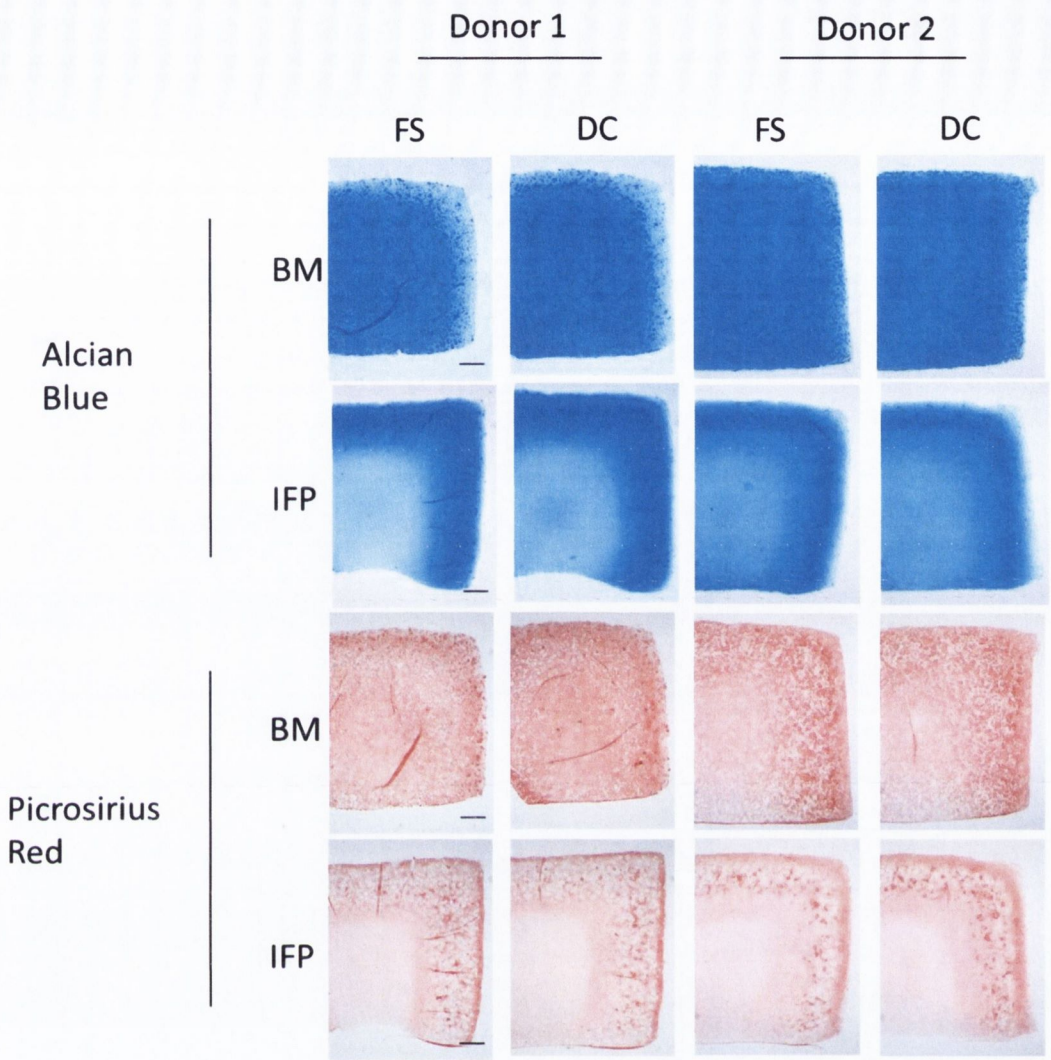

Figure 3.7. Histological staining of FS and DC BM and IFP constructs from donor 1 (left) and donor 2 (right) at day 42. Upper two rows: Alcian blue staining for proteoglycan; lower two rows: Picrosirius red for collagen. Scale bar: 500 μm.

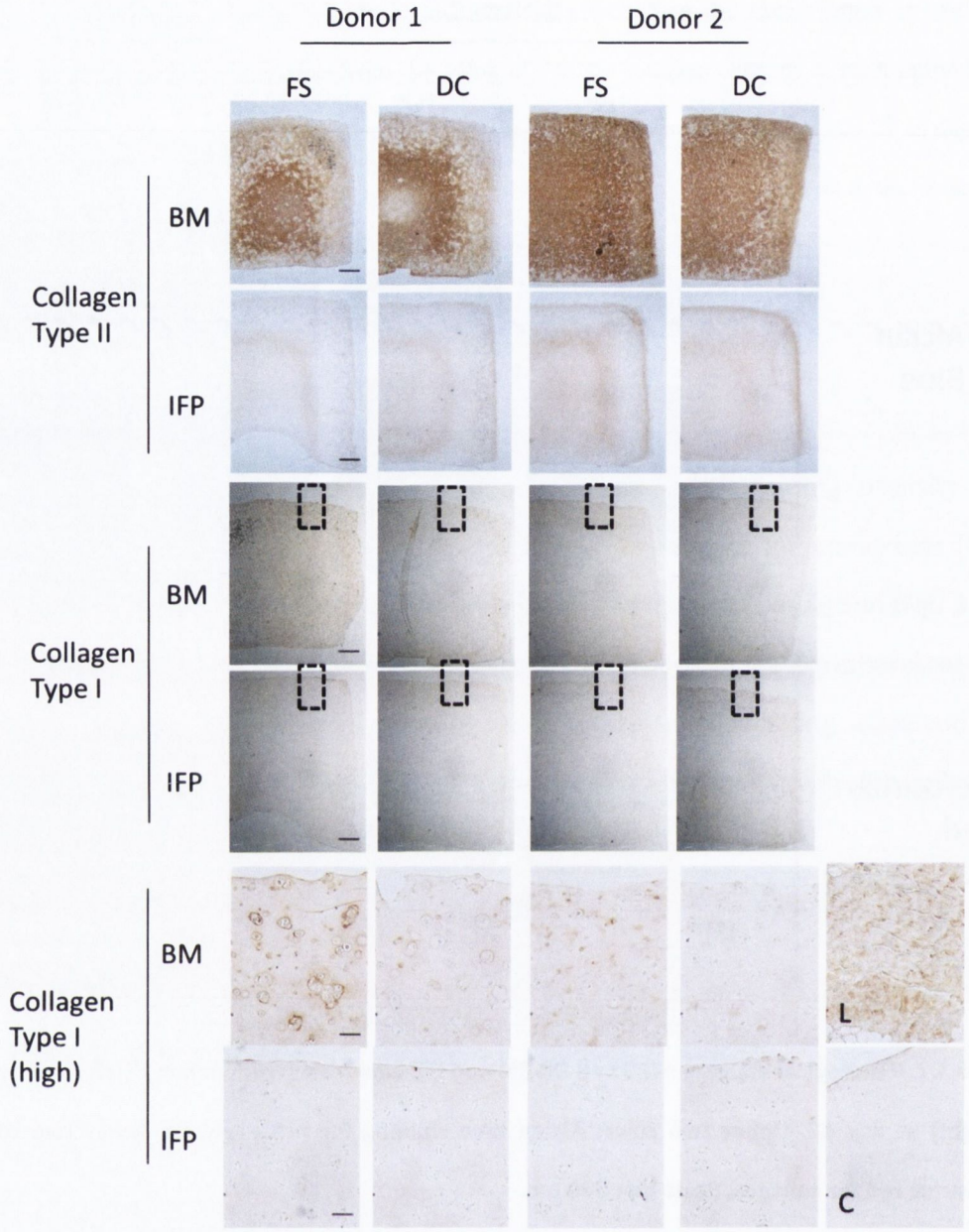

Figure 3.8. Immunohistological staining of FS and DC BM and IFP constructs from donor 1 (left) and donor 2 (right) at day 42. Upper two rows: immunohistological staining for collagen type II, scale bar: 500 μm. Middle two rows: immunohistological staining for collagen type I, scale bar: 500 μm; Box region indicates area from where high magnification images (lower two rows) were taken. Lower two rows: immunohistological staining for collagen type I at the peripheral region of the samples (high magnification); L: ligament (positive control); C: cartilage (negative control). Scale bar: 50 μm.

3.3.3. The influence of DC on the spatial development of engineered cartilage

Overall, the application of DC did not dramatically alter the spatial accumulation of GAG or collagen in the top and bottom of engineered tissues (Supplementary Figs. 3.2 A-F), although it made matrix distribution more homogeneous in IFP constructs from donor 2 (Supplementary Figs. 3.2G, 3.2H). Histological staining with Alcian Blue was less intense around the periphery of BM constructs, particularly for donor 1 (Fig. 3.9). The pericellular matrix (PCM) in the peripheral region of DC constructs stained more intensely for GAG compared to FS controls (Fig. 3.9). The extracellular matrix (ECM) in this region of DC tissues also stained more intensely for GAG and collagen (Fig. 3.9).

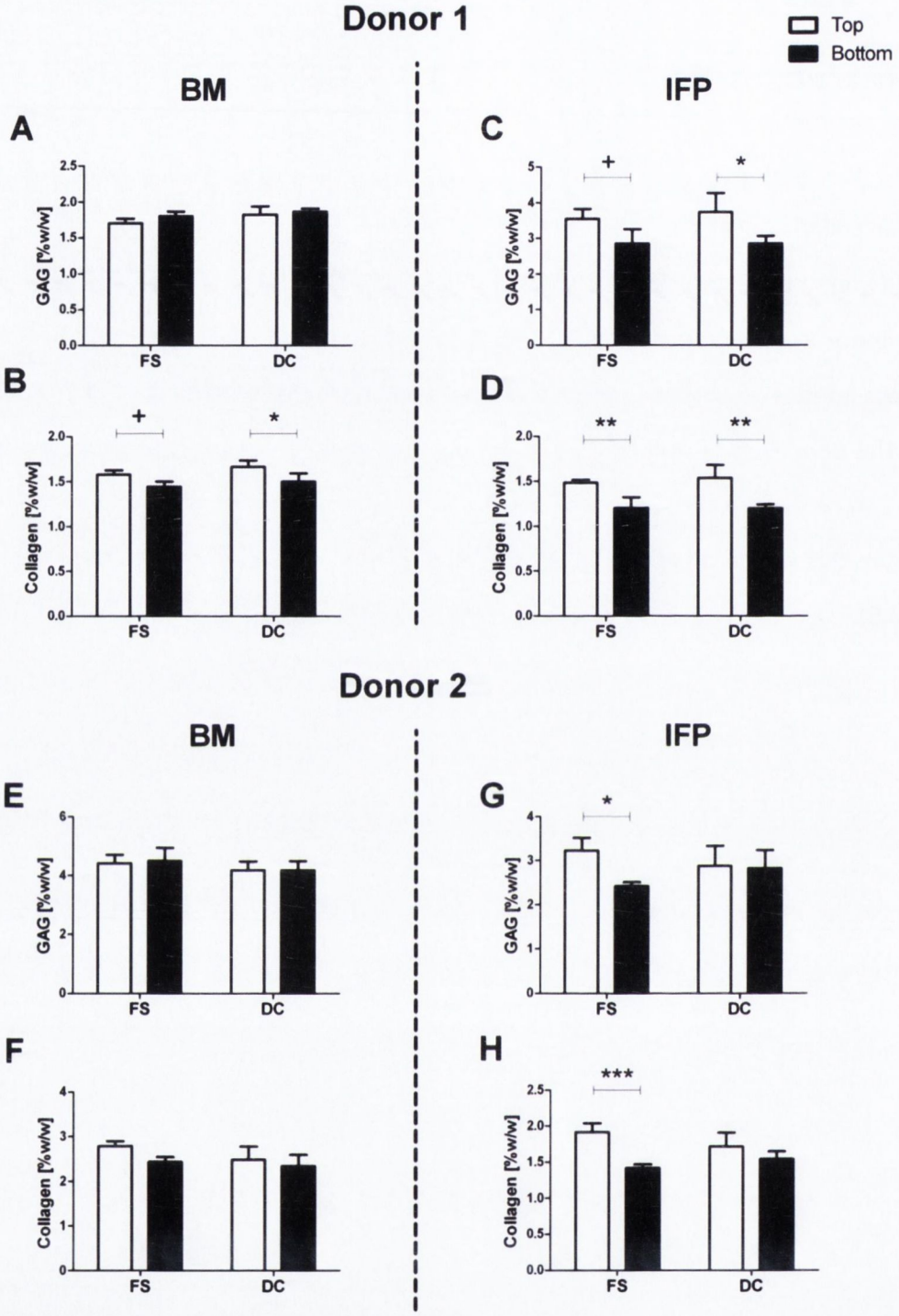

Supplementary Figure 3.2. Biochemical content of top and bottom halves of FS and DC BM (left) and IFP constructs (right) from donor 1 (A, B, C, D) and donor 2 (E, F, G, H) at day 42. (A, C, E, G) GAG content (%w/w); (B, D, F, H) collagen content (%w/w). +: $p<0.1$; *: $p<0.05$, **: $p<0.01$; ***: $p<0.001$.

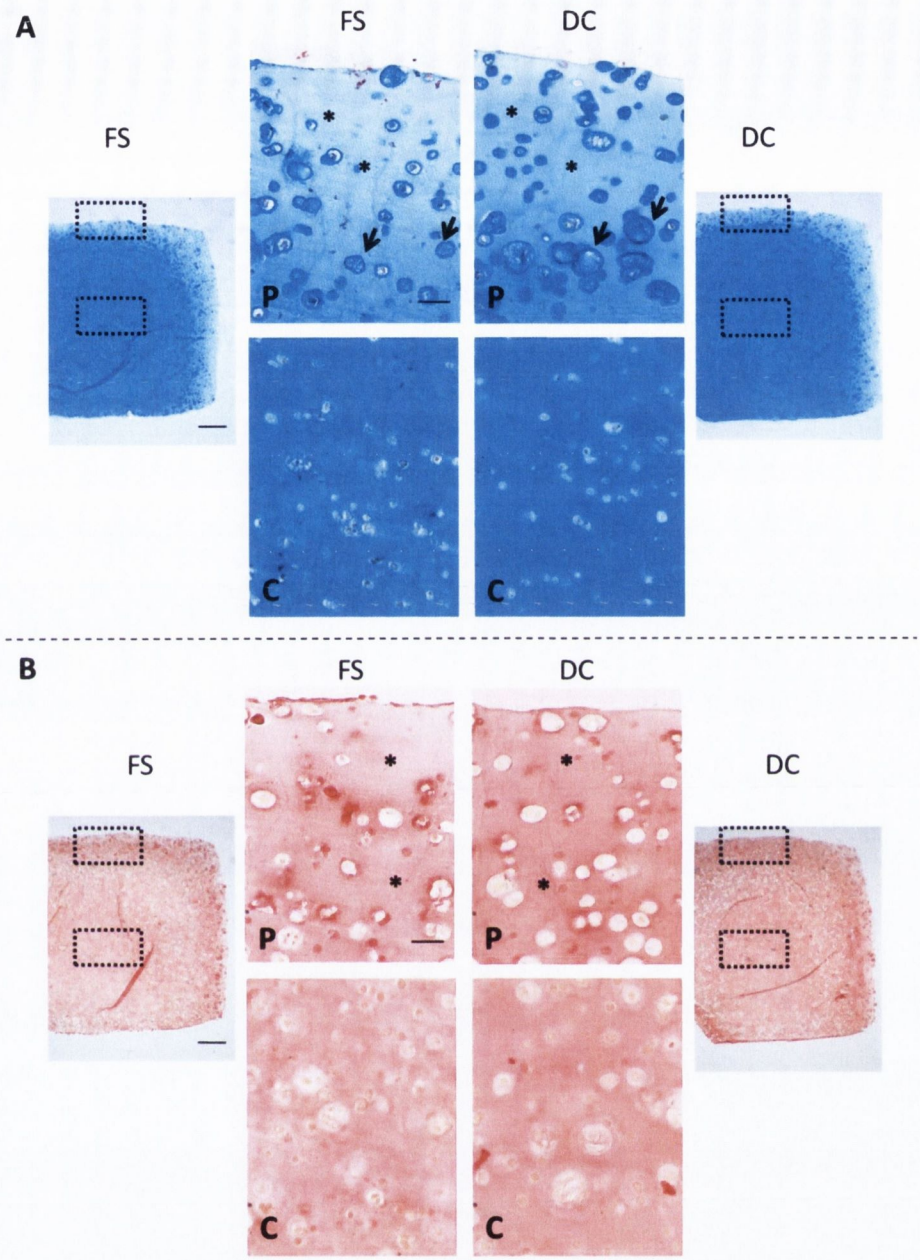

Figure 3.9. Histological staining of FS and DC BM constructs from donor 1 at the peripheral and central region of the tissue at day 42. (A) Alcian blue staining for proteoglycan; (B) Picrosirius red staining for collagen. P: peripheral region; C: central region. Box region in low magnification images (side two columns) indicates area from where high magnification images (middle two columns) were taken. Asterisks and arrows in high magnification images indicate ECM and PCM respectively. Scale bar in low magnification images: 500 μm; scale bar in high magnification images: 50 μm.

3.3.4. The influence of DC on hypertrophy of chondrogenically primed BM-MSCs

Alizarin red staining and μCT scans were carried out to assess mineralization of the engineered cartilaginous constructs. At day 42, positive staining was found in FS BM constructs, while tissues subjected to DC stained negatively (Fig. 3.10A). In spite of this, no significant difference in ALP activity in the medium of FS and DC constructs was found (data not shown). μCT scans of mineral deposition within the constructs were consistent with the results of the histological analysis (Fig. 3.10B). In three out of four samples, less mineral was measured in DC samples compared to FS controls (Fig. 3.10C). All IFP constructs stained negatively for mineralization (Fig. 3.10A). Furthermore, no ALP activity was measured in the culture medium (data not shown).

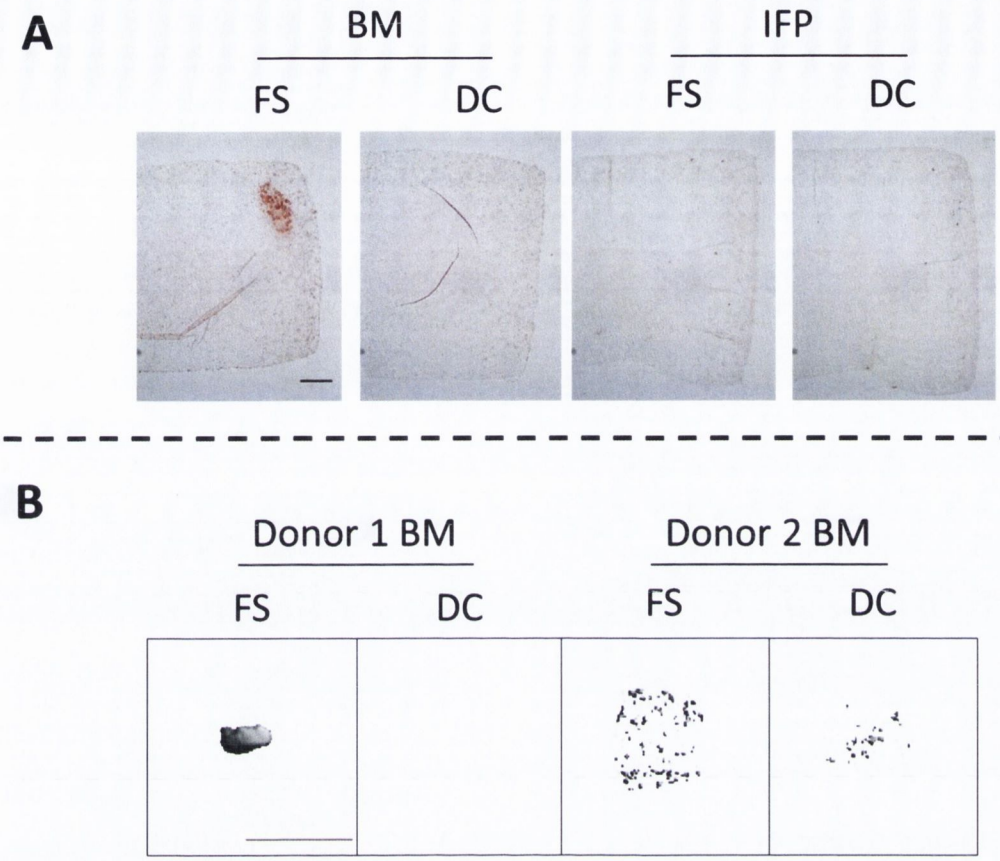

C

	FS (mineral volume mm^3)	DC (mineral volume mm^3)
Donor 1 BM	0.1859	0
	0	0
Donor 2 BM	0.0285	0.0014
	0.0073	0.0006
Mean ± SD	0.0554 ± 0.0878	0.0005 ± 0.0007

Figure 3.10. Assessment of mineralization in FS and DC BM and IFP constructs from donor 1 and donor 2 at day 42. (A) Alizarin red staining of mineral deposition in FS and DC BM and IFP constructs from donor 1 at day 42; scale bar: 500 μm. Images represent the main finding for both donors. (B) 3D images obtained with μCT scan of mineral deposition within FS and DC BM constructs from both donors. Scale bar: 1mm. (C) Volume of minerals in FS and DC BM constructs from both donors. Two constructs per group were scanned using μCT.

3.4. Discussion

The global objective of this study was to explore how dynamic compression would influence the functional development of cartilaginous grafts engineered using different sources of MSCs. In agreement with previous studies (Huang et al., 2010, Bian et al., 2012, Thorpe et al., 2013, Mauck et al., 2007, Kisiday et al., 2009), we showed the application of dynamic compression (DC) can be beneficial to the development of cartilaginous grafts engineered using BM-MSCs, with loading having the potential to increase matrix accumulation and the mechanical properties of the graft while simultaneously suppressing collagen type I accumulation and mineral deposition. In contrast, DC did not have a dramatic effect on the functional development of cartilaginous grafts engineered using IFP-MSCs, with no significant changes observed in matrix synthesis or in mechanical properties of engineered tissues subjected to loading.

While some donor to donor variability was observed, MSCs isolated from both BM and IFP tissue generated cartilaginous constructs with a proteoglycan content, measured as a percentage of wet weight, approaching that observed in the skeletally immature tissue (Gannon et al., 2012) (Fig. 3.1B). This in turn led to the development of tissues with mechanical properties of a similar order of magnitude to native skeletally immature tissue, with the equilibrium modulus reaching up to 300 kPa (Fig. 3.5). Perhaps the most striking difference between the tissues engineered using BM and IFP derived MSCs was the spatial accumulation of matrix within the hydrogel. Greater levels of extracellular matrix (ECM) accumulation was observed around the periphery of IFP constructs from both donors, while a more homogenous distribution of ECM observed in BM constructs (Fig. 3.2). This may be due to the fact that IFP-MSCs are more metabolically active than BM-MSCs, leading to the development of nutrient deprived regions towards the centre of the constructs. (Indeed, IFP-MSCs and BM-MSCs are known to be phenotypically different (Vinardell et al., 2012b).) The

greater levels of proliferation observed in IFP constructs may also be contributing to the development of such a nutrient deprived core region in the engineered tissue. Alternatively, it may be possible that nutrient deprived regions develop in the centre of both IFP and BM constructs, but that BM-MSCs are better equipped to thrive in such conditions than IFP-MSCs. Evidence against this hypothesis can be found in recent studies which demonstrate that BM-MSCs are sensitive to nutrient supply and undergo superior chondrogenesis under optimal nutrient conditions (Farrell et al., 2012). Further studies are required to compare the metabolic requirements of different sources of MSCs, as if differences do exist then the culture conditions to optimize the functional development of cartilage grafts will need to be optimized for specific MSC types.

Dynamic compression did not appear to enhance the development of cartilage grafts engineered using IFP-MSCs. This may be due to the fact that these cells possess a strong intrinsic potential to generate a matrix rich in proteoglycans, which has already approached the levels that is observed in native skeletal immature tissue, following TGF-β3 stimulation in free swelling conditions, and hence chondrogenesis of IFP-MSCs is not further enhanced following the application of DC. Furthermore, when dynamic compression was observed to increase ECM synthesis in BM constructs, these changes were relatively small. As previous studies provide support for the hypothesis that mechanical load promotes chondrogenesis of human MSCs through the TGF-β pathway by up-regulating TGF-β gene expression and protein synthesis (Li et al., 2010), it is perhaps unsurprising that dynamic compression has only a small effect on ECM synthesis in culture environment containing abundant TGF-β3. Further work is required to identify if alternative loading periods or magnitudes would have a more positive impact on MSC chondrogenesis.

The spatial differences in ECM accumulation observed in BM and IFP constructs (and indeed between MSCs taken from the same tissue source but from different donors) may provide an alternative explanation for why DC did not consistently result in an

increase in matrix synthesis. Finite element models have demonstrated that localization of ECM to the outer layer of the engineered tissue, similar to that observed in IFP constructs from both donors, can result in an order of magnitude increase in the peak volumetric strain (i.e. a measure of volume changes) and deviatoric strain (i.e. a measure of shear deformation at constant volume) in the tissue, but to a reduction in the peak pore pressure in the centre of the construct (Khoshgoftar et al., 2013). Therefore the spatial mechanical environment in the IFP and BM grafts are very different, even though the same global deformation is being applied to each engineered tissue. It is therefore possible that the more homogenous ECM distribution observed in the BM-MSCs seeded construct is leading to the development of a more chondrogenic mechanical environment when these tissues are subjected to DC. Similarly, donor to donor variability in the response of MSCs to loading may also potentially be explained by variations in ECM accumulation. The fact that BM-MSCs from donor 1 responded anabolically to the application of DC, while donor 2 did not, may be due to the greater levels of ECM accumulation observed in the grafts generated from donor 2, which may necessitate alterations to the magnitude of global deformation applied to the engineered tissue as it develops to create a pro-chondrogenic mechanical environment at the cellular level (Khoshgoftar et al., 2013). These results also serve to highlight the challenges of exploring donor dependent variability in the response of MSCs to biophysical cues. Given that spatial ECM accumulation determines the local cellular mechanical environment in engineered tissues subjected to DC, and that ECM develops uniquely with the engineered tissue of each donor, it is difficult if not impossible to attribute differences in matrix synthesis in response to DC between the different donors to either donor dependent MSC mechano-responsiveness, differences in ECM accumulation between donors or a combination of both.

It was found that a small, but significant, increase in GAG and collagen accumulation (~8% increase in GAG and collagen accumulation with the application of DC) lead to a relatively higher increase (~25%) in the equilibrium modulus of the BM constructs

(Figs. 3.4, 3.5). Previous studies have found that the delayed application of dynamic compression to cartilaginous tissues engineered using BM-MSCs can lead to improvements in the mechanical properties of the grafts without significantly changing the bulk levels of GAG and collagen accumulation within the tissue (Huang et al., 2010). DC did however lead to an altered distribution of matrix components within the engineered tissue, which may in turn contribute to the improved apparent mechanical properties (Huang et al., 2010). While such dramatic changes in ECM distribution were not observed in this study, which may be due to the fact that we only applied 1 hour of DC compared to 4 hours used in other studies, subtle changes in PCM and ECM accumulation were observed following the application of loading. For example, the superficial region of BM constructs, which generally stain weakly for GAG, appeared more intensely stained in loaded constructs (Fig. 3.9). Any loading regime that leads to the development of a more homogenous engineered tissue should lead to increased construct mechanical properties independent of any increase in biochemical composition (Khoshgoftar et al., 2012).

In agreement with a number of recent studies (Thorpe et al., 2012, Bian et al., 2012, Vinardell et al., 2012a, Steward et al., 2012), we also found that mechanical cues would appear to be critical to the maintenance of the cartilage phenotype in chondrogenically primed BM-MSCs. Collagen type I accumulation and mineralization within BM constructs was suppressed by the application of DC (Figs. 3.8, 3.10). This suggests that much of the concern associated with hypertrophy and endochondral ossification of chondrogenically primed BM-MSCs could be associated with the absence of mechanical cues within most *in vitro* culture conditions and many *in vivo* models (such as subcutaneous implantation) used to access the phenotypic stability of tissue engineered grafts. Under the appropriate mechanical environment within load bearing cartilage defects, it may be that BM-MSCs will generate phenotypically stable articular cartilage. In contrast, constructs engineered using IFP-MSCs showed no type I collagen deposition or mineralization. This is line with the findings from

others, which showed cartilage tissues engineered using this cell type do not proceed along the endochondral pathway in general (Vinardell et al., 2012b).

In conclusion, both BM and IFP derived MSCs were capable of generating cartilaginous tissues with near native levels of GAG content and mechanical properties approaching that observed in skeletally immature animals. Collagen accumulation, as has been observed in numerous cartilage tissue engineering studies, was still significantly lower than the native tissue. The application of dynamic compression could at best lead to small increases in ECM accumulation, although not for all donors or cell types. It is difficult to argue that such small increases in ECM synthesis would warrant the use of bioreactors in a clinical context. Whether the potential increases in mechanical properties of the graft, or the suppression of hypertrophy, merits their use requires further *in vivo* studies.

Acknowledgements

Funding was provided by the European Research Council Starter Grant (StemRepair – Project number 258463) and a SFI President of Ireland Young Researcher Award (08/Y15/B1336).

Chapter IV

Engineering zonal cartilaginous tissue using infrapatellar fat pad derived mesenchymal stem cells by modulating the spatial environment within the developing construct

4.1. Introduction

Articular cartilage (AC) is a highly organised tissue with spatially-varying structure and composition (Klein et al., 2009a). It's typically divided into three zones: the superficial, middle and deep zone, with each zone displaying distinct biological and mechanical properties and functions (Klein et al., 2009b). Cellular morphology, collagen network organisation and extracellular matrix (ECM) composition all vary through the depth of the tissue (Klein et al., 2009a, Klein et al., 2009b, Mow and Guo, 2002). In human adult AC, the collagen content is highest in the superficial zone and its content (as a % of dry weight) decreases with depth whereas proteoglycan content increase with depth and is highest in the deep zone (Muir et al., 1970). This unique depth dependent structure and composition is crucial to the mechanical functions of AC (Wilson et al., 2007, Gannon et al., 2012, Roth and Mow, 1980, Williamson et al., 2003). For example, the high collagen content and its densely packed parallel structure in the superficial zone provides the tissue with the necessary tensile strength to withstand the challenging loading conditions experienced in this region during joint movement (Roth and Mow, 1980, Williamson et al., 2003). This densely packed collagen structure is also believed to contribute to the low permeability of the superficial zone (Mansour and Mow, 1976, Maroudas et al., 1968), which in turn contributes to the dynamic properties of the tissue (Gannon et al., 2012). The increase of glycosaminoglycan (GAG) content from the superficial region to the deep zone has also been shown to correlates with the increase in the compressive modulus with depth through the tissue (Wilson et al., 2007, Klein et al., 2007).

Despite the importance of this zonal structure and composition to the function of AC, to date relatively few studies have attempted to engineer zonal constructs with a structure and composition mimicking that of the native tissue. Early efforts involved isolating chondrocytes from different zones of AC and incorporated them separately into specific regions of the construct in an attempt to engineer zonal cartilage tissue

(Kim et al., 2003, Klein et al., 2003, Sharma et al., 2007). Challenges with this approach include the difficulty to distinguish different zones in a diseased cartilage and the relatively low availability of zonal chondrocytes, which may limit the clinical translation of this approach. Alternative strategies include varying the stiffness (Ng et al., 2009, Ng et al., 2006, Ng et al., 2005) or composition (Nguyen et al., 2011b) through the depth of a scaffold. For example, Nguyen et al. has demonstrated that unique biomaterial compositions can direct bone marrow derived mesenchymal stem cells (BM-MSCs) into specific chondrocytic phenotypes corresponding to the various zones of AC (Nguyen et al., 2011a), and that by incorporating these different biomaterial compositions into a three-layer cell seeded scaffold, it is possible to create a construct with spatially-varying mechanical and biochemical properties similar to the native cartilage (Nguyen et al., 2011b). Potential limitations associated with such approach include the development of a distinct boundary between gel layers, with potentially poor integration and mechanical discontinuity at the interface of layers.

An alternative approach to engineer zonal cartilage is to attempt to recapitulate aspects of the tissue microenvironments which may be responsible for the formation of the zonal structure in AC during tissue development and maturation (Thorpe et al., 2013). Among such environmental cues, oxygen tension and mechanical environment are the two factors known to play a key role in regulating chondrogenesis. Physiologically AC exists in a low oxygen tension environment, and this oxygen tension also decreases from the cartilage surface to the depth of the tissue (Zhou et al., 2004). Meanwhile, the tissue experiences various mechanical stimuli such as compression and tension during joint movement (Mow and Guo, 2002). A previous study (Thorpe et al., 2013) from our lab has used partial confinement of cell seeded hydrogels to create a gradient in oxygen tension through the depth of the construct mimicking that of the native tissue. By coupling such confinement of BM-MSCs seeded hydrogels with dynamic compression, which generated high levels of tensile stain across the top of the construct, it was possible to engineer constructs with zonal

gradients mimicking certain aspects of native cartilage. However, the overall biochemical and mechanical properties of the engineered tissue were significantly lower than those of the native cartilage. Furthermore, hypertrophy and mineralization were also found in the engineered tissues.

The previous chapter of this thesis demonstrated that IFP-MSCs can be used to engineer cartilage grafts with bulk equilibrium mechanical properties approaching that of the native tissue; and that cartilage grafts engineered using this cell type do not undergo hypertrophy or endochondral ossification in general. Furthermore, these engineered tissues were spatially heterogeneous, demonstrating that IFP-MSCs are sensitive to the gradients in regulatory factors that develop within cell seeded hydrogels. Therefore, the objective of this study was to explore if cartilage tissue with a native-like composition, both in terms of absolute levels of matrix accumulation and its spatial distribution, can be engineered by spatially modulating environmental cues through the depth of IFP-MSC seeded hydrogels. Based on a previous study from our lab (Thorpe et al., 2013), we sought to achieve this through the combined application of partial construct confinement and dynamic compression, which has been shown to spatially modulate both the nutrient availability (including oxygen tension) and mechanical cues within MSC seeded hydrogels. To achieve this goal, we first sought to explore how the height of IFP-MSC seeded constructs would influence the spatial development of the engineered tissue, as nutrient availability is strongly dependent on the size of engineered tissues. We next sought to explore how modulating the gradients in nutrients within such engineered tissues, by partially confining the constructs, would modulate the development of the constructs. The next phase sought to explore how the application of dynamic compression would influence the functional development of engineered cartilage, and if its impact would also depend on the height of the engineered tissue. The final phase of the study sought to explore whether the combination of partial confinement and dynamic compression would lead to development of a cartilage construct with a zonal composition mimicking that of the native tissue.

4.2. Materials and Methods

4.2.1. Cell Isolation and Expansion

Porcine IFP-MSCs were isolated from the entire IFP of the knee joint (n=2, 3-4 months old, ~50kg) using a previously described protocol (Buckley and Kelly, 2012). Cells were then seeded at a density of $5x10^3$ cell/cm^2 in high-glucose Dulbecco's modified Eagle's medium (hgDMEM) GlutaMAX™ supplemented with 10% fetal bovine serum and 1% penicillin (100 U/mL)-streptomycin (100 µg/mL) (all GIBCO, Biosciences, Dublin, Ireland) and expanded to passage two (P2) in a humidified atmosphere of 5% CO_2 at 37°C. Fibroblast-growth factor-2 (ProSpec-Tany TechnoGene Ltd, Israel) was added into the medium during the whole expansion period at a concentration of 5 ng/ml to promote the growth and chondrogenic potential of the IFP-MSCs (Buckley and Kelly, 2012).

4.2.2. Hydrogel construct fabrication and culturing

At the end of P2, cells were harvested and encapsulated in agarose (Type VII) as previously described (Thorpe et al., 2010) to obtain a final gel concentration of 2% and a cell density of 20 x 10^6 cells/ml. The agarose-gel suspension was then cast between stainless steel plates, one of which was overlaid with a patterned Polydimethylsiloxane layer, allowed cool to room temperature (RT), and cored to produce cylindrical constructs with a diameter of 6 mm and a height of either 2 mm or 4 mm (4 mm height constructs were fabricated using cells isolated from a different donor). All resulted constructs were with patterns on one surface. Each type of constructs (2 mm/4 mm height) were then maintained respectively in a 58 cm^2 culture dish (6 constructs per dish; Nunclon; Nunc, VWR, Dublin, Ireland) in either 6 ml (per 2 mm height constructs) or 9 ml (per 4 mm height constructs) of

chondrogenic medium consisting of hgDMEM GlutaMAX™ supplemented with penicillin (100 U/ml)-streptomycin (100 µg/ml), 100 µg/ml sodium pyruvate, 40 µg/ml L-proline, 4.7 µg/mL linoleic acid, 50 µg/ml L-ascorbic acid-2-phosphate, 1.5 mg/ml bovine serum albumin, 1 × insulin–transferrin–selenium, 100 nM dexamethasone (all from Sigma-Aldrich, Dublin, Ireland) and 10 ng/ml recombinant human transforming growth factor-β3 (TGF-β3; ProSpec-Tany TechnoGene Ltd). Care was taken to ensure that the constructs remained patterned surface up throughout the culture period and that they did not flip over to stabilise the oxygen and glucose gradient within them. Media was exchanged twice weekly. At each exchange media was sampled and stored at -85°C for biochemical analysis.

4.2.3. Experimental design

Both 2 mm and 4 mm constructs were first maintained in unconfined free swelling (UFS) conditions in a chondrogenic medium for 21 days to allow matrix establishment (Haugh et al., 2011). At this point, samples were confined to half of their height using custom made Polytetrafluoroethylene confinement chambers and subjected to dynamic compression of 10% strain (1Hz, 2 hours/day, 5 days/week) for a further 21 days as previously described (Thorpe et al., 2013) (see CDC group; Fig. 4.1), while samples remained in UFS conditions were used as a control. The effect of these boundary conditions was to lower the oxygen tension in the bottom of the construct and increase the magnitude of strain in the top of the tissue to more closely recapitulate the in vivo microenvironment within articular cartilage. Samples that were confined but still in FS conditions (CFS) and samples that remained unconfined but subjected to DC (UDC) were also kept to study to effects of confinement alone and dynamic compression alone on the development of the tissue (Fig. 4.1). Constructs (n=6 per group) were assessed at day 0, 21 and 42.

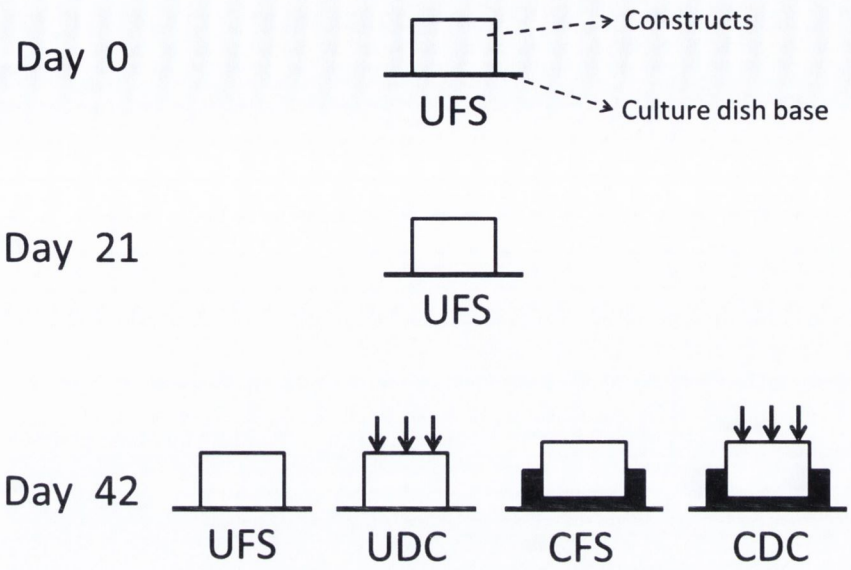

Figure 4.1. Experimental design. Constructs were first cultured in unconfined free swelling (UFS) conditions until day 21, and care was taken to ensure constructs did not flip over during the whole culture period to maintain a stable oxygen and glucose gradient within them. Samples were then confined to half of their height and subjected to dynamic compress (CDC) until day 42 while samples remained in UFS conditions were used as controls. Constructs that were confined but still in free swelling (CFS) conditions and constructs that remained unconfined but subjected to dynamic compression (UDC) were also kept to study the effects of confinement alone and dynamic compression alone on the development of the tissue.

4.2.4. Computational modelling of oxygen, glucose and mechanical environment within developing constructs

Modelling of oxygen, glucose availability within developing constructs

The bellowing modelling was kindly carried out by my colleague Adam O'Reilly. The diffusion of oxygen and glucose was modelled using a mass balance relation combined with Fick's law for diffusion (Sengers et al., 2005, Thorpe et al., 2013, Zhou et al., 2004). The reaction term in the equation followed Michaelis-Menten kinetics:

$$\frac{\partial c}{\partial t} = D\nabla^2 c - n\frac{Q_m c}{K_m + c}$$

Here, c is the solute concentration [mol L^{-1}], D is the diffusion coefficient [cm^2 s^{-1}], n is the cell density [cells L^{-1}], Q_m is the maximum consumption rate [mol h^{-1}] and Km is the concentration at half the maximum consumption rate [mol L^{-1}]. The values of the parameters for each solute diffusion model were obtained from the literature. For the oxygen model; $Qm,0_2$ = 38.88 fmol h^{-1} $cell^{-1}$ (Buckley et al., 2012) and; $Km,0_2$ = 6 x 10^{-6} mol m^{-3} (Sengers et al., 2005). Similarly, for the glucose diffusion model; Qm,glucose = 61.2 fmol h^{-1} $cell^{-1}$ and; Km,glucose = 0.35 x 10^{-3} mol m^{-3} (Sengers et al., 2005). For both models the diffusion coefficient in 2 % agarose was calculated using the Mackie and Meares relation:

$$\frac{D_{ag}}{D_{H_20}} = \frac{n_f^2}{(2 - n_f)}$$

Assuming that n_f = 0.98 for 2 % agarose; for the oxygen model, where $D_{H20},0_2$ = 3.0 x 10^{-5} cm^2s^{-1}, $D_{ag},0_2$ = 2.77 x 10^{-5} cm^2 s^{-1}. Similarly, for the glucose model, D_{H20},glucose = 0.92 x 10^{-5} cm^2 s^{-1} and D_{ag},glucose = 0.85 x 10^{-5} cm^2 s^{-1}.

Using COMSOL, an axisymmetric model was constructed for both the confined and the unconfined case. In accordance with the experimental procedure, both groups were initially modelled as unconfined for the first 21 days, before being split into their respective groups for the remaining 21 days. The initial value for glucose in the media was 25 mM while for the oxygen model the initial value in the media was 208.5 µM; a value which corresponded to an oxygen tension of 21 %. For the oxygen model there was also an essential boundary condition of 208.5 µM at the free surface to account for the diffusion of oxygen into the media from the atmosphere. A media change was modelled every 3.5 days at which point the oxygen and glucose concentrations in the media were returned to their initial values.

Modelling of mechanical environment within developing constructs

The bellowing modelling was kindly carried out by my colleague Adam O'Reilly. The peak fluid pressure and the maximum strain in the axial and radial directions were

estimated during the dynamic compression loading phase for both the confined and unconfined groups at day 21. Using the finite element package FEBio, a pseudo axisymmetric model was developed for both construct geometries, each of which were compressed to 10 % strain over 0.5 seconds. In order to characterise the heterogeneous distribution of collagen and sGAG through the construct, an algorithm developed by the Kelly lab was employed. Briefly, this made use of histology images to calculate the material parameters in each element of the geometry based on its pixel intensity relative to the total number of pixels in the image.

Alcian blue and picrosirius red histology images were used to quantify the distribution of sGAG and collagen respectively. The algorithm involved splitting each image into elements corresponding to the mesh of the stiffness model. The relative pixel intensity was then used to determine the percentage wet weight of the ECM component in each element of the image. The material parameters for the stiffness model used to characterise the mechanical properties of each element were then updated with respect to the ECM concentration. The parameters relating to the sGAG were updated using the same algorithm outlined in the studies conducted by Narmoneva et al. and Khoshgoftar et al. (Narmoneva et al., 1999, Khoshgoftar et al., 2012) while the material parameters related to the collagen were changed using a simple linear approach outlined by Nagel et al. (Nagel and Kelly, 2012).

The governing stress equation used for the mechanical model was the same as the one used by Nagel et al. (Nagel and Kelly, 2012) with the exception that fluid pressurization during loading was also considered. Fluid pressure was accounted for using the permeability model detailed in the study conducted by Holmes & Mow (Holmes and Mow, 1990). The total stress was thus given by:

$$\sigma_{total} = -\Delta\pi I + \sigma_{collagen} + \sigma_{agarose} - \mathrm{p}I$$

Here; $\Delta\pi$ was the Donnan osmotic pressure which was dependent on the concentration of sGAG in the element; σ_{fibres} was the stress in the collagen fibre

network, this was assumed to be isotropic and dependent on the concentration of collagen in the element; σAgarose was the stress in the agarose hydrogel which was constant and isotropic; p accounted for the fluid pressure, this was assumed to be independent of the concentration of extra cellular matrix (ECM) components.

The method was validated by using it to predict the stress relaxation curve of the unconfined stiffness tests conducted at day 21 on the 2 mm and 4 mm constructs. Both cases produced curves which matched the experimental data with an $R^2 > 0.95$.

4.2.5. Assessment of mechanical properties

Construct mechanical properties were tested (n=3/4 per group) using a standard materials testing machine with a 5 N load cell (Zwick Roell Z005, Herefordshire, UK) as previously described (Buckley et al., 2009). Briefly, constructs were immersed in phosphate buffered saline (PBS) bath (RT) and placed between two impermeable platens. A preload of 0.01 N was used to ensure direct contact between construct and platen surfaces. An unconfined stress-relaxation test was then performed, which consisted of a ramp compression up to 10% strain of the sample thickness followed by a hold period of 30 minutes until equilibrium was reached. The equilibrium compressive modulus of the sample was calculated from the equilibrium force. A dynamic test consisting of a cyclic strain amplitude of 1% at 1 Hz for 10 cycles was performed directly after the equilibrium test to determine the dynamic modulus.

4.2.6. Quantitative biochemical analysis

After mechanical testing, constructs were maintained in PBS for 30 mins to allow them to recover to their initial thickness, after which constructs (n=3/4 per group) were transversely sliced into two halves for determination of the spatial distribution of matrix within the engineered tissue. The top and bottom halves of the samples

were weighed (wet) and stored separately at -85 °C for subsequent analyses. Samples were digested with 125 μg/ml papain in 0.1 M sodium acetate, 5 mM L-cysteine HCl, 0.05 M EDTA, pH 6.0 (all Sigma-Aldrich) under constant rotation at 60 °C for 18 hours. The DNA content of the samples was measured using the Hoechst bisBenzimide H33258 dye assay with calf thymus DNA as a standard as previously described (Kim et al., 1988). GAG content was quantified using the dimethylmethylene blue dye-binding assay (Blyscan, Biocolor Ltd., Northern Ireland), with a chondroitin sulphate standard. Collagen content was determined through measurement of the hydroxyproline content (Kafienah and Sims, 2004) and calculated using a hydroxyproline-to-collagen ratio of 1:7.69 (Ignat'eva et al., 2007). GAG/collagen accumulation within constructs was normalized to construct wet weight and to DNA content. GAG/collagen release into the media during the whole culture period was also analysed using the methods described above. Total GAG/collagen synthesis was calculated by the sum of GAG/collagen accumulation within constructs and release into media.

4.2.7. Histology and immunohistochemistry

Whole constructs (n=2 per group) were fixed with 4% paraformaldehyde (Sigma-Aldrich), wax embedded and sectioned perpendicularly to the disk surface at a thickness of 5 μm. Sections were stained histologically with 1% alcian blue 8GX in 0.1M HCl for GAG distribution and with picro-sirius red for collagen distribution (all Sigma–Aldrich). Sections were immunohistochemically stained for collagen type II using a mouse monoclonal collagen type II antibody (1:100; 1 mg/mL; Abcam) as previously described (Thorpe et al., 2010). Constructs were also immunohistochemically stained for proteoglycan 4 (PRG4) expression with a mouse monoclonal antibody (1:50; 0.5 mg/mL; Novus Biologicals, Littleton, USA) using a modified protocol. Briefly, Sections were enzymatically treated with 1 mg/ml pronase (64072 PUK/g; Millipore Ireland, Cork, Ireland) in a humidified environment at 37 °C

for 12 mins. Slides were then blocked with blocking buffers consisting of PBS containing 1% bovine serum albumin and 10% goat serum (all Sigma-Aldrich) for 2 hours at RT and sections were incubated with the primary antibody diluted in blocking buffer at 4 °C over night. After washing in PBS/0.05% Tween20 (Sigma–Aldrich), sections were blocked for peroxidase activity using hydrogen peroxide (Sigma–Aldrich), followed by an incubation for 1 hour in the secondary antibody, anti-mouse IgG biotin antibody produced in goat (1:133; 2 mg/mL; Sigma-Aldrich). Colour was developed using the Vectastain ABC kit followed by exposure to peroxidase DAB substrate kit (both Vector Laboratories, Peterborough, UK). Sections of porcine cartilage and ligament were used as positive and negative controls for collagen type II staining respectively. For PRG4 staining, cartilage (superficial zone) was used as positive control and cartilage without the addition of primary antibody was used as negative control.

4.2.8. Statistical analysis

Statistics were performed using MINITAB 15.1 software (Minitab Ltd., Coventry, UK). A two-sample T-test was used for data sets containing only two groups. For data sets which contain more than two groups, a general linear model for analysis of variance with Tukey's test for multiple comparisons was used. Significance was determined at $p<0.05$ and a trend towards significance was determined at $p<0.1$. All graphical results are presented as mean ± standard deviation.

4.3. Results

4.3.1. Construct height determines the spatial development of tissue engineered cartilage

The availability of regulatory factors such as oxygen and glucose within engineered tissues will depend on the size of the cell seeded construct. Therefore we first sought to explore how the height of IFP-MSC seeded agarose hydrogels would determine the availability of oxygen and glucose within the construct and hence the spatial development of the engineered tissue. Cell seeded constructs of either 2 mm or 4 mm in height were fabricated (where the top surface of the constructs was patterned) and care was taken to ensure they did not flip over during the culture period to help maintain a stable oxygen and glucose gradient through the engineered tissues. Finite element models (undertaken by my colleague Adam O'Reilly) predicted that a low oxygen microenvironment develops in the bottom core of 2 mm hydrogels (≤5% O_2, see red circle area), while an even lower oxygen tension is predicted in the bottom of the 4 mm gels, with an average oxygen tension of 1.24% within the bottom half of the construct (Fig. 4.2A). Models also predicted sufficient and relatively homogeneous glucose availability within both 2 mm and 4 mm constructs, with no dramatic differences observed between them (Fig. 4.2B). The 2 mm constructs stained reasonably homogenously for GAG and collagen, while a larger core region staining less intensely for GAG and collagen was observed in the 4 mm gels (Fig. 4.2C and D).

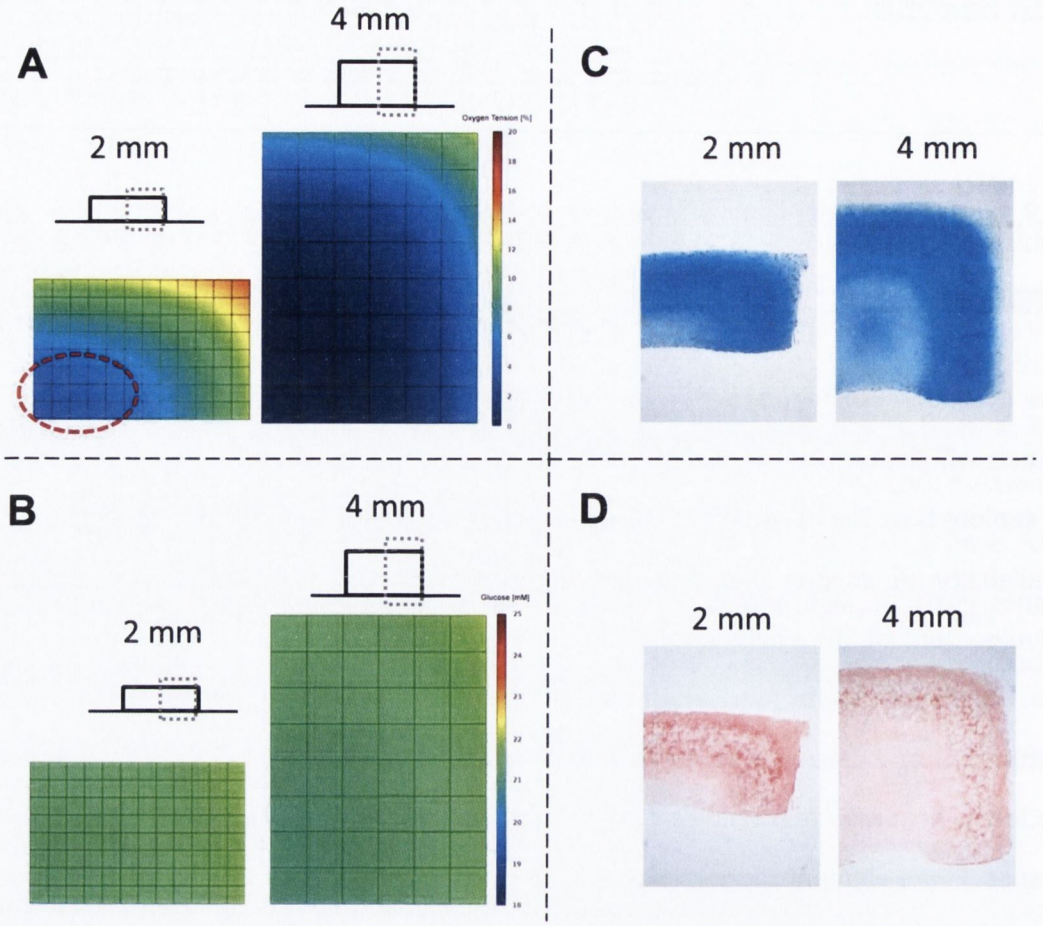

Figure 4.2. Oxygen and glucose environment and matrix distribution with 2 mm and 4 mm samples at day 42. (A) An axisymmetric computational model predicting oxygen environment and (B) an axisymmetric computational model predicting glucose environment within both 2 mm and 4 mm samples. The resulted oxygen/glucose concentration data was calculated from the regions within constructs which were indicated by grey boxes. (C) Alcian blue staining of GAG and (D) Picro-sirius red staining of collagen distribution within both samples at day 42. Histology images were taken at 2x magnification, and they represent approximately 2/3 of the whole sample.

To further explore the spatial development of the engineered tissues they were sliced half way along their height and the biochemical content of the 'top' and 'bottom' of the engineered tissue was measured (Fig. 4.3). At day 42, both 2 mm and 4 mm gels contained significantly higher levels of DNA compared to day 0 (data not shown), suggesting cells proliferated during this time period. The DNA content was higher in the top of both 2 mm and 4 mm tissues compared to the corresponding bottom region of each construct ($p<0.05$; Fig. 4.3A), indicating greater cell proliferation in this region of the engineered tissue. There was a trend ($p<0.1$) towards greater GAG accumulation (as a % of wet weight) in the bottom of the 2 mm constructs (Fig. 4.3B), which was significant ($P<0.01$) when GAG content was normalised to DNA content (Fig. 4.3D). Greater ($P<0.001$) collagen accumulation (as a % of wet weight) was observed in the top of the 4 mm constructs (Fig. 4.3C), however no significant difference was observed if collagen content was normalised to DNA content (Fig. 4.3E).

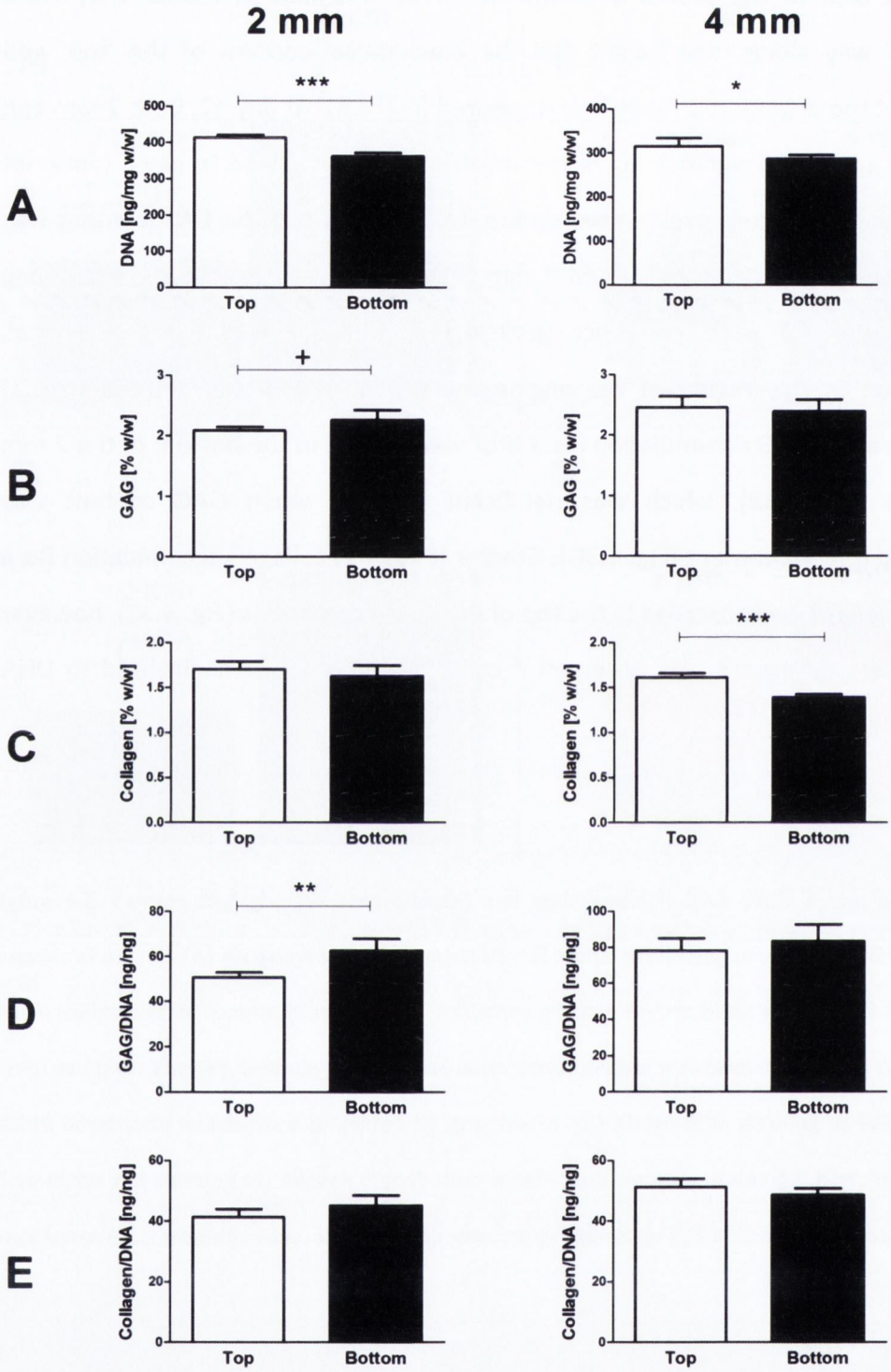

Figure 4.3. Biochemical content of the top and bottom halves of 2 mm and 4 mm unconfined free swelling (UFS) samples at day 42. (A) DNA content [ng/mg w/w]; (B) GAG content [% w/w]; (C) Collagen content [% w/w]; (D) GAG/DNA [ng/ng] and (E) Collagen/DNA [ng/ng]. +: trend, $p<0.1$; *: $p<0.05$; **: $p<0.01$; ***:$p<0.001$.

4.3.2. Modulating spatial oxygen and glucose availability within stem cell seeded hydrogels by partially confining the constructs alters matrix synthesis and the spatial development of the engineered tissue

As a low oxygen environment is known to enhance chondrogenesis of stem cells (Buckley et al., 2010a, Meyer et al., 2010), we next sought to determine how reducing oxygen availability to the bottom of stem cell seeded hydrogels, by radially confining the bottom half of the engineered tissue, would influence the matrix synthesis and distribution of the construct. We have previously shown that this approach can be used to increase GAG accumulation within the bottom of BM-MSC seeded hydrogels (Thorpe et al., 2013). Confining the hydrogels was predicted to lower the oxygen tension in the bottom of both the 2 mm and 4 mm gels, particularly towards the periphery of the gels (Fig. 4.4, see red circles). It was also predicted to increase oxygen levels in the top of the engineered tissue (the confinement chamber moved the construct higher in the culture media and hence nearer the oxygen source), leading to the development of a steeper oxygen gradient through the depth of the construct. A reduction in glucose availability throughout the hydrogels was also predicted in both the 2 mm and 4 mm confined gels, nevertheless this reduced glucose level (~ 18 mM) is still predicted to be sufficient for maintaining cell viability (Fig. 4.4). Partial confinement of free swelling (CFS) hydrogels was found to increase both total GAG and collagen synthesis in the 2 mm gels compared to unconfined free swelling (UFS) constructs ($p<0.05$), however no significant difference was observed when total GAG or collagen synthesis was normalised to DNA content (Fig. 4.5A and B). In the 4mm gels, partial confinement reduced total GAG synthesis and this was also significant when total GAG synthesis was normalised to DNA content ($p<0.05$; Fig. 4.5A). Looking at the spatial development of the engineered tissues, it was found that confinement increased the DNA and collagen content within the top of both 2 mm and 4 mm gels ($p<0.05$; Fig. 4.5C and E). This increase in collagen content was

not significant when normalised to DNA content (Supplementary Fig. 4.1B). Furthermore, confinement increased GAG accumulation throughout the 2 mm gels, but reduced GAG accumulation throughout the 4 mm gels ($p<0.05$; Fig. 4.5D). Histologically, it appeared that confinement increased GAG accumulation around the bottom periphery of the gels (Fig. 4.6).

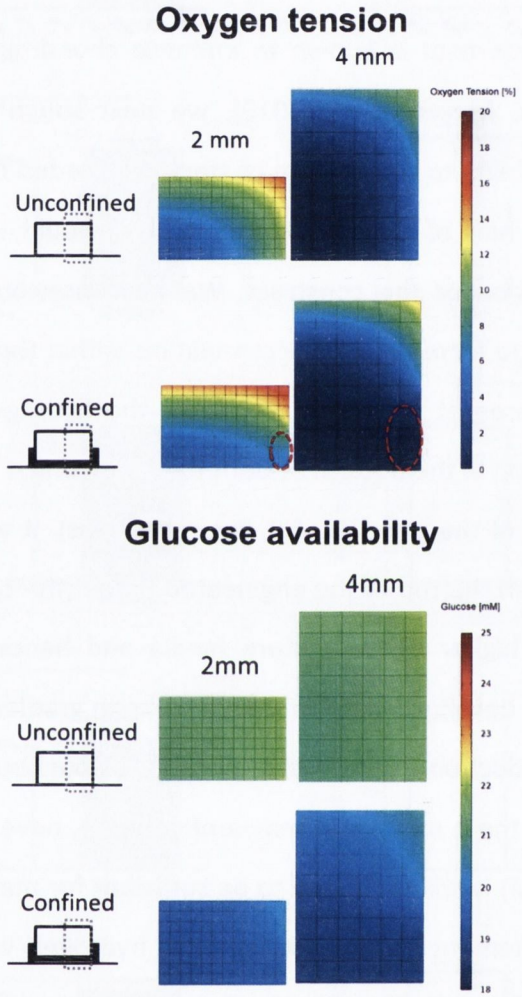

Figure 4.4. An axisymmetric computational model predicting oxygen and glucose environment with unconfined and confined free swelling 2 mm and 4 mm samples at day 42. The resulted oxygen/glucose data was calculated from regions within constructs which were indicated by grey boxes. Red circles highlight regions with lowered oxygen tension in the 2 mm and 4 mm confined samples.

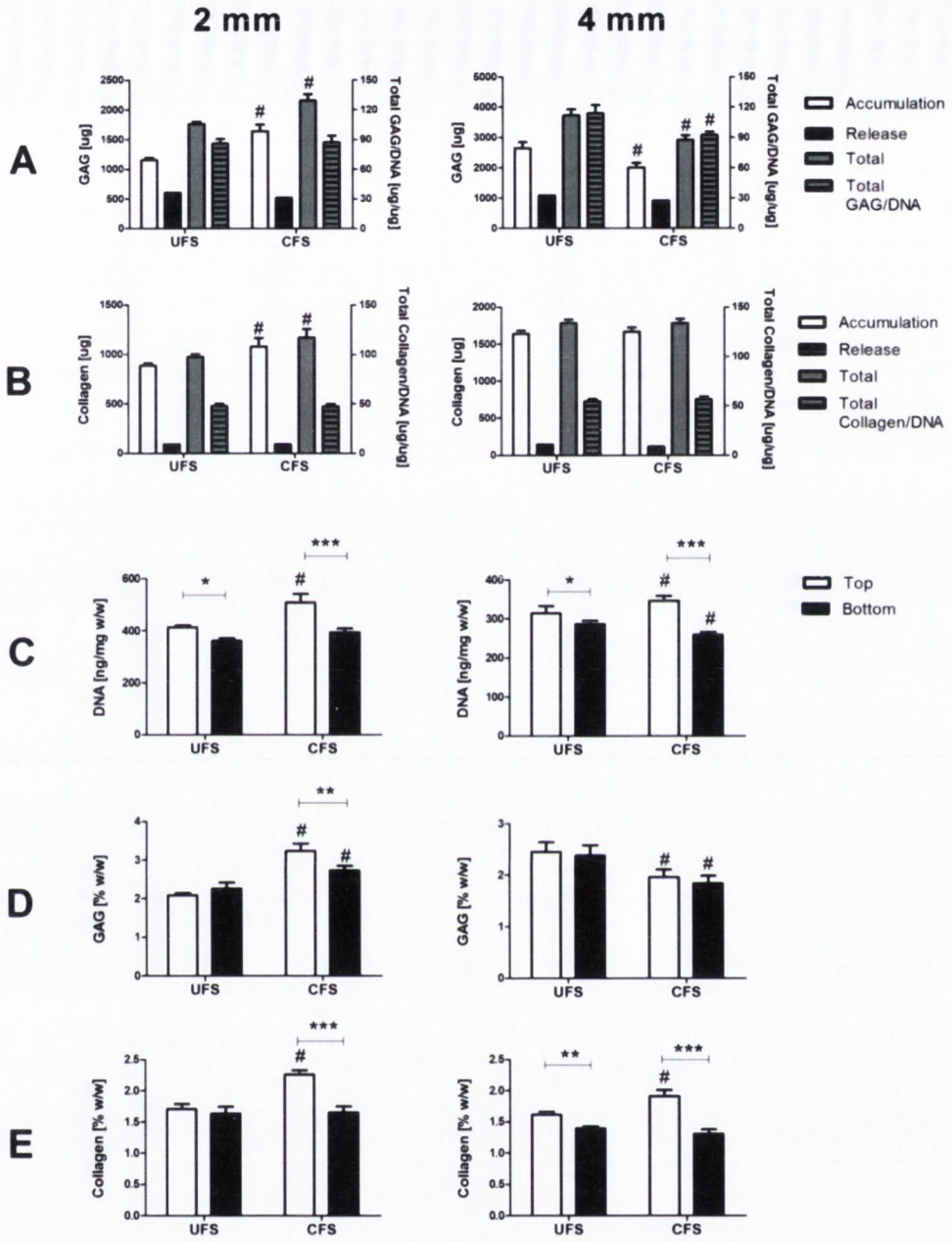

Figure 4.5. (A) GAG content [μg] and (B) collagen content [μg] accumulated within constructs, released into media and total synthesized (accumulated+released) in unconfined free swelling (UFS) and confined free swelling (CFS) 2 mm and 4 mm constructs at day 42. Total GAG/DNA [μg/μg] and total collagen/DNA [μg/μg] value were also plotted on the right Y axis within each graph. (C) DNA content [ng/mg w/w], (D) GAG content [%w/w] and (E) collagen content [%w/w] of the top and bottom halves of the UFS and CFS 2 mm and 4 mm samples at day 42. #: $p<0.05$ vs. UFS; *: $p<0.05$; **: $p<0.01$; ***: $p<0.001$.

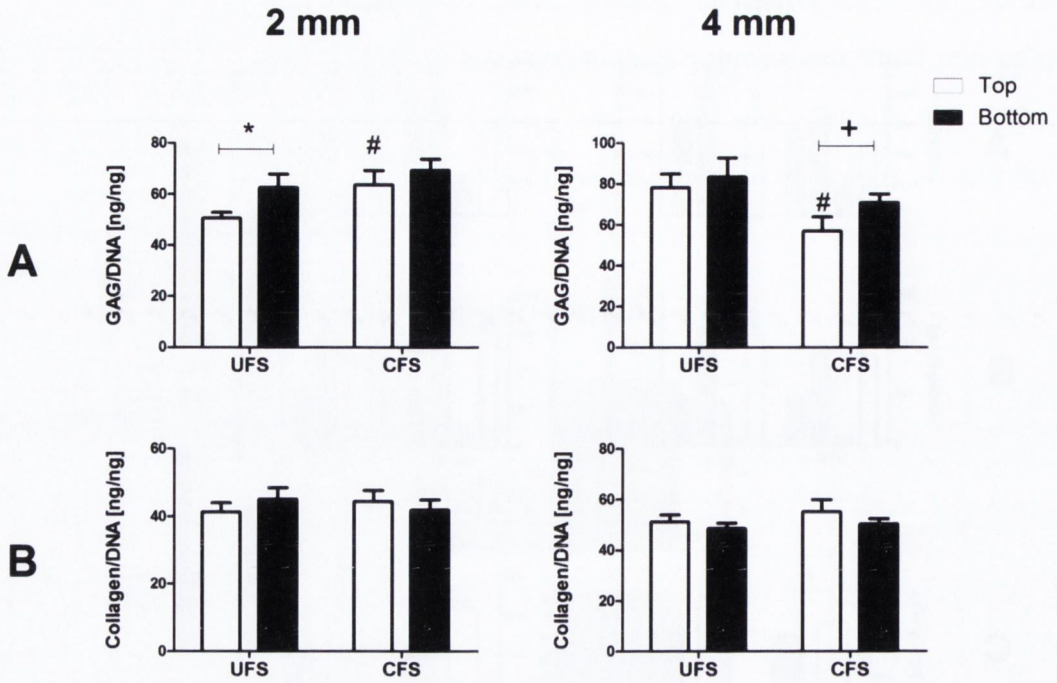

Supplementary Figure 4.1. (A) GAG/DNA [ng/ng] and (B) collagen/DNA [ng/ng] value of the top and bottom halves of UFS and CFS 2 mm and 4 mm constructs at day 42. #: $p<0.05$ vs. UFS; +: trend, $p<0.1$; *: $p<0.05$.

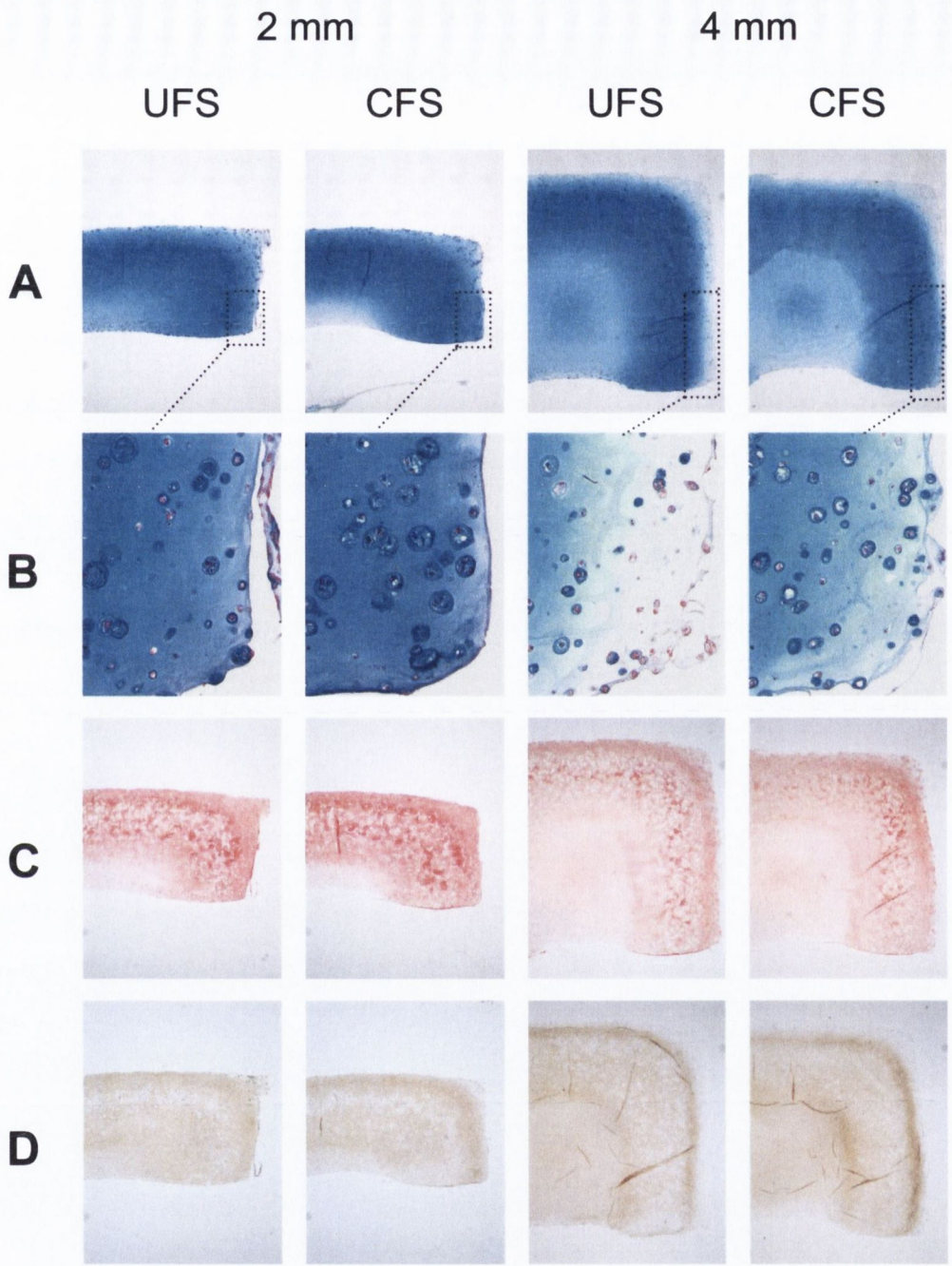

Figure 4.6. Histological staining of matrix deposition within UFS and CFS 2 mm and 4 mm constructs at day 42. (A) Alcian blue staining for GAG, (C) picro-sirius red staining for collagen and (D) Immunohistochemical staining for collagen type II accumulation within samples. All images were taken at 2x magnification, showing 2/3 of the whole construct. (B) Alcian blue staining for GAG deposition at the bottom periphery of the samples (indicated by box regions in (A)) and images were taken at 20x magnification.

4.3.3. The development of tissue engineered cartilage subjected to dynamic compression depends on the height of the construct

We and others have previously shown that the application of delayed dynamic compression (DC) can enhance the development of cartilage grafts engineered using MSCs (Thorpe et al., 2013, Huang et al., 2010, Bian et al., 2012). After 3 weeks in unconfined free swelling (UFS) culture, 2 mm and 4 mm IFP-MSC seeded hydrogels were subjected to DC. Computational finite element simulations of the mechanical environment under such loading conditions predicted a very low fluid pressure in both 2 mm and 4 mm unconfined dynamically compressed (UDC) gels (~0.02 MPa; Fig. 4.7A). Tensile and compressive strains were relatively homogenous through the depth of both the 2 mm and 4 mm constructs, with no dramatic differences in strain level predicted between the 2 mm and 4 mm gels (Fig. 4.7A). GAG and collagen accumulation within the construct increased in the 2 mm UDC gels compared to UFS controls ($p<0.05$; Fig. 4.8A and B). In contrast, DC reduced GAG ($p<0.05$) and collagen ($p<0.1$) accumulation within the 4 mm gels (Fig. 4.8A and B). The reduction in GAG accumulation in the 4 mm gels could be partially explained by an increase in GAG release to the media (Fig. 4.8A). When normalised to DNA content, total (accumulated + released) GAG and collagen synthesis was not significantly affected by the application of DC in either the 2 mm or the 4 mm gels (Fig. 4.8A and B).

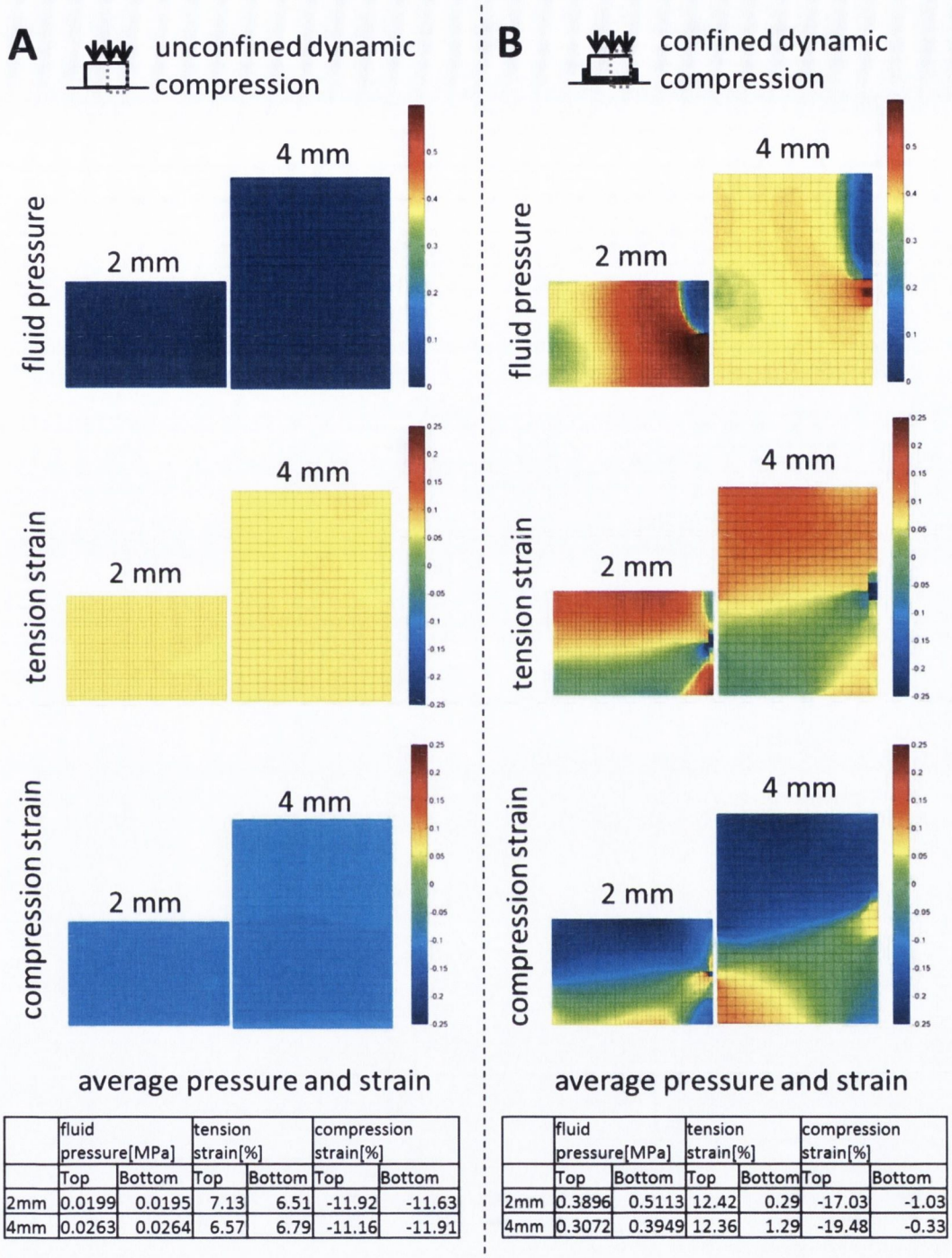

	fluid pressure[MPa]		tension strain[%]		compression strain[%]	
	Top	Bottom	Top	Bottom	Top	Bottom
2mm	0.0199	0.0195	7.13	6.51	-11.92	-11.63
4mm	0.0263	0.0264	6.57	6.79	-11.16	-11.91

	fluid pressure[MPa]		tension strain[%]		compression strain[%]	
	Top	Bottom	Top	Bottom	Top	Bottom
2mm	0.3896	0.5113	12.42	0.29	-17.03	-1.03
4mm	0.3072	0.3949	12.36	1.29	-19.48	-0.33

Figure 4.7. An axisymmetric computational model predicting the mechanical environment of fluid pressure [MPa], tension strain [%, positive] and compression strain [%, negative] within (A) unconfined dynamically compressed (UDC) and (B) confined dynamically compressed (CDC) 2 mm and 4 mm constructs at day 21. The mechanical environment data were calculated from regions within constructs, which were indicated by grey boxes.

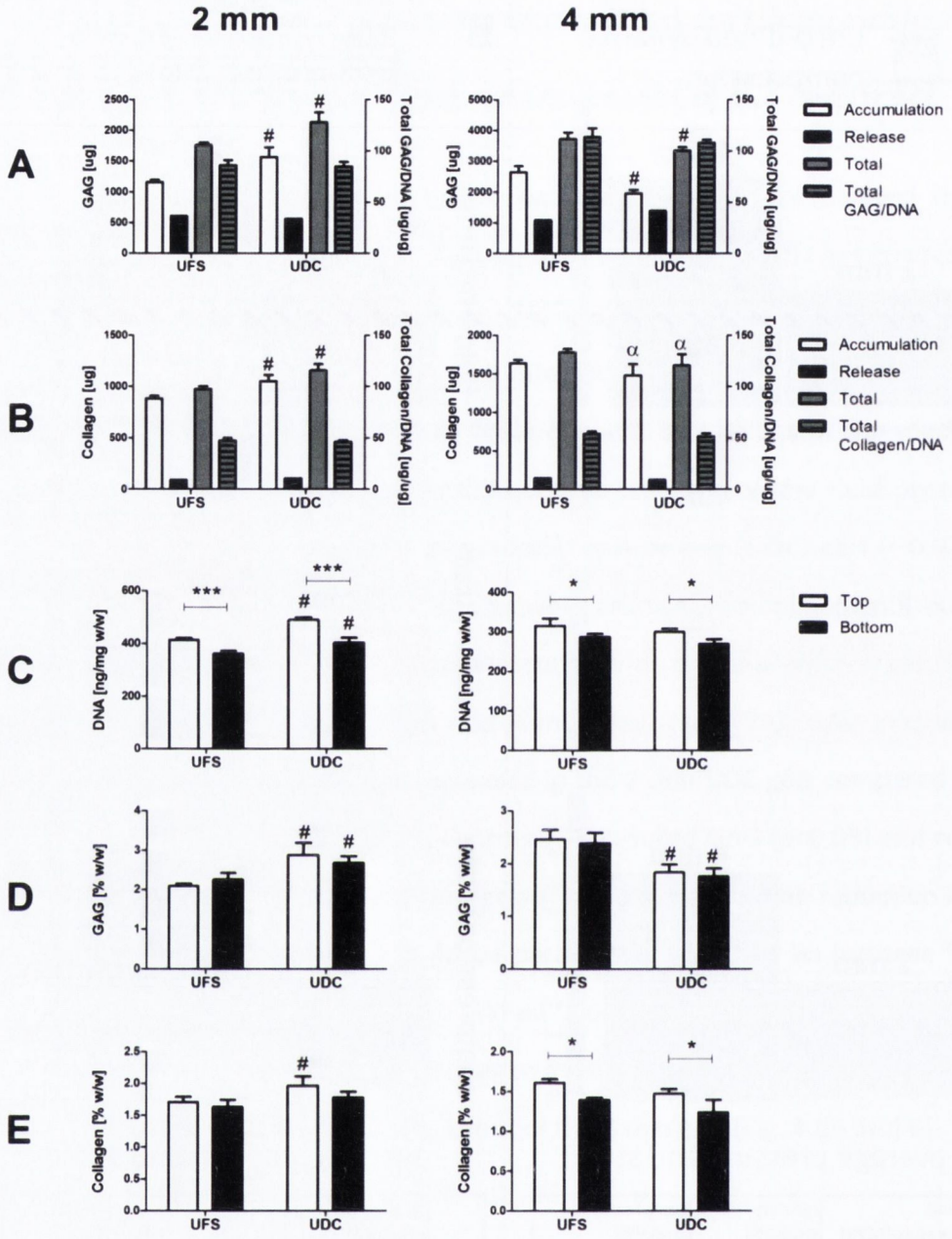

Figure 4.8. (A) GAG content [μg] and (B) collagen content [μg] accumulated within constructs, released into media and total synthesised (accumulated+released) in unconfined free swelling (UFS) and unconfined dynamically compressed (UDC) 2 mm and 4 mm constructs at day 42. Total GAG/DNA [μg/μg] and total collagen/DNA [μg/μg] value were also plotted on the right Y axis within each graph. (C) DNA content [ng/mg w/w], (D) GAG content [%w/w] and (E) collagen content [%w/w] of the top and bottom halves of the UFS and UDC 2 mm and 4 mm samples at day 42. α: trend, $p<0.1$ vs. UFS; #: $p<0.05$ vs. UFS; *: $p<0.05$; ***: $p<0.001$.

DC was found to significantly increase the DNA and GAG content in both the top and bottom of 2 mm gels, and to significantly increase the collagen content in the top of the same gels ($p<0.05$; Fig. 4.8C, D and E). These differences were no longer significant when matrix levels were normalised to DNA content (Supplementary Fig. 4.2). The increased levels of matrix accumulation due to the application of loading translated into improvements in the mechanical properties of the engineered tissues. The equilibrium modulus of the 2 mm UDC gels was found to be 95.3 kPa, compared to 43.3 kPa for the UFS controls ($p<0.01$). The dynamic modulus of the 2 mm UDC gels was found to be 1452 kPa, compared to 969 kPa for the UFS controls ($p\leq0.001$; data not shown). Although histology staining showed no obvious difference in matrix accumulation between the 2 mm UDC and UFS constructs; immunohistochemically, enhanced staining for type II collagen was observed at the top of 2 mm UDC gels compared to UFS gels (Fig. 4.9C). In contrast to the 2 mm gels, DC reduced GAG accumulation throughout the 4 mm gels ($p<0.05$; Fig. 4.8D and Supplementary Fig. 4.2A). This decrease in GAG accumulation also translated into decreases in the mechanical properties of the tissues. The equilibrium modulus of the 4 mm UDC gels was found to be 67.7 kPa, compared to 87.4 kPa for the UFS controls ($p<0.01$). The dynamic modulus of the 4 mm UDC gels was found to be 593.5 kPa, compared to 818.3 kPa for the UFS controls ($p<0.01$; data not shown). Histologically, 4 mm UDC gels appeared similar to UFS controls, albeit that Alcian Blue staining appeared slightly more homogenous within UDC gels (Fig. 4.9).

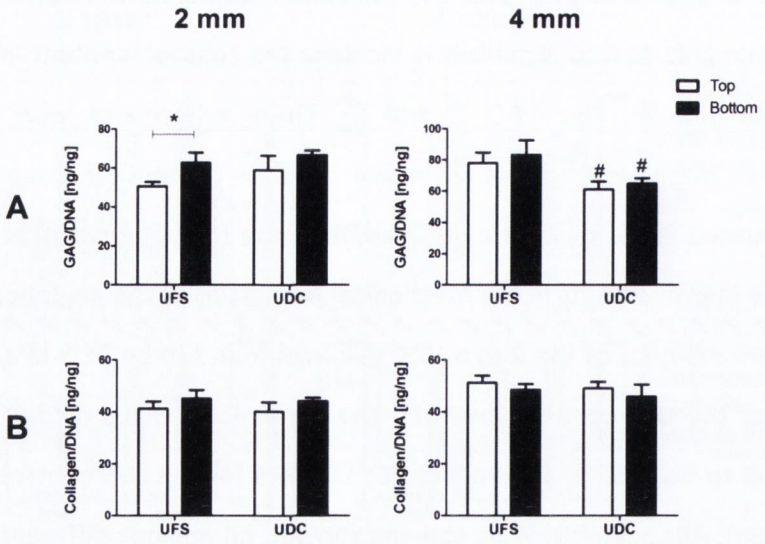

Supplementary Figure 4.2. (A) GAG/DNA [ng/ng] and (B) collagen/DNA [ng/ng] value of the top and bottom halves of UFS and UDC 2 mm and 4 mm constructs at day 42. #: $p<0.05$ vs. UFS; *: $p<0.05$.

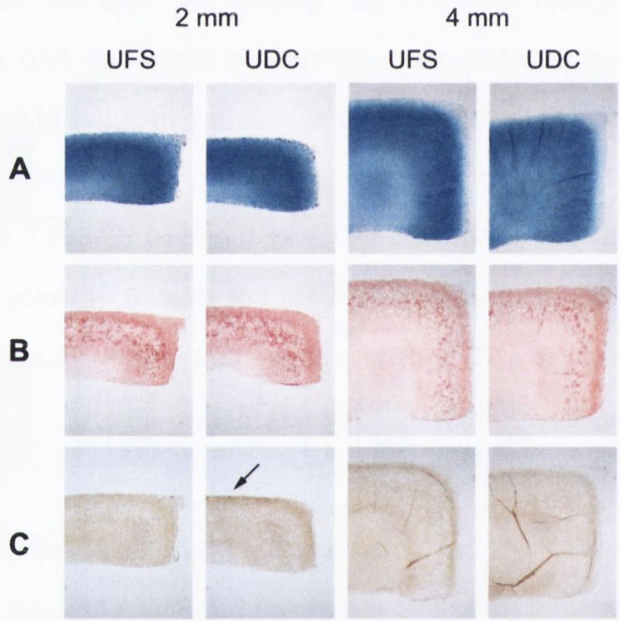

Figure 4.9. Histological staining of matrix deposition within UFS and UDC 2 mm and 4 mm constructs at day 42. (A) Alcian blue staining for GAG, (B) picro-sirius red staining for collagen and (C) Immunohistochemical staining for collagen type II accumulation within samples. Arrow indicates the enhanced staining for collagen type II at the superficial region of 2 mm UDC constructs. All images were taken at 2x magnification, showing 2/3 of the whole construct.

4.3.4. Coupling partial confinement and dynamic compression can lead to the development of engineered cartilage with zonal features mimicking certain aspects of the native tissue

Separately confinement and DC have been shown to generally enhance the development of 2 mm gels, but were not necessarily beneficial to the development of 4 mm gels. Therefore we were interested in exploring how the combination of both factors would influence the development of the engineered tissues. Partially confining the hydrogels was predicted to alter the mechanical environment in both 2 mm and 4 mm confined dynamically compressed (CDC) hydrogels, leading to a higher fluid pressure inside the constructs and to dramatically increased strain levels across the top of the constructs (Fig. 4.7). Overall, there was no synergistic effect of coupling confinement and DC on overall levels of matrix accumulation compared to the application of confinement alone or DC alone (data not shown). There was however some important differences in the zonal development of CDC constructs compared to UFS controls and other previously reported experimental groups. In both the 2 mm and the 4 mm gels, the combination of confinement and DC was found to lead to the development of an engineered tissue that spatially best resembled native articular cartilage. Collagen accumulation was significantly greater in the top of 2 mm CDC gels ($p<0.05$; Fig. 4.10C), which was not observed in UFS controls (this was also not observed in UDC gels, see Fig. 4.8E, but was found in CFS gels, see Fig. 4.5E). No significant difference was observed in GAG accumulation between the top and bottom of 2 mm CDC gels (Fig. 4.10B; however GAG accumulation was higher in the top of 2 mm CFS gels, see Fig. 4.5D, a non-native gradient in matrix levels). When normalised to DNA levels, GAG synthesis was found to be greater in the bottom of CDC gels compared to the top ($p<0.05$; Supplementary Fig. 4.3A).

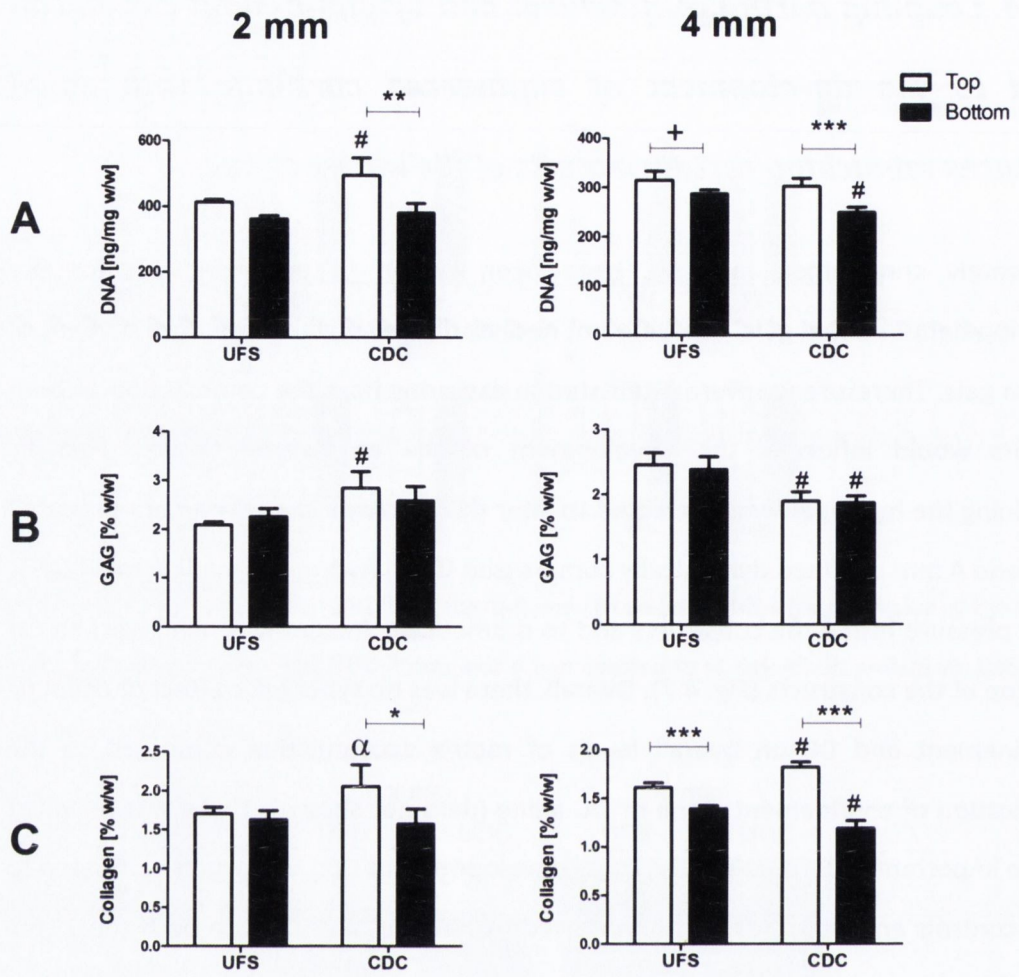

Figure 4.10. (A) DNA content [ng/mg w/w], (B) GAG content [%w/w] and (C) collagen content [%w/w] of the top and bottom halves of the unconfined free swelling (UFS) and confined dynamically compressed (CDC) 2 mm and 4 mm samples at day 42. α: trend, $p<0.1$ vs. UFS; #: $p<0.05$ vs. UFS; +: trend, $p<0.1$; *: $p<0.05$; **: $p<0.01$; ***: $p<0.001$.

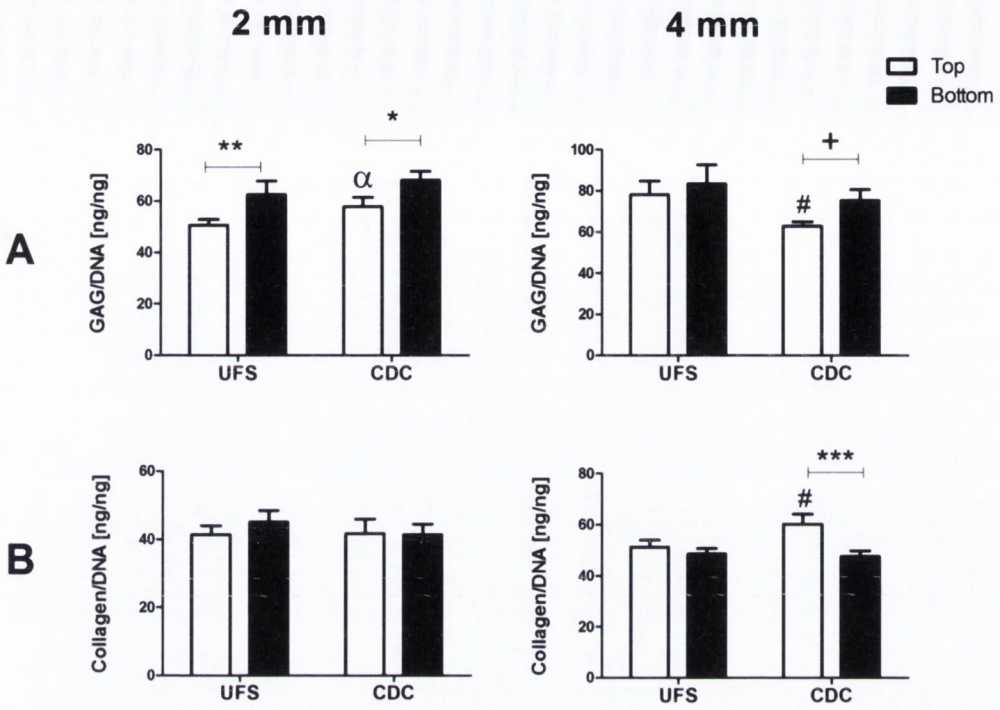

Supplementary Figure 4.3. (A) GAG/DNA [ng/ng] and (B) collagen/DNA [ng/ng] value of the top and bottom halves of UFS and CDC 2 mm and 4 mm constructs at day 42. α: trend, $p<0.1$ vs. UFS; #: $p<0.05$ vs. UFS; +: trend, $p<0.1$; *: $p<0.05$; **: $p<0.01$; ***: $p<0.001$.

A similar gradient in collagen and GAG accumulation was observed in the 4 mm CDC gels (Fig. 4.10B and C). In fact, while the combination of confinement and DC was not beneficial to overall levels of matrix accumulation in the 4 mm gels, it did again lead to the development of a tissue with a zonal composition mimicking aspects of the native tissue. GAG/DNA was higher ($p<0.1$) and collagen/DNA was lower ($p<0.001$) in the bottom of the 4 mm CDC constructs compared to the top (supplementary Fig. 4.3), which was not observed in any other group. Furthermore, the superficial region of both the 2 mm and 4 mm CDC constructs best mimicked that of the native tissue, staining weakly for proteoglycans and strongly for type II collagen deposition (Fig. 4.11A and B). In addition, PRG4 staining was stronger in the superficial region of 4 mm CDC constructs compared to UFS controls (Fig. 4.11C) and indeed UDC constructs (data not shown).

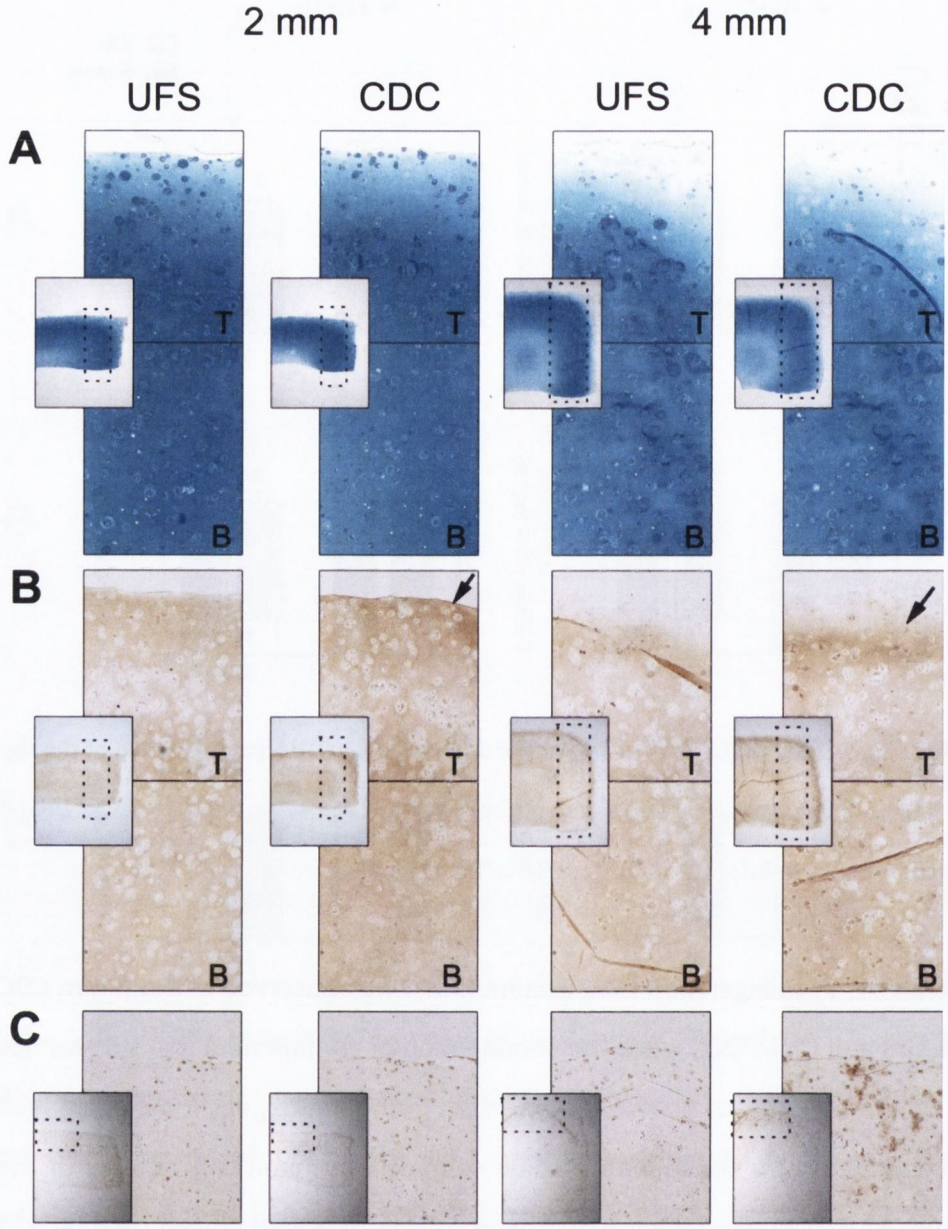

Figure 4.11. GAG, collagen type II and PRG 4 distribution within UFS and CDC 2 mm and 4 mm constructs at day 42. (A) Alcian blue staining for GAG and (B) Immunohistochemical staining for collagen type II accumulation in the top and bottom halves of the sample. T: top; B: bottom. Arrows indicate the enhanced collagen type II deposition in the superficial region of both 2 mm and 4 mm CDC constructs. (C) Immunohistochemical staining for PRG4 expression at the top surface of the sample. Images were taken at 10x magnification. All inserted images were taken at 2x magnification, and box regions indicate area where 10x magnification images were taken.

4.4. Discussion

Generating cartilage grafts with a structure and composition mimicking that of the native cartilage remains a key challenge in the field of tissue engineering. This study aimed to explore if IFP-MSCs can be used to engineer cartilage tissue with native-like levels of matrix accumulation and distribution. IFP-MSCs were encapsulated in agarose hydrogel to make constructs of either 2 mm or 4 mm in height. Constructs were confined to half of their height and subjected to dynamic compression (DC) in an attempt to mimic the spatial oxygen levels and mechanical environment within articular cartilage. Differences in both the predicted oxygen environment and matrix distribution were observed between 2 mm and 4 mm UFS hydrogels. Confinement alone lowered the oxygen tension in the bottom of both 2 mm and 4 mm gels, but only lead to increases in GAG accumulation in 2 mm gel. Similarly the effect of DC alone also depended on the height of the gels, with DC increasing GAG and collagen accumulation in 2 mm gels but decreasing GAG accumulation in 4 mm gels. When confinement was coupled with DC, an altered mechanical environment within constructs was predicted, with increased strain levels within the top of both 2 mm and 4 mm confined dynamically compressed (CDC) gels. This correlated with an increase in total collagen accumulation and collagen type II deposition at the top of both 2 mm and 4 mm CDC gels compared to the UFS controls. Furthermore, both 2 mm and 4 mm CDC gels contained a superficial region that stained weakly for GAG and strongly for collagen type II, with positive staining for PRG4 further observed in 4 mm CDC gels, thus mimicking certain aspects of the zonal composition in articular cartilage. Although the engineered tissue did not quite achieve native levels of matrix accumulation (approaching 3% GAG and 2% collagen as a percentage of wet weight) and biomechanical function (approaching 100 kPa for the equilibrium modulus), they may have attained the necessary function and zonal composition to thrive within a load bearing defect (Nagel and Kelly, 2013).

A low oxygen microenvironment (~5%) was predicted to develop in the bottom core of the 2 mm IFP-MSC seeded UFS hydrogels (Fig. 4.2A), which correlated with higher levels of GAG synthesis (as indicated by GAG/DNA levels) in the bottom of the engineered tissue (Fig. 4.3D). No significant difference in collagen synthesis at per cell level (collagen/DNA) was found between the top and bottom of these tissues (Fig. 4.3E). Similarly, Buckley *et al.* reported increased GAG/DNA but not collagen/DNA level in IFP-MSC seed hydrogel cultured in 5% oxygen compared to 20% oxygen environment (Buckley et al., 2010a). An even lower oxygen tension was predicted in the bottom of 4 mm UFS gels, with an average oxygen concentration of 1.24% across the bottom half. However, it didn't affect either GAG or collagen synthesis at per cell level in the bottom of the tissue (Fig. 4.3D and E). Therefore, while there is evidence to demonstrate that a hypoxic environment (~5% oxygen) can promote chondrogenesis of the stem cells (Buckley et al., 2010a, Meyer et al., 2010); an even lower oxygen environment may not necessarily guarantee improvements to the development of the tissue. In fact, a previous study has even shown significant decreases in cell metabolism and proteoglycan synthesis when freshly-excised articular cartilage was cultured in an environment with oxygen tension <2% (Lee and Urban, 1997).

Significant higher levels of collagen accumulation were observed in the top of the 4 mm gels compared to the bottom (Fig. 4.3C), which is likely attributed to the higher cell proliferation in this region of the engineered tissues (Fig. 4.3A). In fact, this greater cell proliferation at the top of the constructs was also observed in 2 mm gels (Fig. 4.3A) as well as all other reported experimental groups (2 mm and 4 mm CFS, UDC and CDC). It may be explained by the fact that the higher oxygen tension environment generated in the top of the gels promoted a more proliferative phenotype of the cells, as a higher cell proliferation has been seen in adipose derived stem cells cultured at 20% oxygen compared to 5% oxygen (Wang et al., 2005).

Partially confining the gels was predicted to lower the oxygen tension in the bottom of both 2 mm and 4 mm gels, steepening the oxygen gradient as well as reducing glucose availability throughout the gels (Fig. 4.4). The prediction of the increased oxygen tension but decreased glucose availability at the top of the confined gels can be explained by the fact that the confinement chamber moved gels higher in the culture media, and this caused constructs more near to the oxygen source but also less glucose was available above the top surface of the gels. The most dramatic impact of partial confinement was that it increased the DNA content and collagen accumulation within the top of both 2 mm and 4 mm gels (Fig. 4.5C and E), indicating greater cellular proliferation in this region of the engineered tissue. As previously discussed, the increased oxygen tension at the top of the gels may contribute to this enhanced cell proliferation. The increase in cell number was accompanied by an increase in GAG accumulation within the 2 mm confined gels, while a reduction in GAG accumulation was observed in the 4 mm confined gels (Fig. 4.5D). This could be explained by the fact that the confinement had a more critical impact on oxygen levels in the 4 mm gels compared to the 2 mm gels, with the average oxygen tension predicted to decrease from 1.24% to 0.24% (anoxic conditions) in the bottom of 4 mm gels. A previous study has shown significantly decreased matrix production of chondrocytes in anoxic conditions (oxygen tension <0.1%) (Grimshaw and Mason, 2000).

The development of tissue engineered cartilage subjected to DC was found to depend on the height of the construct. In 2 mm gels the application of DC was found to increase GAG and collagen accumulation and the mechanical functionality of the engineered graft, while in 4mm high gels it lead to a reduction in matrix accumulation and mechanical properties of the tissue (Fig. 4.8). The reduction in GAG accumulation within the 4 mm gels could be partially explained by increased GAG release to the media in response to mechanical loading (Fig. 4.8A). The fact that the radial surface area of the 4 mm gels is twice that of the 2 mm gels may partially explain why such GAG loss is higher in the thicker gels. The increased levels of matrix accumulation in

the mechanically loaded 2 mm gels appeared to be driven by increased cell proliferation in these constructs. The finding that this only occurred in the 2 mm gels and not the 4 mm gels is unlikely due to the difference in mechanical environment between them, as predictions showed similar tension and compression strain levels and very low fluid pressures (~0.02 MPa, physiological level is ~10 MPa) in both gels (Fig. 4.7). One important difference observed between these constructs is that 2 mm gels have higher levels of matrix accumulations than 4 mm gels (3% vs. 2% GAG). A previous study has shown that active solute uptake in agarose hydrogel disk subjected to DC increased as the concentration of the gel increased (Albro et al., 2010). Therefore the solute/nutrients transport may be greater in 2 mm gels compared to 4 mm gels, which may attribute to the increased cell proliferation in 2 mm gels. In 2 mm gels the application of DC was also found to lead to increases in type II collagen deposition, particularly at the top surface of the engineered tissue. This suggests that the unique combination of mechanical cues and oxygen tension (Fig. 4.2A) in this region of the 2 mm constructs preferentially supports collagen type II deposition.

Articular cartilage (AC) is characterised by its unique depth dependent composition. The collagen content is highest at the superficial zone and decreases with depth while the proteoglycan content is very low in the superficial zone and increases with depth (Muir et al., 1970). This depth dependent composition together with the collagen network organisation is crucial to the biomechanical properties of the tissue (Wilson et al., 2007, Gannon et al., 2012, Roth and Mow, 1980, Williamson et al., 2003). Subjecting IFP-MSC seeded hydrogels to both confinement and DC appeared to lead to the development of an engineered tissue that best mimicked the depth dependent composition of native AC. While confinement lead to greater collagen accumulation in the top of engineered tissues, mimicking the native tissue, it also lead to greater GAG accumulation in the top of the 2 mm gels due to increased cell proliferation (Fig. 4.5D and E). However, by coupling confinement and DC it was possible to engineer a tissue where GAG levels were not higher in the top of the

tissue but where collagen levels were (Fig. 4.10B and C). Furthermore, the superficial region of CDC constructs best resembled that of the native tissue (Fig. 4.11A and B). Of particular importance was the finding that the combination of partial confinement and DC lead to increased PRG4 deposition at the top surface of the 4 mm gels (Fig. 4.11C). PRG4 is a molecule expressed by the chondrocytes on the surface of articular cartilage to provide boundary lubrication and low-friction properties for the tissue, and it has been shown to be up-regulated in chondrocytes by the application of mechanical stimuli (Grad et al., 2005, Nugent-Derfus et al., 2007). The attainment of a high collagen content and expression of PRG4 in the superficial region of the engineered tissue, may better equip grafts to withstand the challenging loading environment in the joint following implantation.

In conclusion, by regulating the spatial environment through the depth of the engineered tissue, it is possible to engineer cartilage constructs with zonal compositions mimicking certain aspects of articular cartilage using IFP-MSCs. The attained zonal composition may better equip the engineered tissue to achieve a long-term stable cartilage repair.

Chapter V

Engineering tissues that mimic the zonal characteristics of articular cartilage using decellularized cartilage scaffolds seeded with infrapatellar fat pad derived mesenchymal stem cells

5.1. Introduction

Tissue engineering holds great promise for creating viable grafts for repairing cartilage defects. In general, however, most attempts have resulted in the development of homogeneous tissues that do not recapitulate the complex structure and organization of normal articular cartilage. In skeletally mature articular cartilage, the cell morphology and arrangement, extracellular matrix (ECM) composition and structure, and the compressive and tensile modulus all vary through the depth of the tissue (Klein et al., 2009a, Klein et al., 2009b). While it has been possible to engineer cartilage grafts with bulk mechanical properties approaching that of the native tissue (Huang et al., 2010, Mauck et al., 2006), no approaches to date has led to the development of engineered tissues with native-like depth-dependent mechanical properties. The acquisition of these depth-dependent properties in tissue engineered grafts is desirable and may bring benefits such as a better integration into the surrounding native cartilage and long-term mechanical stability, by providing a depth-dependent structure and composition that matches the surrounding native environment (Klein et al., 2009a, Klein et al., 2009b). Therefore, it remains an ongoing challenge in the field of tissue engineering to regenerate cartilage grafts with structure, composition and mechanical properties mimicking the native tissue.

While the previous chapter and other studies have made some progress in attempting to engineer cartilage grafts with a depth-dependent composition mimicking aspects of the native tissue (Klein et al., 2003, Kim et al., 2003, Ng et al., 2009, Ng et al., 2005, Nguyen et al., 2011a, Nguyen et al., 2011b, Thorpe et al., 2013), no strategy has been developed to recapitulate the Benninghoff collagen architecture of skeletally mature articular cartilage. In mature cartilage tissue, the collagen fibers are densely packed and horizontally aligned in the superficial zone but perpendicularly aligned in the deep zone, with the fibers in the middle zone displaying a random organization (Klein et al., 2009a, Klein et al., 2009b). This

depth-dependent collagen architecture together with the spatial-varying ECM composition, are believed to contribute to the overall stiffness and strength of the tissue (Korhonen et al., 2008, Roth and Mow, 1980, Williamson et al., 2003). An alternative approach to tissue engineering grafts with a native-like collagen architecture might be to decellularize native cartilage in such a way that the depth-dependent organization of the tissue is maintained, and to then re-populate this decellularized scaffold with adult stem cells that will function to replace key matrix components (e.g. proteoglycans) lost during the decellularization process. Furthermore, such seeded cells would also function to maintain and turnover the construct following implantation. Decellularized ECM-derived biological scaffolds have been developed from various tissues, such as dermis, urinary bladder, small intestine and heart valves (Crapo et al., 2011). Similar strategies have been adopted using decellularized cartilage grafts for cartilage tissue engineering applications (Kheir et al., 2011, Elder et al., 2010, Schwarz et al., 2012a, Schwarz et al., 2012b). For example, it has been shown that decellularization of a porcine cartilage-bone construct is possible, with near-complete removal of genomic DNA, but accompanied by a significant loss in tissue sulfated glycosaminoglycan (sGAG) content (Kheir et al., 2011). However, limited cellular infiltration into the decellularized scaffold was observed after subcutaneous implantation. Furthermore, it is still not clear if such decellularized scaffolds would support robust chondrogenesis when re-populated with adult stem cells.

The overall objective of this study was to decellularized articular cartilage tissue and re-populate the resulting ECM-derived scaffolds with infrapatellar fat pad derived mesenchymal stem cells (IFP-MSCs) to engineer cartilage grafts with structure, composition and depth-dependent mechanical properties mimicking that of the native tissue. Specifically, the first goal of this study was to develop a methodology to decellularize articular cartilage tissue to produce ECM-derived scaffolds where the collagen structure and content of the native tissue is maintained. I also sought to manipulate the bulk architecture of these scaffolds to facilitate their re-population

with stem cells. The second aim of the study was to explore if re-populating such cartilage ECM-derive scaffolds with IFP-MSCs can lead to the development of engineered cartilage with a Benninghoff collagen architecture and depth-dependent mechanical properties mimicking the native tissue. As the Benninghoff collagen architecture is only fully developed in skeletally mature articular cartilage and not in skeletally immature tissue, it is hypothesized that only by re-populating decellularised cartilage scaffolds derived from skeletally mature joints with IFP-MSCs is it possible to engineer tissues with structure, composition and depth-dependent mechanical properties similar to native tissue.

5.2. Materials and methods

5.2.1. Tissue retrieval

Porcine osteochondral plugs (Ø 6 mm, 10 mm in thickness) were obtained from skeletally immature (n=2; 4 month old) and mature (n=2; 18 month old) animals within 24 h of slaughter as previously described (Gannon et al., 2012). Briefly, samples were taken from the medial and lateral trochlear ridges of the femoropatellar groove of the knee joints using the Osteochondral Autograft Transfer System (Athrex, Naples, FL, USA). Samples were then stored in phosphate buffered saline (PBS; Sigma-Aldrich, Dublin, Ireland) at -85℃ until required.

5.2.2. Decellularization

Osteochondral plugs from skeletally immature and mature donors were thawed in a PBS bath at 37℃ for 1 h. The sub-chondral bone was then removed and the remaining cartilage was trimmed to approximately 1 mm in thickness to produce cartilage disks with a uniform size (Ø 6 mm, ~1 mm in thickness). These cartilage disks were then decellularized using the following protocol. Samples were first subjected to two freeze-thaw cycles. Freezing was carried out at -85℃ for 3 h until crystal formation, while thawing occurred in a PBS bath at 37℃ for 1 h. Channels (see Fig. 5.1) were then introduced into the cartilage disks using flat-ended needles, aimed to improve decellularization and to facilitate subsequent cellular infiltration and migration into the scaffolds (i.e. re-cellularization).

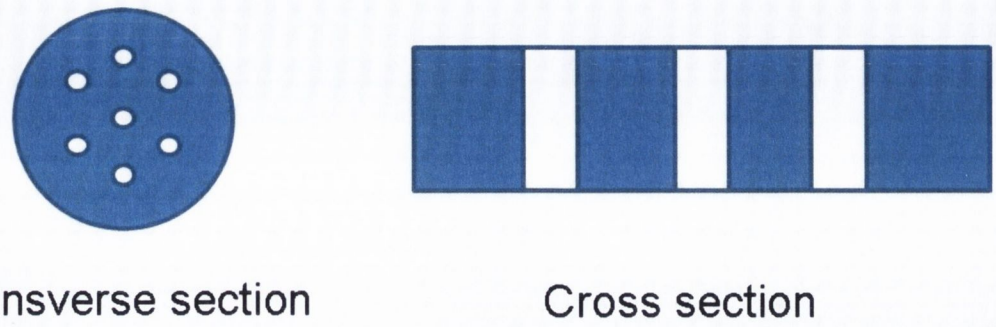

Figure 5.1. Transverse and cross section of channeled cartilage disks. In total 7 channels were introduced to each cartilage disk.

These channeled disks were then incubated in hypotonic buffer (10 mM Tris-HCl/2 mM EDTA, pH 8.0) supplemented with 100mM KCl, 5 mM $MgCl_2$ and 100 mM dithiothreitol (DTT; all Sigma-Aldrich), for 24 h at room temperature (RT). This was followed by another two cycles of incubation in hypotonic buffer supplemented with 0.5% (w/v) sodium dodecyl sulfate (SDS; Sigma-Aldrich), for 18 h at 30℃ each time, with 100 mM DTT also added in the first cycle. The presence of the KCl, $MgCl_2$ and DTT was to facilitate the removal of cell membranes and antigens by increasing the solubility of these proteins in the decellularization solution (Wong et al., 2011). Samples were then washed in PBS for 6 h twice at RT before being treated with 800U/ml hyaluronidase (Sigma-Aldrich) in PBS for 12 h at 37℃. (This step was introduced to remove the hyaluronic acid and proteoglycan inside the cartilage disks, based on the assumption that the removal of glycosaminoglycan (GAG) may lead to the development of a more porous decellularized tissue.) After the hyaluronidase treatment, samples were washed in PBS for 6 h twice at RT, subjected to another freeze-thaw cycle, and then incubated in hypotonic buffer containing 25 U/ml DNase, 25 U/ml RNase (both Sigma-Aldrich), 5 mM $MgCl_2$ and 150 mM NaCl for 16 h at 37℃. Samples were again washed in PBS twice and subjected to another freeze-thaw cycle, before treatment with 0.5 M NaOH in a sonication bath for 5 h at RT. This NaOH

(which digests small collagen fibers) and sonication treatment also aimed to increase the porosity of the decellularized tissues (Sheridan et al., 2012). Finally, following 3 washes in PBS and one more freeze-thaw cycle, samples were left swelling in diH_2O for 6 h at 4℃ and then freeze-dried at -45℃ to produce a scaffold that is suitable for long-term storage. Before cell seeding, scaffolds were sterilized by incubation in PBS containing penicillin (500 U/mL)-streptomycin (500 µg/mL), 0.5 µg/ml amphotericin B (both GIBCO, Biosciences, Dublin, Ireland) three times for 24 h in total, followed by another three washes in PBS for a total period of 24 h. All decellularization and sterilization procedures were carried out under gentle agitation at RT unless stated otherwise.

5.2.3. Cell Isolation and Expansion

Human infrapatellar fat pad derived mesenchymal stem cells (IFP-MSCs) were isolated from the infrapatellar fat pad tissue of a patient (male, 19 years old) undergoing joint arthroplasty at Mater Misericordiae University Hospital under ethical approval, as previously described (Liu et al., 2013). Cells were then seeded at a density of $5x10^3$ cell/cm^2 in high-glucose Dulbecco's modified Eagle's medium (hgDMEM) GlutaMAX™ supplemented with 10% fetal bovine serum, penicillin (100 U/mL)-streptomycin (100 µg/mL), 0.25 µg/ml amphotericin B (all GIBCO, Biosciences) and 5 ng/ml Fibroblast-growth factor-2 (ProSpec-Tany TechnoGene Ltd, Israel) and expanded to passage two (P2) in a humidified atmosphere of 5% CO_2 at 37°C.

5.2.4. Cell seeding and construct culture

At the end of P2, cells were trypsinized and seeded onto both sides of the decellularized scaffolds at a density of 250,000 cells/side, within an agarose ring (3% agarose, Ø 8 mm, ~7 mm in height) placed in the center of the each well of the 12-well-plates, which was also coated with 3% agarose. The agarose ring was used to

provide a confined area to promote cellular attachment onto the scaffolds and to prevent cells from escaping from the scaffolds during early media changes. After the first cell seeding onto one side of the scaffolds, a resting period of 45 mins was allowed for cells to attach to them. The scaffolds were then turned over for cell seeding onto the other side. After another 45 mins, 200 µl chondrogenic medium was then added into each agarose well and cells were incubated at 37 °C for a further 12 hrs to allow complete cell attachment occur. Full amount of fresh medium was then added the next day, and each cell seeded scaffold was cultured in 2 ml chondrogenic medium, consisting of hgDMEM GlutaMAX™ supplemented with penicillin (100 U/ml)-streptomycin (100 µg/ml), 100 µg/ml sodium pyruvate, 40 µg/ml L-proline, 4.7 µg/mL linoleic acid, 50 µg/ml L-ascorbic acid-2-phosphate, 1.5 mg/ml bovine serum albumin (BSA), 1 × insulin–transferrin–selenium, 100 nM dexamethasone (all from Sigma-Aldrich) and 10 ng/ml recombinant human transforming growth factor-β3 (TGF-β3; ProSpec-Tany TechnoGene Ltd), for a total period of 4 weeks. Care was taken to ensure the cell-seeded scaffolds did not flip over throughout the culture period, with the articular surface side of the scaffold facing upward, in order to mimic the decreasing oxygen gradient through the depth of the native tissue. Medium was changed twice per week. In the first two weeks, constructs were cultured on a rotational platform (Sigma-Aldrich), which was found to facilitate cell migration into the scaffolds and channels. In the last 2 weeks of culture, rotation was stopped to provide a steady culture condition for the seeded cells. Constructs were assessed on day 1, 14 and 28.

5.2.5. Live/dead assay

The viability of cells within the constructs (n=2 per group) was assessed throughout the culture period, using a live/dead assay kit (VWR International, Ireland). Briefly, constructs were cross sectioned into halves along the channels and rinsed 5 times in PBS before incubated in PBS containing 2 mM Ethidium Homodimer-1 and 4 mM

Calcein for 1 h at 37 °C. Samples were again washed 5 times in PBS to remove excessive dye and then visualized immediately under an Olympus FluoView™ FV1000 confocal microscope. Images were taken and stacked through the radius of the channels. Calcein stains live cells (shown green) while ethidium Homodimer-1 stains the nucleus of dead cells (shown red).

5.2.6. DAPI and actin staining

The cellular alignment within the scaffolds (n=2 per group) was also assessed throughout the culture period using a protocol adapted from Steward et al. (Steward et al., 2014). Briefly, constructs were cross sectioned into halves along the channels, fixed in 4% paraformaldehyde (PFA; Sigma-Aldrich) overnight at 4℃ and rinsed with PBS. After this, samples were permeabilized in PBS containing 0.5% (v/v) Triton X-100 (Sigma-Aldrich) for 45 min at RT, rinsed again with PBS, and then incubated in a PBS solution containing 1.5% (w/v) BSA, 10 µg/ml 4',6-diamidino-2-phenylindole (DAPI) and 5 U/mL rhodamine phalloidin (both from VWR) for 1.5 h at RT. Excessive dye was then removed by rinse in PBS, and samples were visualized immediately under an Olympus FluoView™ FV1000 confocal microscope. Images were taken and stacked through the radius of the channels. DAPI stains the nuclear of the cells (shown blue) and rhodamine phalloidin stains the F-actin of the cytoskeleton of the cells (shown red).

5.2.7. Mechanical test

Bulk mechanical test

The bulk mechanical properties of the day 28 seeded constructs were measured using a modified protocol described by Buckley et al (Buckley et al., 2009). Samples 3 mm in diameter were cored from the center region of the constructs for mechanical testing. Briefly, samples (n=3 or 4 per group) were immersed in PBS bath and placed

between two impermeable patterns. A preload of 0.2 N was first applied to ensure good contact between the sample surface and the loading platen. Samples were hold at this preload for 10 minutes until they were fully relaxed. Next, an unconfined stress-relaxation test was performed, consisting of a ramp compression up to 20% strain of the sample thickness, followed by a hold period of 30 mins until equilibrium of the samples was reached. A dynamic test consisting of a cyclic strain amplitude of 1% at 1 Hz for 10 cycles was then performed to determine the dynamic modulus of the tissue.

Depth-dependent mechanical test

The depth dependent mechanical testing of the samples was kindly carried out by my colleague Johnnie Chu. For day 1 samples, the cell-seeded constructs were tested awhole; while for day 28 samples, cores 4 mm in diameter were removed from the center region of the cell-seeded constructs. This facilitated the creation of a flatter sample for mechanical testing, as an uneven layer of tissue was found to form across the surface of the day 28 constructs. Prior to depth-dependent mechanical testing, samples (both day 1 and 28) were cross sectioned into two halves along the channels and then placed in a PBS solution containing 1 μg/ml Hoechst 33342 dye (Sigma-Aldrich) for 1.5 hours, which stains the nuclei of the cells seeded into the scaffolds. Samples were then placed into a custom-built microscopic unconfined compression rig (Gannon, 2013) with the cross section of the sample (reveals the plane of the cells seeded into the channels) being monitored by a fluorescent microscope during the whole testing period.

After a preload of 0.4 N , samples were compressed such that offset strains of 2.5, 5.0, 7.5, 10.0, 12.5% and 15.0% strains were achieved, where a relaxation period of up to 30 minutes was implemented between each bulk strain increment. The strain fields across the samples were then obtained from VIC-2D software using the images obtained at each offset strain, from which the average local strains within different zones of the engineered tissue were also obtained. The average equilibrium stress

was also obtained at each offset strain, using a load cell connected in series with the platens to determine the applied stress. Subsequently the local zonal equilibrium compressive modulus was obtained from the applied stress and the local zonal strain values.

5.2.8. Quantitative biochemical analysis

After bulk mechanical testing, samples were maintained in PBS for 30 mins to allow them to recover to their initial thickness. The wet weight of the samples was then recorded (core and annulus were pooled for day 28 cell-seeded constructs) and samples were stored at -85 °C for biochemical analyses. The biochemical content of the samples (n=3 or 4 per group) was assessed as previously described (Thorpe et al., 2010). Briefly, Samples were digested with 125 μg/ml papain in 0.1 M sodium acetate, 5 mM L-cysteine HCl, 0.05 M EDTA, pH 6.0 (all Sigma-Aldrich) under constant rotation for 18 hours at 60 °C. The DNA content of the samples was then measured using the Hoechst bisBenzimide H33258 dye assay with calf thymus DNA as a standard (Kim et al., 1988). sGAG content was quantified using the dimethylmethylene blue dye-binding assay (Blyscan, Biocolor Ltd., Northern Ireland), with a chondroitin sulphate standard. Collagen content was determined through measurement of the hydroxyproline content (Kafienah and Sims, 2004) and calculated using a hydroxyproline-to-collagen ratio of 1:7.69 (Ignat'eva et al., 2007).

5.2.9. Histology and PLM

Samples (n=2 per group) were cut into halves along the channels, fixed in 4% PFA overnight at 4°C, wax embedded and cross sectioned at 5 μm for histological analysis. Sections were stained with haematoxylin and eosin (H&E) to assess cellular content, and 1% alcian blue 8GX in 0.1 M HCL counter-stained with nuclear fast red to visualise GAG content (all Sigma-Aldrich). The collagen content and fiber orientation

was assessed by pre-incubating sections in bovine testicular hyaluronidase before staining in picro-sirius red (Sigma-Aldrich) and visualizing under normal bright filed and polarization respectively. The hyaluronidase treatment step was performed as previously described (Kiraly et al., 1997), in order to remove all sGAG in the sections and thus enhancing the visualisation of the collagen architecture.

5.2.10. Statistical analysis

Statistics were performed using MINITAB 15.1 software (Minitab Ltd., Coventry, UK). A two-sample T-test was used for data sets containing only two groups. For data sets which contain more than two groups, a general linear model for analysis of variance with Tukey's test for multiple comparisons was used. Significance was determined at $p \leq 0.05$. All numerical and graphical results are presented as mean ± standard deviation.

5.3. Results

5.3.1. Effective decellularization of articular cartilage is accompanied by a complete loss in sGAG while maintaining tissue collagen content

A protocol was developed to decellularize articular cartilage tissue using 4 month old cartilage samples. Histological analysis of decellularized cartilage tissue revealed that the developed protocol resulted in near complete removal of cellular nuclei and a dramatic reduction in tissue sulfated glycosaminoglycan (sGAG) content (Fig. 5.2). In contrast, the protocol did not appear to affect the tissue collagen content, as evidenced by no change in the intensity of picrosirius red staining post-decellularization (Fig. 5.2). Quantitative biochemical analysis of decellularized tissues agreed with these histological findings. The decellularization procedure led to a significant reduction (~88%, $p \leq 0.001$) in the DNA content of the samples, near-complete removal of sGAG, while maintaining the collagen content (Fig. 5.3A). The DNA/dry weight level of the decellularized cartilage samples was ~388 ng/mg, significantly lower than that of native tissue (Fig. 5.3B; $p \leq 0.001$). Collagen was found to account for ~90% of the dry weight of the decellularized samples, significantly higher than that of the native tissue (Fig. 5.3B; $p \leq 0.001$), which is most likely due to the removal of sGAG from the decellularized samples.

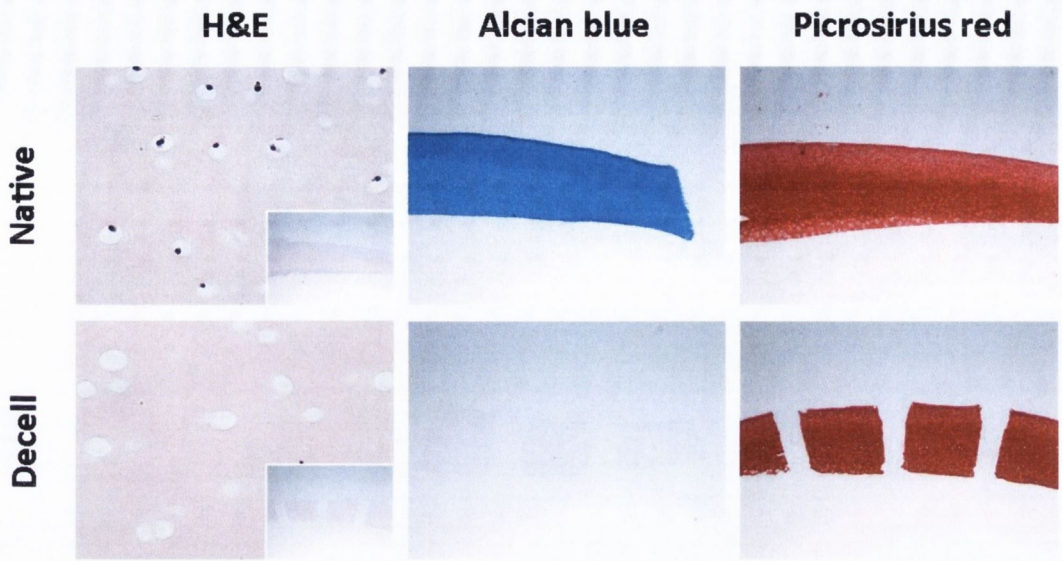

Figure 5.2. H&E, Alcian blue and Picrosirius red staining of the 4 month old native and decellularized articular cartilage. Images for H&E were taken at 40x, with inserted images taken at 2x. Images for Alcian blue and Picrosirius red were all taken at 2x.

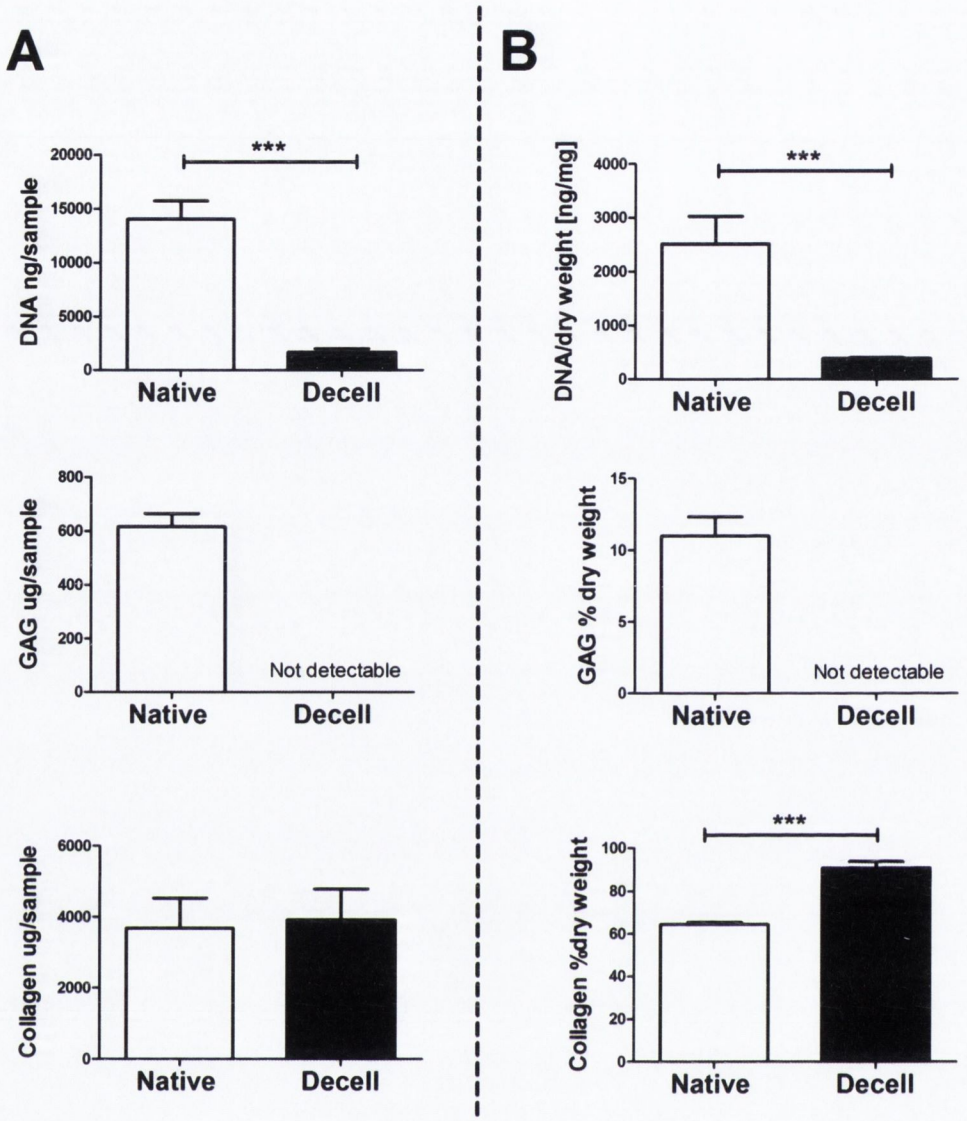

Figure 5.3. A: DNA, GAG and collagen content of the 4 month old native and decellularized articular cartilage. B: DNA/dry weight (ng/mg), GAG %dry weight and collagen %dry weight level of the 4 month old native and decellularized articular cartilage. ***: $p \leq 0.001$.

5.3.2. The depth-dependent collagen architecture of skeletally mature and immature cartilage is maintained post-decellularization

Skeletally immature (4 month old) and mature (18 month old) articular cartilage tissues were then decellularized using the above protocol to produce decellularized ECM-derived scaffolds for cartilage regeneration. After decellularization, a significantly higher level of DNA and collagen content was found in the decellularized skeletally mature scaffolds than immature scaffolds ($p \leq 0.05$ and $p \leq 0.001$ respectively); however when normalized to the dry weight of the scaffolds, these differences were no longer significant (Table 5.1). No sGAG was detected in both decellularized immature and mature scaffolds (Table 5.1). H&E staining revealed a near-complete removal of nuclei through the depth of both decellularized scaffolds, while alcian blue staining also showed a complete removal of sGAG in both groups (Fig. 5.4). Importantly, PLM revealed that the depth-dependent collagen architecture of skeletally immature and mature cartilage was maintained post-decellularization, with horizontally aligned collagen fibers observed in both superficial and deep zone of the decellularized immature samples, and horizontally aligned collagen fibers in the superficial zone but perpendicularly aligned collagen fibers in the deep zone of the decellularized mature samples (Fig. 5.4).

	Immature	Mature	Immature vs. Mature
DNA (ng/sample)	1747 ± 383.6	2419 ± 270.5	*
Collagen (ug/sample)	3563 ± 200	4551 ± 290.2	***
GAG (ug/sample)	Not detectable	Not detectable	-
Dry weight (mg/sample)	4.07 ± 0.26	5.25 ± 0.38	**
DNA/dry weight (ng/mg)	426.2 ± 68.29	460.2 ± 29.63	ns
Collagen % dry weight	87.6 ± 2.64	86.71 ± 2.56	ns
Wet weight (mg/sample)	23.07 ± 1.30	22.41 ± 2.34	ns
DNA/wet weight (ng/mg)	75.4 ± 14.3	108.1 ± 7.2	**
Collagen % wet weight	15.47 ± 0.97	20.42 ± 1.88	**

Table 5.1. DNA, GAG and collagen content, dry and wet weight, DNA/dry weight (ng/mg), collagen %dry weight, DNA/wet weight (ng/mg) and collagen %wet weight of the decellularized skeletally immature and mature cartilage scaffolds. ns: not significant; *:$p \leq 0.05$; **: $p \leq 0.01$; ***: $p \leq 0.001$.

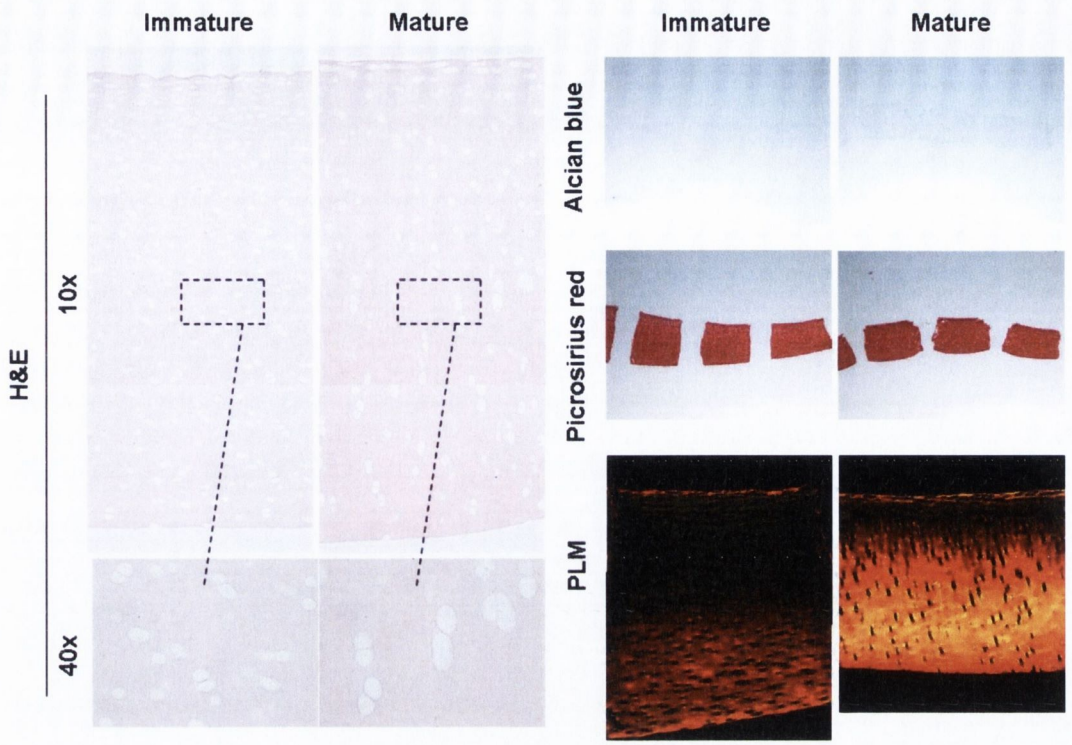

Figure 5.4. H&E, Alcian blue and Picrosirius red staining and PLM images of collagen architecture of decellularized skeletally immature and mature cartilage ECM-derived scaffolds. H&E images were taken at 10x, showing cell removal through the depth of the decellularized tissue, with images shown by box region taken at 40x. Images for Alcian blue and Picrosirius red were all taken at 10x. Regions with bright color in PLM images indicate the existence of an organized collagen alignment (either horizontal or perpendicular) in these regions, leading to birefringence. Dark regions indicate the lack of collagen alignment in these areas.

5.3.3. Decellularized cartilage scaffolds support stem cell attachment, viability and proliferation

The decellularized skeletally immature and mature cartilage scaffolds were then seeded with human IFP-MSCs and cultured for a total period of four weeks, with the viability of the cells inside the scaffolds monitored throughout the culture period. One day after cell seeding, viable cells were found throughout the channels, attaching to the walls of both decellularized immature and mature scaffolds (Fig. 5.5A). After 14 days of culture, significant cell proliferation was observed in both groups, with cells filling the channels and covering the periphery of the scaffolds. Channels were still well cellularized by day 28. Some dead cells were observed in the bottom regions of both decellularized scaffolds, nevertheless most cells still remained viable (Fig. 5.5A). DNA analysis showed significantly more cells had attached to the decellularized immature scaffolds on day 1 compared to the mature scaffolds (Fig. 5.5B; $p \leq 0.05$). However, significant cell proliferation was found in both decellularized scaffolds over the culture period (a near 5-fold increase in DNA content was observed in immature scaffolds and also a near 13-fold increase in DNA content was observed in mature scaffolds, both $p \leq 0.001$), such that by day 28 there was no significant difference in the DNA content of both constructs (Fig. 5.5B).

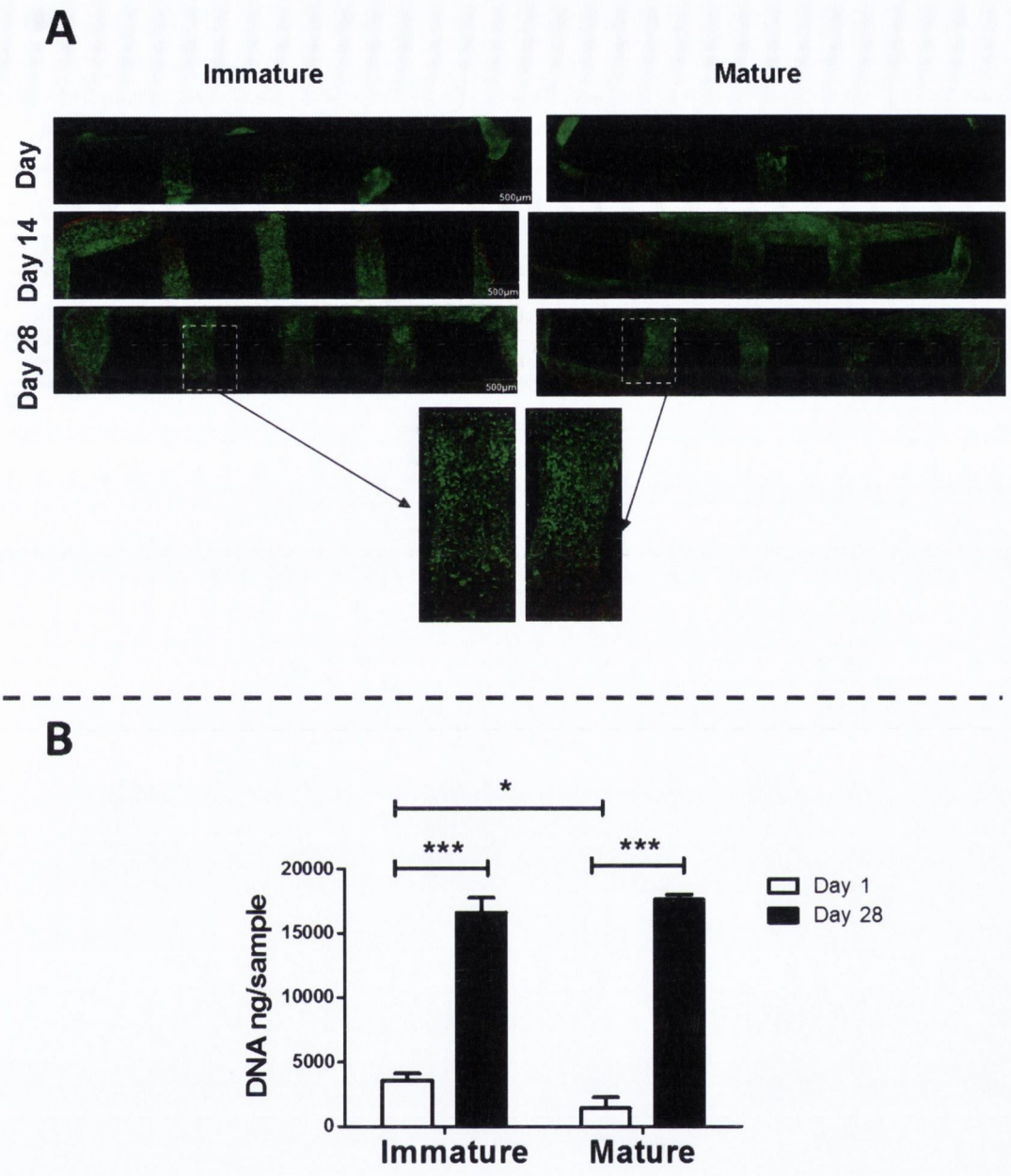

Figure 5.5. A: viability of IFP-MSCs seeded in decellularized immature and mature cartilage scaffolds at day 1, 14 and 28. Live cells appear green and dead cells appear red. Arrows indicate magnified images shown in box regions (channels). B: DNA content of the cells seeded in decellularized immature and mature cartilage scaffolds at day 1 and 28. The DNA content of the cells is calculated by subtracting the residual DNA content of the scaffolds from the total DNA content of the constructs.*: $p \leq 0.05$; ***: $p \leq 0.001$.

5.3.4. IFP-MSCs secreted comparable amounts of sGAG but higher levels of collagen in skeletally mature compared to immature cartilage scaffolds

After 28 days of culture, IFP-MSCs had secreted similar levels of sGAG in both decellularized scaffolds, but significantly higher levels of collagen in decellularized mature scaffolds compared to immature scaffolds ($p \leq 0.05$). Similar results were observed when levels of matrix synthesis were normalized to DNA levels (Fig. 5.6; $p \leq 0.05$). The ratio of collagen:sGAG synthesis in the decellularized immature scaffolds was ~0.4 compared to ~1.4 in the decellularized mature scaffolds ($p \leq 0.05$), approaching that observed in the native tissue (Fig. 5.6).

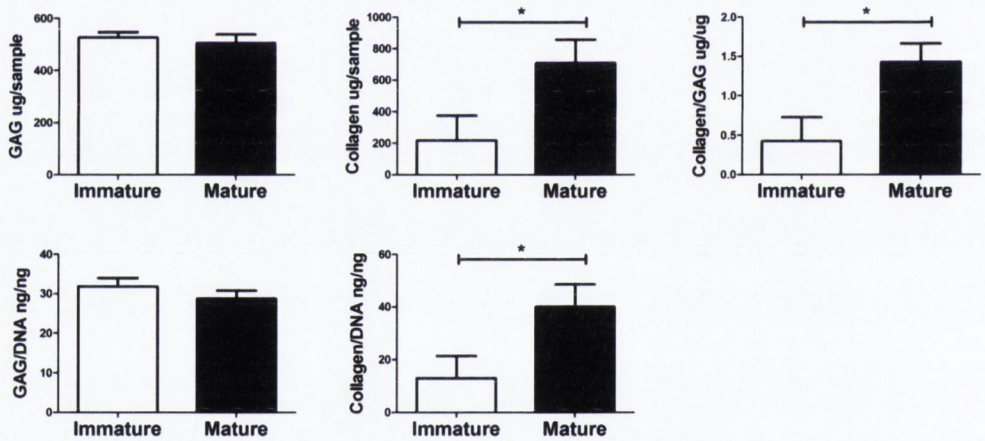

Figure 5.6. GAG, collagen, collagen/GAG (μg/μg), GAG/DNA (ng/ng) and collagen/DNA (ng/ng) level of the matrix secreted by IFP-MSCs inside the cell seeded decellularized immature and mature cartilage scaffolds at day 28. The GAG or collagen or DNA level of matrix secreted by cells is calculated by subtracting the residual GAG or collagen or DNA level of the decellularized scaffolds from the total GAG or collagen or DNA level of the constructs. *: $p \leq 0.05$.

Histologically, Alcian blue staining demonstrated sGAG deposition within the channels of both decellularized groups after 14 days of culture. This sGAG deposition continued with time in culture. By day 28, a cartilaginous tissue staining strongly for alcian blue filled more than half of most channels in both decellularized scaffolds, as well as covering the periphery of the scaffolds (Fig. 5.7). However, the bottom regions of both decellularized scaffolds stained less intensely for sGAG deposition, which is possibly due to lower cell viability in these regions (shown in Fig. 5.5A). Cells displayed a round chondrocyte-like morphology in both decellularized scaffolds (Fig. 5.7). There was some evidence of cell migration from the channels or periphery into the body of the scaffolds; however overall the scale of such migration appeared to be small. There was little evidence of cell synthesized sGAG diffusing into the body of the scaffolds (Fig. 5.7).

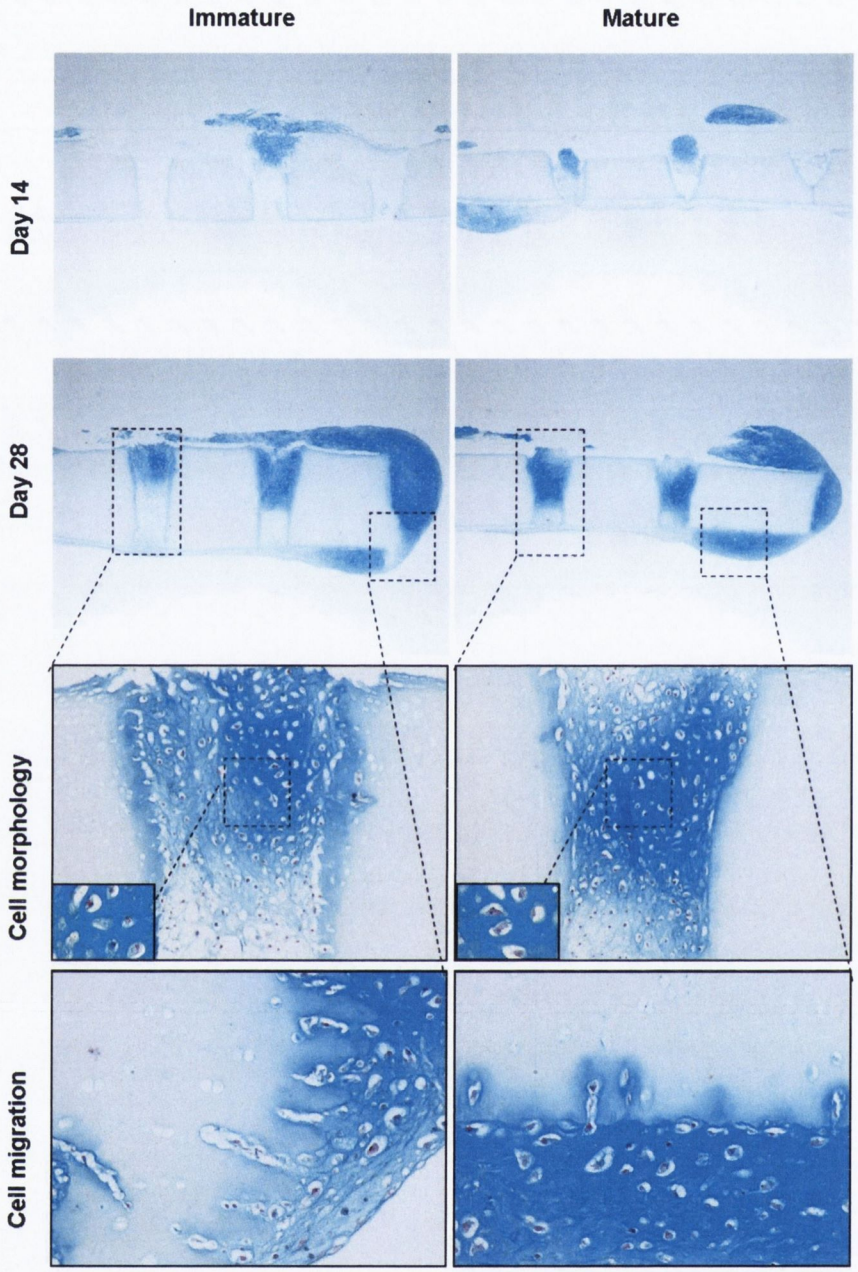

Figure 5.7. Alcian blue staining of cell seeded decellularized immature and mature cartilage scaffolds at day 14 and 28. Images from first and second row were taken at 2x. Images from third row were taken at 10x, showing cell morphology and GAG distribution within the channels, with inserted images taken at 40x. Images from last row were taken at 20x, showing cell migration into the ECM of the decellularized scaffolds at sites shown in box regions in images from the second row.

Positive staining for collagen deposition was observed in the channels of both decellularized scaffolds on day 14. By day 28, newly deposited collagen also filled more than half of the depth of the most channels and covered the periphery of both decellularized scaffold types (Fig. 5.8). Less collagen deposition was observed in the bottom region of both decellularized scaffolds.

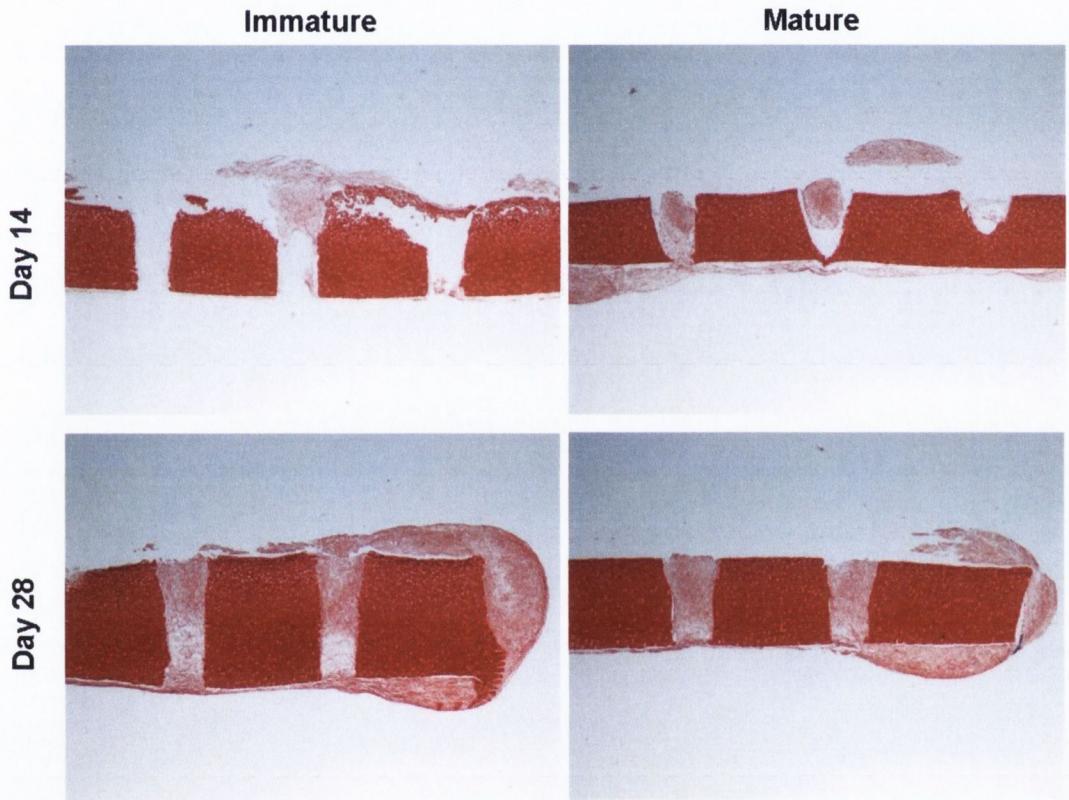

Figure 5.8. Picrosirius red staining of cell seeded decellularized immature and mature cartilage scaffolds at day 14 and 28. All images were taken at 2x.

5.3.5. Cellular and neo-matrix alignment in decellularized cartilage is driven by the underlying collagen architecture of the scaffold

The alignment of the cells seeded within the decellularized scaffolds was assessed throughout the culture period. On day 1, cells displayed a spread shape in both decellularized scaffolds. In the decellularized immature scaffolds, cells were generally aligned horizontally in each channel, whereas cells were generally aligned perpendicularly in the channels of mature scaffolds (Fig. 5.9). This cellular alignment was predominant in some channels but less obvious in others. A similar pattern of cellular alignment was found in the channels of both decellularized scaffolds at day 14. For both groups, a small portion of cells had re-organized their actin cytoskeleton, from a spread, tense structure into a more confined and round shape, resembling a chondrocyte-like phenotype (Fig. 5.9). By day 28, most cells displayed this round shape, thus the cellular alignment pattern was no longer obvious. However, some cells were still found to be spread and horizontally aligned in the channels of decellularized immature scaffolds, but perpendicularly aligned in the channels of decellularized mature scaffolds, similar to that observed on day 1.

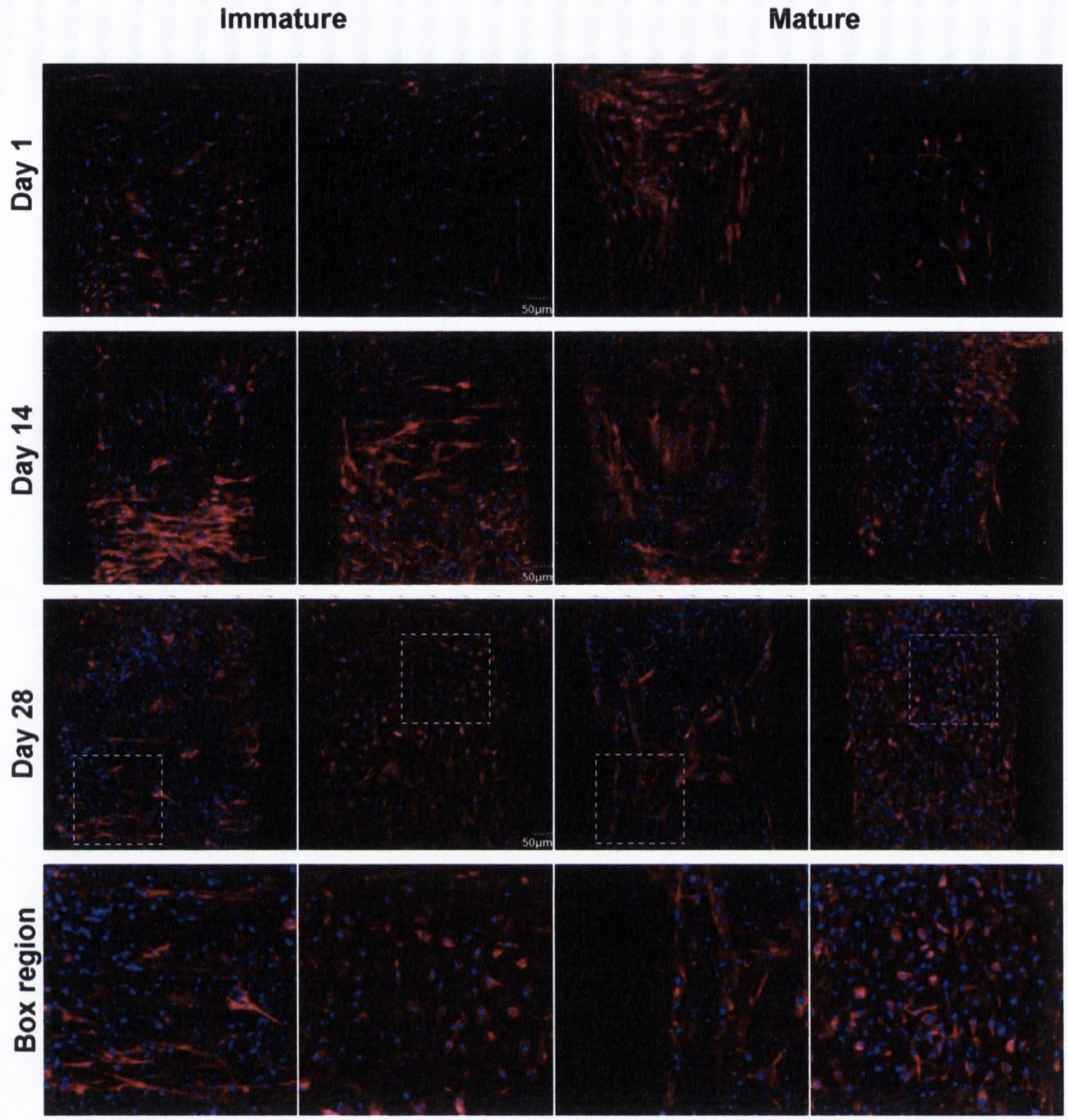

Figure 5.9. DAPI and F-actin staining showing cell alignment within the channels of cell seeded decellularized immature and mature cartilage scaffolds at day 14 and 28. Images in first and third column represent the highest degree of cell alignment observed in the two groups at corresponding time points, while images in second and fourth column represent the average degree of cell alignment observed in the two groups. Images from first to third row were all taken at 20x. Images from the fourth row show the magnified images of the box regions in third row.

The alignment of collagen fibers secreted by cells within the channels was assessed using PLM. On day 14, the new synthesized collagen fibers appeared to be perpendicularly aligned in the channels of the decellularized mature scaffolds, mimicking the alignment of the native collagen fibers within the decellularized scaffolds (Fig. 5.10). Collagen fiber alignment was less obvious in the immature scaffolds, which may be due to lower levels of matrix deposition within these scaffolds at this time point (see Fig. 5.8). A more obvious and predominant pattern of collagen fiber alignment was observed by day 28 in both scaffold types. Collagen fibers were found to be perpendicularly aligned through the depth of the channels in the mature scaffolds. In the immature scaffolds, the deposited collagen fibers were found to be horizontally aligned in the lower region of the channels but perpendicularly aligned in the upper regions of the channels (Fig. 5.10).

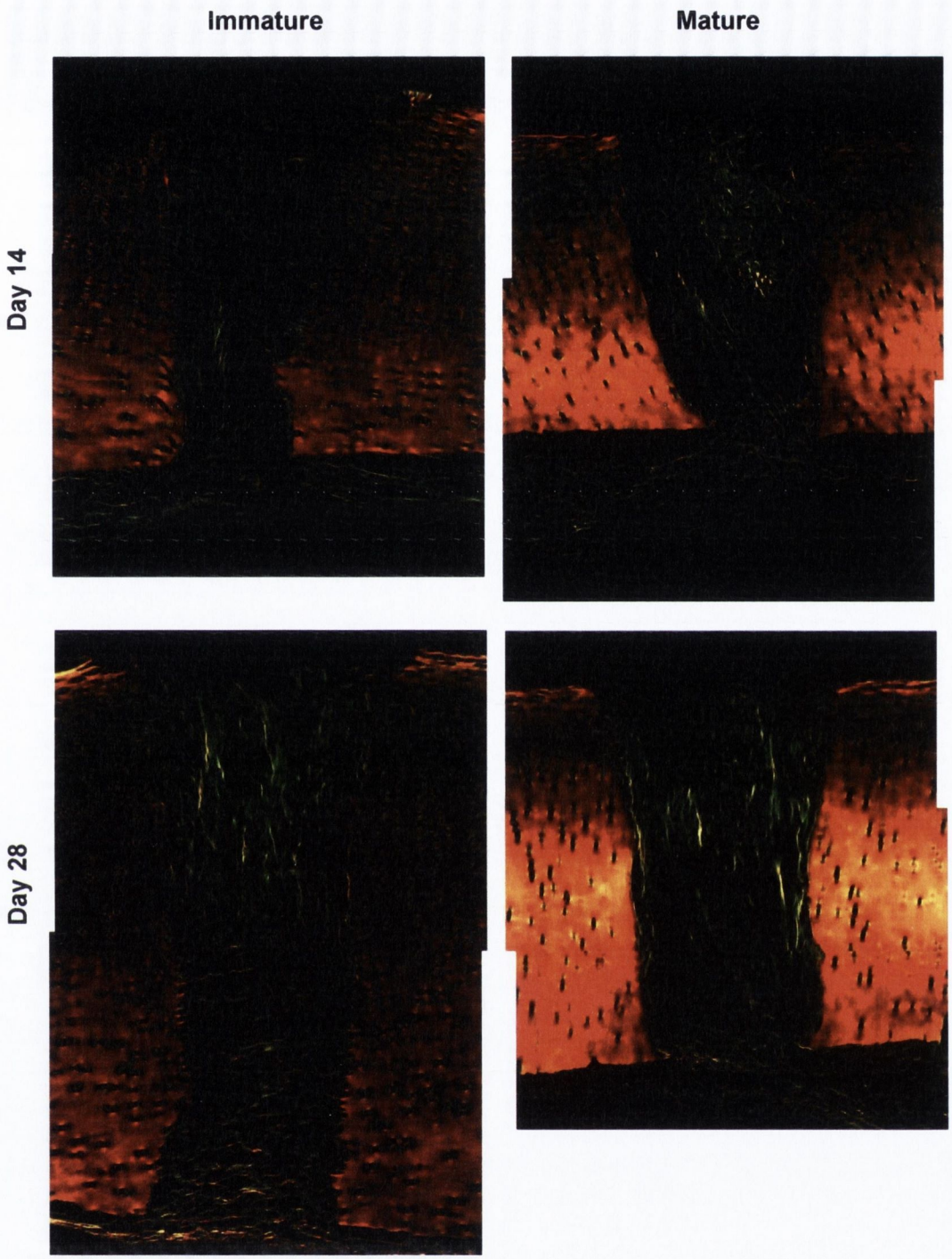

Figure 5.10. PLM images of collagen alignment within the channels of the cell seeded decellularized immature and mature cartilage scaffolds at day 14 and 28. All images were taken at 10x.

5.3.6. Re-population of decellularized skeletally mature cartilage scaffolds with IFP-MSCs leads to the development of engineered cartilage with mechanical properties mimicking the native tissue

By day 28, the total sGAG content of the engineered grafts (including cell synthesized and the residual in the decellularized scaffold) as a percentage of wet weight was ~1% for both scaffold types (Fig. 5.11A). The total collagen as a percentage of wet weight level was significantly higher in the mature grafts compared to immature grafts ($p \leq 0.001$), approaching that found in native articular cartilage (~10%; Fig 5.11A). The dynamic modulus of the immature grafts remained steady over the 28 days of culture whereas the dynamic modulus of the mature grafts increased significantly. At day 28, the dynamic modulus of mature grafts reached 2132 kPa, significantly (~twice) higher than that of the immature grafts (Fig. 5.11B; $p \leq 0.001$).

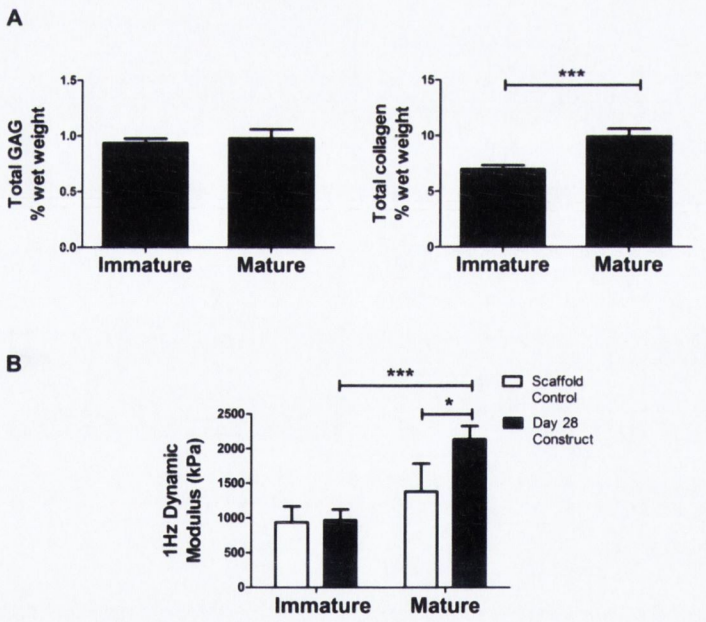

Figure 5.11. A) Total GAG %wet weight and total collagen %wet weight level of the engineered immature and mature cartilage grafts at day 28; B) 1Hz dynamic modulus (kPa) of the immature and mature cartilage scaffold controls and cell seeded constructs at day 28. *: $p \leq 0.05$; ***: $p \leq 0.001$.

The equilibrium modulus through the depth of IFP-MSCs seeded constructs (at 5% global offset strain) was computed after 1 and 28 days of culture. There was little evidence of an increase in the equilibrium compressive modulus with depth in IFP-MSCs seeded scaffolds after 1 day of culture (Fig. 5.12A). In contrast, a notable trend towards an increase in modulus with depth was observed after 28 days of culture, particularly for mature grafts.

We next sought to determine if re-populating the decellularized cartilage scaffolds with IFP-MSCs would lead to the development of cartilaginous tissues demonstrating the characteristic strain softening behavior (a reduction in compressive modulus with increases in applied strain) observed in the native tissue. To test this, the compressive modulus in the deep zone of the engineered tissue was computed for increasing levels of applied strain. There was little evidence of such strain softening behavior directly after seeding the scaffold with IFP-MSCs (day 1). In contrast, there was a notable reduction in modulus with increasing levels of applied strain in engineered tissues after 28 days of culture (Fig. 5.12B). Specifically, the modulus of mature constructs after 28 days of culture decreased from 4.42 MPa at 2.5% offset strain to 0.36 MPa at 10% offset strain ($p \leq 0.05$), compared to 0.2 MPa at 2.5% offset strain and 0.09 MPa at 10% offset strain at day 1. Strain softening was less obvious in the immature constructs, where the modulus after 28 days of culture decreased from 0.96 MPa at 2.5% offset strain to 0.29 MPa at 10% offset strain, compared to 0.19 MPa at 2.5% offset strain and 0.06 MPa at 10% offset strain at day 1.

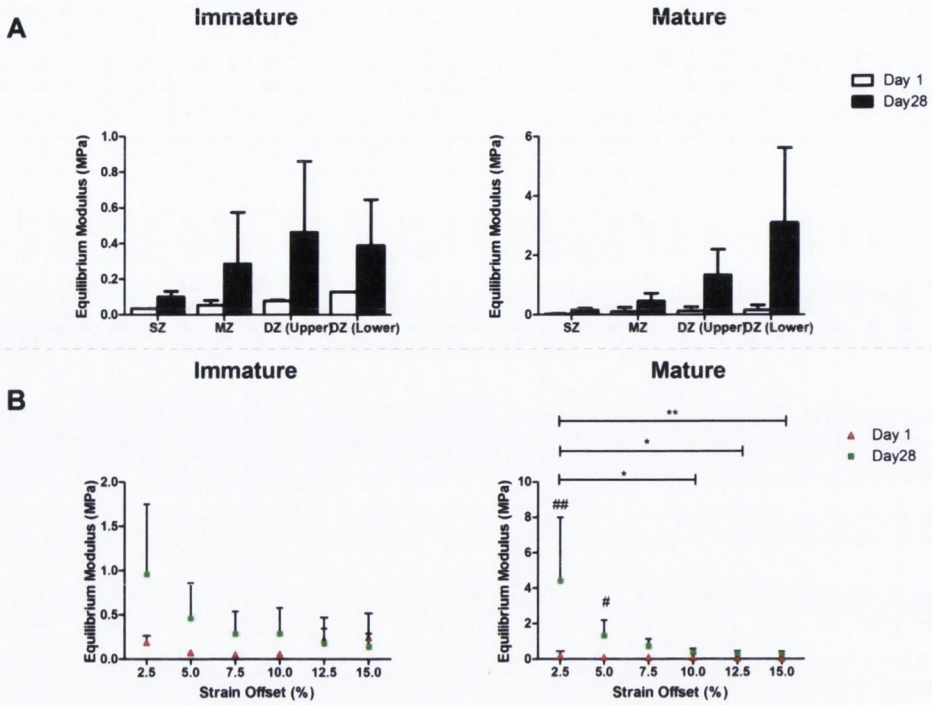

Figure 5.12. A: The equilibrium modulus (for a global compressive strain of 5%) of the superficial zone (SZ), middle zone (MZ), upper deep zone (DZ-upper) and lower deep zone (DZ-lower) of the day 1 and 28 cell seeded decellularized immature and mature scaffolds. B: The equilibrium modulus of the upper deep zone of the day 1 and 28 cell seeded decellularized immature and mature scaffolds for 2.5%, 5% 7.5%, 10%, 12.5% and 15% global strain. *:p≤0.05; **: p≤0.01; #:p≤0.05 vs. day1; ##: p≤0.01 vs. day1.

5.4. Discussion

The overall objective of the study was to repopulate decellularized cartilage grafts (herein termed *scaffolds*) with IFP-MSCs, with the aim of engineering functional cartilage constructs with structure, composition and depth-dependent mechanical properties equivalent to the native tissue. First, a decellularization protocol was developed, which resulted in a ~88% reduction in DNA content and near complete removal of GAG, while maintaining the collagen content and architecture of the native tissue. Decellularized scaffolds derived from skeletally immature and mature cartilage grafts were then seeded with IFP-MSCs and cultured for 4 weeks. Both scaffold types supported stem cell attachment, viability and proliferation, with cells seeded in skeletally mature scaffolds displaying significantly higher levels of proliferation and collagen synthesis compared to those seeded in immature scaffolds. Cellular and neo-matrix alignment was found to depend on the underlying collagen architecture of the scaffolds. The impact of this was that cartilage tissues engineered using stem cell laden scaffolds derived from skeletally mature grafts demonstrated a collagen structure and content, depth-dependent mechanical properties, and a straining softening behaviour characteristic of native mature articular cartilage. To the best of our knowledge this is the first time such native tissue-like functionality has been recapitulated in engineered cartilaginous grafts.

Decellularization resulted in a ~88% reduction in the DNA content of cartilage tissues. The decellularization was more effective for the immature cartilage tissues, which may be due to the fact that the ECM of the mature tissue is denser and more organized, hence creating a greater barrier for the diffusion of decellularization solutions and the removal of residual DNA. Previous studies have reported similar, higher or lower levels of DNA removal post-decellularization. For example, after a 6 day wash in a hypotonic buffer containing 0.1% (w/v) SDS, Kheir et al. showed a near complete (~99%) removal of genomic DNA from the decellularized cartilage-bone constructs (Kheir et al., 2011). While using a 20 times higher SDS concentration (2%)

but a shorter incubation period (8 h), Elder al. reported only a 40% reduction in DNA content of the decellularized articular cartilage tissue (Elder et al., 2010). It should be noted however that the measured levels of DNA remaining in decellularized scaffolds are still higher than recommended limits proposed in the literature for decellularized ECM derived scaffolds (<50 ng dsDNA per mg ECM dry weight) to prevent an adverse host response (Crapo et al., 2011). While such stringent criteria may not be required for implantation into articular cartilage defects, regions often described as immune-privileged (Benders et al., 2013), additional work is warranted to further reduce the DNA content of decellularized tissues.

Both the collagen content and collagen network organization appeared unaffected by the decellularization procedure. Previous studies have also shown that SDS does not affect the collagen content, structure or tensile properties of articular cartilage when used at appropriate concentrations and incubation periods (Elder et al., 2010, Kheir et al., 2011). A near-complete removal of GAG was observed, which was to be expected due to the inclusion of hyaluronidase treatment into the decellularization procedure. This step was included based on the assumption that the removal of GAG would lead to a more porous scaffold, thereby facilitating removal of DNA and recellularization of the scaffold. It should be noted however that many decellularization procedures that lack hyaluronidase treatment, but which contain one or more cycles of SDS washes, can lead to significant or even complete removal of GAG in articular cartilage (Elder et al., 2010, Kheir et al., 2011).

Decellularized cartilage was found to provide a substrate supportive of stem cell proliferation. This may be explained, at least in part, by the significant increase in surface area provided by the introduction of channels into the cartilage grafts. It is well established in the tissue engineering literature that increases in scaffold porosity and/or surface area support stem cell proliferation (Murphy et al., 2010, Matsiko et al., 2014). The residual (primarily type II) collagen network within the decellularized tissue may also be supporting cellular growth. Previous studies have found that type

II collagen promoted cell proliferation at a dose-dependent manner (Qi and Scully, 1997), and resulted in a significantly higher biosynthesis rate in chondrocytes compared to type I collagen (Bosnakovski et al., 2006, Nehrer et al., 1997, Veilleux et al., 2004). Furthermore, any growth factors potentially reserved in the scaffolds after decellularization may be supportive of stem cell proliferation. Some cell death was observed towards the bottom of the channels within the decellularized scaffolds. This is likely due to nutrient transfer limitations within such regions of the engineered tissues leading to cell death.

Scaffolds derived from skeletally mature cartilage were found to provide a substrate more supportive of stem cell proliferation and collagen synthesis than those derived from immature tissue. Previous studies in our lab have reported that the thickness of collagen fibers increases dramatically with skeletal maturity, from approximately 20 nm in 4 week old cartilage to nearly 200 nm in 3 year old cartilage (Gannon, 2013). Studies have demonstrated that increases in fiber diameter in electrospun scaffolds can lead to increases in cell proliferation (Badami et al., 2006), thus suggesting that the larger sized fibers in the skeletally mature scaffolds may be supporting greater levels of cell proliferation. Chondrogenesis in electrospun scaffolds has also been shown to depend on the fiber diameter, with enhanced collagen type II expression observed on scaffolds with a 300 nm fiber diameter (Noriega et al., 2012), similar to the collagen fiber diameter of the mature tissues. Other differences between scaffolds derived from immature and mature cartilage, such as the type of collagen present in the tissue and it structural alignment, may also be contributing to the findings of enhanced proliferation and collagen matrix synthesis in the scaffolds derived from mature articular cartilage.

The alignment of cells, and the collagen they synthesized, strongly depended on the underling alignment of the collagen network in the decellularized scaffolds, and this was achieved through the seeded cells sensing the collagen fiber alignment on the surface area of the channels. In scaffolds derived from skeletally mature tissue, the

collagen network that formed in the channels mimicked the classic Benninghoff architecture that is characteristic of fully developed articular cartilage. Previous studies have also shown that the underlying substrate architecture can direct cellular and neo-matrix alignment (Gilchrist et al., 2014, Guillemette et al., 2009, Ma et al., 2011) and even the biosynthesis activity of the cells (Ma et al., 2011).

Critically, the impact of re-populating decellularized cartilage scaffolds derived from skeletally mature donors with IFP-MSCs was the development of engineered constructs with mechanical properties (i.e. depth-dependent compressive modulus, strain softening) that mimicked the native tissue after 4 weeks in culture. Following decellularization, which resulted in a complete loss in tissue GAG content, neither the immature or mature grafts displayed such mechanical behavior and had mechanical properties dramatically lower than the native tissue (Gannon, 2013). This is in agreement with previous studies that have demonstrated how proteoglycans electrostatically and non-electrostatically contribution to the compressive properties of articular cartilage (Canal Guterl et al., 2010). The mechanical properties of the engineered tissues dramatically improved over 28 days in culture. At low offset strains (2.5% strain), the equilibrium modulus of the deep zone of tissues engineered using mature scaffolds exceeded 4 MPa, which compares to approximately 9 MPa for the native tissue (Gannon, 2013). Furthermore, the characteristic strain softening behavior of the native tissue re-emerged following the deposition of proteoglycans inside the scaffold. These newly deposited proteoglycans will promote the development of an osmotic swelling pressure within the engineered tissue, which in turns will generate a state of pre-stress or tension within the existing collagen network. High loads are initially required to relieve this pre-stress as the tissue is compressed, but once the fibers are no longer in tension they no longer contribute to the compressive properties of the tissue and hence the engineered construct starts to appear softer with increasing levels of applied strain. The fact that the collagen fibers are thicker and aligned predominantly perpendicular to the direction of applied strain in the deep zone of the mature scaffolds likely explains why the development

of proteoglycan induced swelling in these constructs leads to greater increases in compressive modulus with depth in these constructs compared to the immature scaffolds.

One of the limitations of this study is the limited cellular infiltration into the body of scaffolds, likely due to dense nature of the cartilage ECM. This challenge has previously been reported when attempting to re-populate decellularized cartilaginous grafts (Kheir et al., 2011, Schwarz et al., 2012a). For example, cellular infiltration only ~200 μm into the body of a decellularized cartilage-bone scaffold has been reported 3 months after implantation into nude mice. Such challenges may potentially be overcome by increasing the number of channels in the decellularized scaffolds, which may accelerate the in vivo host cell infiltration and tissue remodelling process. Even without such modifications, it may be that such scaffolds will be adequately re-cellularized following implantation into a load-bearing orthotopic defect. Another limitation is that the GAG level of the engineered grafts is still lower than that of the native tissue, in part because all GAG was removed from the scaffolds during decellularization. Further studies may seek to retain some level of GAG in the decellularized scaffolds, which may improve the mechanical properties of the scaffolds.

In conclusion, this study highlights the importance of scaffold architecture on engineering zonal cartilage grafts. Scaffolds derived from decellularized articular cartilage tissue, which maintain the original collagen content and structure of the native tissue, can facilitate the regeneration of cartilage grafts with native-like structure, composition and depth-dependent mechanical properties. The limitation with cell infiltration into the body of the scaffolds may be overcome by approaches such as the introduction of larger numbers of channels into the scaffolds. Alternatively, the results of this study may inspire the design of novel scaffolds derived from natural or synthetic polymers to produce biomaterials that mimic many of the structural features of the decellularized tissue, but which have a higher

porosity to facilitate greater cellular migration. Indeed, many novel scaffold fabrication techniques are now available that may facilitate this (Moutos et al., 2007, McCullen et al., 2012, Steele et al., 2014). Manipulating scaffold architecture to mimic the collagen architecture of the native tissue appears to be critical for engineering functional articular cartilage grafts.

Chapter VI

Discussion

6.1. Overview

The overall goal of this thesis was to engineer a cartilage graft with depth-dependent structure, composition and mechanical properties mimicking the native tissue. A prerequisite for any cartilage tissue engineering strategy is the identification of a suitable sell source. A previous study from our lab (Thorpe et al., 2013) has shown that cartilage grafts mimicking aspects of the zonal composition of articular cartilage can be engineered using BM-MSCs, by regulating the oxygen and mechanical environment through the depth of the developing constructs. There were, however, limitations associated with this approach including hypertrophy and low mechanical properties of the engineered grafts. This motivated the use of IFP-MSCs in this thesis. However, few studies have investigated how IFP-MSCs would respond to mechanical stimuli, such as dynamic compression. Therefore, in the first study of this thesis, we compared the effects of dynamic compression on chondrogenesis of both BM-MSCs and IFP-MSCs. Both cell types could be used to engineer cartilage grafts with GAG content and bulk compressive mechanical properties approaching those observed in skeletally immature articular cartilage. Although the application of dynamic compression had no significant effect on matrix accumulation or bulk compressive properties of IFP-MSCs laden agarose hydrogels, the cartilage engineered using IFP-MSCs show no mineralization or expression of type I collagen, unlike those engineered using BM-MSCs.

Having identified IFP-MSCs as a promising cell source for engineering phenotypically stable cartilage grafts, we then sought to explore if these cells could be used to engineer cartilaginous tissues with a zonal composition mimicking that of the articular cartilage. IFP-MSCs were encapsulated in agarose hydrogel to make constructs of either 2 mm or 4 mm in height. Constructs were confined to half of their height and subjected to dynamic compression, in an attempt to mimic the spatial oxygen and mechanical environment within articular cartilage. The size of cell seeded constructs was found to dramatically impact spatial nutrient availability and

subsequent matrix deposition within the constructs, with 2 mm high constructs showing a relatively homogeneous matrix distribution, while the 4 mm high constructs contained a bottom core region with little matrix deposition. Confinement coupled with dynamic compression led to an increase in collagen synthesis and type II collagen deposition at the top of both 2 mm and 4 mm constructs, which correlated with the predicted increase in compressive and tensile strain levels at the top of these constructs. Furthermore, the superficial region of both 2 mm and 4 mm confined dynamically compressed (CDC) constructs stained strongly for type II collagen and weakly for GAG, with proteoglycan 4 (PRG4) further observed in 4 mm CDC samples, mimicking certain aspects of the zonal composition of articular cartilage.

While this strategy was able to recapitulate certain aspects of the zonal composition of articular cartilage, there was no evidence that the classic benninghoff collagen architecture of mature articular cartilage was recapitulated in these grafts. Also, the bulk mechanical properties of the engineered grafts were still much lower than those of the native tissue. Therefore, I next explored if re-populating decellularized cartilage ECM-derived scaffolds, where the original tissue collagen structure was maintained, with IFP-MSCs, can lead to the regeneration of cartilage grafts with structure, composition and mechanical properties mimicking native tissue. Skeletally immature and mature articular cartilage were decellularized using a protocol that significantly reduced the DNA content and completely removed the GAG content, while maintaining the collagen content of the tissue. Notably, we also observed that the depth-dependent collagen architecture of both skeletally immature and mature tissue was maintained post-decellularization. These decellularized scaffolds were then seeded with IFP-MSCs and cultured for 4 weeks. Both scaffold types were shown to support cell attachment, viability and proliferation. Interestingly, cells seeded in skeletally mature scaffolds displayed significantly higher proliferation and collagen synthesis compared to those seeded in immature scaffolds. Cellular and neo-matrix alignment within the channels of these decellularized scaffolds was found to depend

on the underlying collagen architecture of the scaffolds. Importantly, cartilage tissues engineered using mature scaffolds seeded with human IFP-MSCs demonstrated a collagen structure and content, depth-dependent compressive properties, and a characteristic straining softening behavior mimicking native mature articular cartilage.

6.2. Is there an ideal approach to engineering zonal cartilage grafts?

This thesis explored two different approaches for zonal cartilage tissue engineering. Each approach has its own advantages and disadvantages, which will be discussed in the following section.

The first approach utilized a bioreactor system to regulate the oxygen and mechanical environment within the developing stem cell laden constructs. This approach led to the development of engineered tissues with a native-like composition through their depth. Engineered grafts displayed a superficial region mimicking that of native tissues, with strong positive staining for type II collagen, weak staining for GAG and expression of PRG4. PRG4 is a molecule expressed by the chondrocytes on the surface of articular cartilage to provide boundary lubrication and low-friction properties for the tissue, and it has been shown to be up-regulated in chondrocytes by the application of mechanical stimuli (Grad et al., 2005, Nugent-Derfus et al., 2007). Notably, the expression of PRG4 was not observed in any other experimental groups within this study, except for the confined dynamically compressed (CDC) constructs. The attainment of a high collagen content and expression of PRG4 in the superficial region of the engineered tissue, may better equip grafts to withstand the challenging loading environment in the joint. Furthermore, the application of confinement and dynamic compression may prime

cells for the low oxygen environment and challenging mechanical conditions they will experience following implantation into a defect within articular cartilage. If cells can pre-adapt to the native-like environment during *in vitro* culture, it may better equip cells to thrive in the complex *in vivo* environment or shorten the adapting period. Lastly, compared to decellularized ECM-derived scaffolds, the agarose used in this study to encapsulate cells is a readily available material, and the cell-laden agarose hydrogel can be made in any size and shape, without risks of disease transmission.

However, it should be noted that there are a few disadvantages about this bioreactor approach. First of all, it requires the use of a complex bioreactor system and relatively complicated handling procedure in the using of this system, which is time-consuming. User friendliness is an important criterion for any bioreactor system, thus the existing bioreactor design need to be improved. Furthermore, even after 6 weeks of culture, the overall mechanical properties of the engineered grafts are still significantly lower than those of native tissues. Also there is no evidence of the acquisition of the Benninghoff collagen architecture of mature articular cartilage in the engineered grafts.

In contrast, the alternative approach which utilized decellularized cartilage ECM-derived scaffolds for engineering zonal cartilage, may overcome some of the limitations mentioned above. First, decellularized cartilage derived scaffolds maintained the collagen architecture of the native tissue. This in turn can be used as a template to direct seeded cells to orient themselves and their synthesized matrix (Gilchrist et al., 2014, Guillemette et al., 2009, Ma et al., 2011), such that the neo-matrix structure/orientation is in line with the existing collagen architecture in the scaffolds. Secondly, the decellularized cartilage scaffolds primarily consist of natural collagen. Since the collagen content of articular cartilage was maintained after decellularization, the engineered grafts reached a total collagen content of 10% of tissue wet weight. This overcomes a current major limitation of tissue engineered cartilage grafts, which is the low collagen content of such tissues. Furthermore,

decellularized cartilage derived scaffolds were not only rich in collagen content, but also may contain various other molecules, such as fibronectin and many growth factors including FGF-2 and TGFβ-3. These molecules have been shown to promote cell attachment, proliferation and differentiation (Arenas-Herrera et al., 2013). Lastly, even over a relatively short culture period (4 weeks), the engineered grafts demonstrated mechanical properties approaching those of mature articular cartilage, likely due to the deposition of sGAG as well as acquisition of a native-like collagen network within the engineered constructs.

Nevertheless, there are also several limitations associated with the decellularized cartilage derived scaffold approach. The decellularized scaffolds are not readily available like many commercial materials. Since raw samples need to be taken from animal donors, certain risks of disease transmission from animal to human is involved. Although the decellularization procedure may possibly inactivate some pathogens, it takes considerable amount of time (in this case 2 weeks). Furthermore, the thickness of the produced scaffolds is limited to that of the animal donor (in this case, scaffolds were ~1mm thick, whereas the average thickness of human articular cartilage is ~2 mm). However, this may be overcome by switching to an alternatively cartilage source, such as bovine articular cartilage. Most importantly, limited cell infiltration into the body of scaffolds was observed over 4 weeks of culture. This was due to the dense nature of the decellularized cartilage ECM, which limited cell migration throughout the construct. The *in vivo* environment is much more complex, with various types of macrophages present which may help in remodelling of an implanted construct, thus perhaps would help to accelerate the cell infiltration (Benders et al., 2013). Mechanical loading associated with the joint may also facilitate this process. Thus, further animal studies where the construct is implanted into a load bearing defect will be required to examine if the host cells can fully re-populate the decellularized scaffolds over time.

To conclude, comparing the two approaches discussed above, I am of the belief that the second approach (decellularization of articular cartilage tissues) may represent a better way to engineer zonal cartilage grafts, given the importance of the acquisition of the collagen architecture on mechanical properties of the engineered tissue. However, the ideal approach to zonal cartilage tissue engineering may involve a combination of both strategies. For example, cell seeded decellularized cartilage scaffolds could be subjected to partial confinement and dynamic compression. Perhaps dynamic compression may facilitate cell infiltration into the scaffolds. Also by priming engineered grafts with a native-like culture environment, it may better equip the engineered grafts to thrive in the very challenging *in vivo* environment.

6.3. Implications for the design of novel scaffolds for zonal cartilage tissue engineering

The last study of this thesis highlighted the impact of scaffold architecture on engineering zonal cartilage grafts. Decellularized cartilage ECM-derived scaffolds, which maintain the original tissue structure, may facilitate the regeneration of cartilage tissue with native-like structure, composition and mechanical properties. Limitations with cell infiltration into the body of scaffolds may be improved by approaches such as the introduction of channels into the scaffolds. Furthermore, the complex *in vivo* environment may also facilitate cell migration into scaffolds.

Alternatively, structurally organized scaffolds mimicking certain aspect of the collagen architecture of articular cartilage may be produced using novel techniques such as bioprinting and/or electrospinning. Bioprinting technology can produce scaffolds with highly reproducible architecture, controlled pore size, geometry and orientation (Woodfield *et al.*, 2004). Therefore, it could be used to produce scaffolds which mimic the collagen fiber alignment in the superficial and deep zone of articular

cartilage to a certain degree, albeit with larger pore size, porosity and inter-connectivity than those of the decellularized cartilage scaffolds produced in this study. However, to the best of my knowledge, it is not clear if current scaffold fabrication techniques can capable of printing fibers at the nanometer scale (Klein et al., 2009a). Compared to micrometer scale fibers, nanometer scale fibers more closely mimic the native collagen fiber size, and can provide a 3D environment more conductive for cell attachment and appropriate differentiation. Micrometer scale fibers tend to provide a 2D environment for cells to attach. For example, it has been shown that small fiber scaffolds promote more robust chondrogenesis than large fiber scaffolds (Li et al., 2006). In contrast, electrospinning technology enables the production of scaffolds with fibers at a nanometer scale. It also allows for the control of the orientation of fibers. Thus, with this technology it is possible to fabricate a scaffold with aligned fiber orientation mimicking the collagen architecture of articular cartilage to a certain degree (McCullen *et al.*, 2012). However, the produced aligned fiber scaffolds tend to have a very small pore size, which could also limit cell migration into the scaffolds. Nevertheless, this may be overcome by the addition of sacrificial fibers, which is spun together with the major fibers but later will be digested to increase the porosity of scaffolds (Baker et al., 2008). Emerging technologies, such as melt electrospinning, may overcome many of these limitations. For example, it has been demonstrated that the predictable deposition location of melt electrospun fibers can be combined with an automated laterally translating collection system to create a direct writing process which allows the design and fabrication of scaffolds with controllable architectures and patterns (Brown et al., 2011).

In conclusion, the author suggests that the ideal scaffold for engineering zonal cartilage grafts should have a structure mimicking the Benninghoff collagen architecture of mature articular cartilage, a suitable pore size and porosity to facilitate cellular migration and infiltration, as well as supporting chondrogenesis of seeded cells.

Chapter VII

Conclusions and Future Directions

7.1. Main findings and conclusions

The overall objective of this thesis was to engineer a cartilage graft with depth-dependent structure, composition and mechanical properties mimicking native tissue using IFP-MSCs. After firstly investigating of effects of dynamic compression on the chondrogenesis of IFP-MSCs, two approaches were then explored to achieve this goal. These were: 1) the use of partial confinement and dynamic compression to regulate the oxygen and mechanical environment within stem cell laden hydrogels; and 2) re-populating decellularized cartilage ECM-derived scaffolds (which maintain the original structure of the native tissue) with human IFP-MSCs. The main conclusions of this thesis are as follows:

- Both BM-MSCs and IFP-MSCs were capable of regenerating cartilage grafts with GAG content and bulk compressive mechanical properties approaching those of the skeletally immature articular cartilage. While, the spatial matrix deposition in the engineered grafts strongly depended on the MSC source.

- Depending on the donor, dynamic compression either enhanced or had no effect on the functional development of cartilage grafts engineered using BM-MSCs. in contrast, the application of dynamic compression (in isolation) had no significant effect on the functional development of cartilage grafts engineered using IFP-MSCs.

- Constructs engineered using BM-MSCs expressed type I collagen and began to calcify *in vitro*, with dynamic compression further suppressing the expression of type I collagen and mineralization. In contrast, constructs engineered using IFP-MSCs showed no evidence of hypertrophy or endochondral ossification.

- The size of cell seeded constructs had a great impact on the spatial nutrient availability and subsequent matrix deposition within the constructs.

- It is possible to engineer cartilage grafts mimicking certain aspects of the zonal composition of articular cartilage, such as high levels of collagen accumulation and expression of PRG4 in the superficial region of engineered tissues, by spatial regulating the oxygen and mechanical environment within IFP-MSCs seeded hydrogels.

- It is possible to decellularize articular cartilage grafts, with significant removal of DNA and GAG content, while maintaining the tissues collagen content and architecture.

- Decellularized cartilage derived scaffolds that keep the original tissue structure can support the attachment, proliferation and chondrogenic differentiation of IFP-MSCs. They also provide a natural template for the seeded IFP-MSCs to align and orient their synthesized matrix in a pattern mimicking the underlying collagen architecture of the scaffold.

- Re-populating decellularized mature cartilage scaffolds with IFP-MSCs can lead to the regeneration of cartilage grafts with a collagen structure and content, depth-dependent compressive properties, as well as a characteristic strain softening behavior mimicking native mature articular cartilage.

To conclude, this thesis highlighted the importance of environmental factors and scaffolds architecture for zonal cartilage tissue engineering. Also it may provide insights into scaffold design for general tissue engineering applications.

7.2. Future directions

While this thesis explored certain approaches for zonal cartilage tissue engineering, there are still a number of key questions that need to be addressed. Furthermore, other strategies could be further explored and evaluated in order to engineer zonal cartilage grafts. The following recommendations are made for future work on the subject of this thesis.

- *In vivo* evaluation of IFP-MSCs seeded decellularized mature cartilage scaffolds in an orthotropic cartilage defect, to explore if host cells can fully re-populate the scaffolds over time and promote good quality hyaline cartilage repair.

- Explore the idea of combining the first and second approach for engineering zonal cartilage grafts (i.e. apply confinement and dynamic compression to IFP-MSCs seeded decellularized mature cartilage scaffolds). Furthermore, to evaluate and compare the long term cartilage repair outcome using constructs engineered using these three approaches (bioreactor, decellularized scaffolds and combined approach).

- Identify methods to improve the porosity of the decellularized scaffolds to facilitate cellular migration and infiltration.

- Explore the possibility of using electrospinning to produce synthetic scaffolds mimicking the collagen architecture of mature articular cartilage.

Chapter VIII

Bibliography

ALBRO, M. B., LI, R., BANERJEE, R. E., HUNG, C. T. & ATESHIAN, G. A. 2010. Validation of theoretical framework explaining active solute uptake in dynamically loaded porous media. *J Biomech,* 43, 2267-73.

ARENAS-HERRERA, J., KO, I., ATALA, A. & YOO, J. 2013. Decellularization for whole organ bioengineering. *Biomedical Materials,* 8, 014106.

BADAMI, A. S., KREKE, M. R., THOMPSON, M. S., RIFFLE, J. S. & GOLDSTEIN, A. S. 2006. Effect of fiber diameter on spreading, proliferation, and differentiation of osteoblastic cells on electrospun poly (lactic acid) substrates. *Biomaterials,* 27, 596-606.

BAKER, B. M., GEE, A. O., METTER, R. B., NATHAN, A. S., MARKLEIN, R. A., BURDICK, J. A. & MAUCK, R. L. 2008. The potential to improve cell infiltration in composite fiber-aligned electrospun scaffolds by the selective removal of sacrificial fibers. *Biomaterials,* 29, 2348-58.

BAKER, B. M., SHAH, R. P., HUANG, A. H. & MAUCK, R. L. 2011. Dynamic tensile loading improves the functional properties of mesenchymal stem cell-laden nanofiber-based fibrocartilage. *Tissue Eng Part A,* 17, 1445-55.

BENDERS, K. E., VAN WEEREN, P. R., BADYLAK, S. F., SARIS, D. B., DHERT, W. J. & MALDA, J. 2013. Extracellular matrix scaffolds for cartilage and bone regeneration. *Trends Biotechnol,* 31, 169-76.

BENYA, P. D. & SHAFFER, J. D. 1982. Dedifferentiated chondrocytes reexpress the differentiated collagen phenotype when cultured in agarose gels. *Cell,* 30, 215-24.

BHOSALE, A. M. & RICHARDSON, J. B. 2008. Articular cartilage: structure, injuries and review of management. *Br Med Bull,* 87, 77-95.

BIAN, L., ZHAI, D. Y., ZHANG, E. C., MAUCK, R. L. & BURDICK, J. A. 2012. Dynamic compressive loading enhances cartilage matrix synthesis and distribution and suppresses hypertrophy in hMSC-laden hyaluronic acid hydrogels. *Tissue Eng Part A,* 18, 715-24.

BOSNAKOVSKI, D., MIZUNO, M., KIM, G., TAKAGI, S., OKUMURA, M. & FUJINAGA, T. 2006. Chondrogenic differentiation of bovine bone marrow mesenchymal stem cells (MSCs) in different hydrogels: influence of collagen type II extracellular matrix on MSC chondrogenesis. *Biotechnol Bioeng,* 93, 1152-63.

BRITTBERG, M., LINDAHL, A., NILSSON, A., OHLSSON, C., ISAKSSON, O. & PETERSON, L. 1994. Treatment of deep cartilage defects in the knee with autologous chondrocyte transplantation. *N Engl J Med,* 331, 889-95.

BRITTBERG, M., PETERSON, L., SJOGREN-JANSSON, E., TALLHEDEN, T. & LINDAHL, A. 2003. Articular cartilage engineering with autologous chondrocyte transplantation. A review of recent developments. *J Bone Joint Surg Am,* 85-A Suppl 3, 109-15.

BROWN, T. D., DALTON, P. D. & HUTMACHER, D. W. 2011. Direct writing by way of melt electrospinning. *Advanced Materials,* 23, 5651-5657.

BUCKLEY, C. T. & KELLY, D. J. 2012. Expansion in the presence of FGF-2 enhances the functional development of cartilaginous tissues engineered using infrapatellar fat pad derived MSCs. *J Mech Behav Biomed Mater,* 11, 102-11.

BUCKLEY, C. T., MEYER, E. G. & KELLY, D. J. 2012. The influence of construct scale on the composition and functional properties of cartilaginous tissues engineered using bone marrow-derived mesenchymal stem cells. *Tissue Eng Part A,* 18, 382-96.

BUCKLEY, C. T., THORPE, S. D., O'BRIEN, F. J., ROBINSON, A. J. & KELLY, D. J. 2009. The effect of concentration, thermal history and cell seeding density on the initial mechanical properties of agarose hydrogels. *J Mech Behav Biomed Mater,* 2, 512-21.

BUCKLEY, C. T., VINARDELL, T. & KELLY, D. J. 2010a. Oxygen tension differentially regulates the functional properties of cartilaginous tissues engineered from infrapatellar fat pad derived MSCs and articular chondrocytes. *Osteoarthritis Cartilage,* 18, 1345-54.

BUCKLEY, C. T., VINARDELL, T., THORPE, S. D., HAUGH, M. G., JONES, E., MCGONAGLE, D. & KELLY, D. J. 2010b. Functional properties of cartilaginous tissues engineered from infrapatellar fat pad-derived mesenchymal stem cells. *J Biomech,* 43, 920-6.

BUSCHMANN, M. D., GLUZBAND, Y. A., GRODZINSKY, A. J. & HUNZIKER, E. B. 1995. Mechanical compression modulates matrix biosynthesis in chondrocyte/agarose culture. *J Cell Sci,* 108 (Pt 4), 1497-508.

CALS, F. L., HELLINGMAN, C. A., KOEVOET, W., BAATENBURG DE JONG, R. J. & VAN OSCH, G. J. 2012. Effects of transforming growth factor-beta subtypes on in vitro cartilage production and mineralization of human bone marrow stromal-derived mesenchymal stem cells. *J Tissue Eng Regen Med,* 6, 68-76.

CANAL GUTERL, C., HUNG, C. T. & ATESHIAN, G. A. 2010. Electrostatic and non-electrostatic contributions of proteoglycans to the compressive equilibrium modulus of bovine articular cartilage. *J Biomech,* 43, 1343-50.

CAPLAN, A. I. 1991. Mesenchymal stem cells. *J Orthop Res,* 9, 641-50.

CAPLAN, A. I. 2005. Review: mesenchymal stem cells: cell-based reconstructive therapy in orthopedics. *Tissue Eng,* 11, 1198-211.

CHEN, S. S., FALCOVITZ, Y. H., SCHNEIDERMAN, R., MAROUDAS, A. & SAH, R. L. 2001. Depth-dependent compressive properties of normal aged human femoral head articular cartilage: relationship to fixed charge density. *Osteoarthritis Cartilage,* 9, 561-9.

CHENG, N. C., ESTES, B. T., YOUNG, T. H. & GUILAK, F. 2013. Genipin-crosslinked cartilage-derived matrix as a scaffold for human adipose-derived stem cell chondrogenesis. *Tissue Eng Part A,* 19, 484-96.

CHUNG, C. & BURDICK, J. A. 2008. Engineering cartilage tissue. *Adv Drug Deliv Rev,* 60, 243-62.

CONNELLY, J. T., VANDERPLOEG, E. J., MOUW, J. K., WILSON, C. G. & LEVENSTON, M. E. 2010. Tensile loading modulates bone marrow stromal cell differentiation and the development of engineered fibrocartilage constructs. *Tissue Eng Part A,* 16, 1913-23.

CRAPO, P. M., GILBERT, T. W. & BADYLAK, S. F. 2011. An overview of tissue and whole organ decellularization processes. *Biomaterials,* 32, 3233-3243.

CREAMER, P. 2000. Osteoarthritis pain and its treatment. *Current Opinion in Rheumatology,* 12, 450-455.

DEMARTEAU, O., WENDT, D., BRACCINI, A., JAKOB, M., SCHAFER, D., HEBERER, M. & MARTIN, I. 2003. Dynamic compression of cartilage constructs engineered from expanded human articular chondrocytes. *Biochem Biophys Res Commun,* 310, 580-8.

DRAGOO, J. L., SAMIMI, B., ZHU, M., HAME, S. L., THOMAS, B. J., LIEBERMAN, J. R., HEDRICK, M. H. & BENHAIM, P. 2003. Tissue-engineered cartilage and bone using stem cells from human infrapatellar fat pads. *J Bone Joint Surg Br,* 85, 740-7.

EISEN, A. Z., JEFFREY, J. J. & GROSS, J. 1968. Human skin collagenase, isolation and mechanism of attack on the collagen molecule. *Biochimica et Biophysica Acta (BBA) - Enzymology,* 151, 637-645.

ELDER, B. D., KIM, D. H. & ATHANASIOU, K. A. 2010. Developing an articular cartilage decellularization process toward facet joint cartilage replacement. *Neurosurgery,* 66, 722-7; discussion 727.

ENGLISH, A., JONES, E. A., CORSCADDEN, D., HENSHAW, K., CHAPMAN, T., EMERY, P. & MCGONAGLE, D. 2007. A comparative assessment of cartilage and joint fat pad as a potential source of cells for autologous therapy development in knee osteoarthritis. *Rheumatology (Oxford),* 46, 1676-83.

ERICKSON, I. E., HUANG, A. H., CHUNG, C., LI, R. T., BURDICK, J. A. & MAUCK, R. L. 2009. Differential maturation and structure-function relationships in mesenchymal stem cell- and chondrocyte-seeded hydrogels. *Tissue Eng Part A,* 15, 1041-52.

EYRE, D. 2002. Collagen of articular cartilage. *Arthritis Res,* 4, 30-5.

FARRELL, M. J., COMEAU, E. S. & MAUCK, R. L. 2012. Mesenchymal stem cells produce functional cartilage matrix in three-dimensional culture in regions of optimal nutrient supply. *Eur Cell Mater,* 23, 425-40.

FEDOROVICH, N. E., SCHUURMAN, W., WIJNBERG, H. M., PRINS, H. J., VAN WEEREN, P. R., MALDA, J., ALBLAS, J. & DHERT, W. J. 2012. Biofabrication of osteochondral tissue equivalents by printing topologically defined, cell-laden hydrogel scaffolds. *Tissue Eng Part C Methods,* 18, 33-44.

GANNON, A. R. 2013. *An Investigation of Structure-Function Relations in Articular Cartilage during Skeletal Maturation.* PhD Thesis, Trinity College Dublin.

GANNON, A. R., NAGEL, T. & KELLY, D. J. 2012. The role of the superficial region in determining the dynamic properties of articular cartilage. *Osteoarthritis Cartilage,* 20, 1417-25.

GANNON, J. M., WALKER, G., FISCHER, M., CARPENTER, R., THOMPSON, R. C., JR. & OEGEMA, T. R., JR. 1991. Localization of type X collagen in canine growth plate and adult canine articular cartilage. *J Orthop Res,* 9, 485-94.

GILCHRIST, C. L., RUCH, D. S., LITTLE, D. & GUILAK, F. 2014. Micro-scale and meso-scale architectural cues cooperate and compete to direct aligned tissue formation. *Biomaterials,* 35, 10015-24.

GONG, Y. Y., XUE, J. X., ZHANG, W. J., ZHOU, G. D., LIU, W. & CAO, Y. 2011. A sandwich model for engineering cartilage with acellular cartilage sheets and chondrocytes. *Biomaterials,* 32, 2265-2273.

GRAD, S., LEE, C. R., GORNA, K., GOGOLEWSKI, S., WIMMER, M. A. & ALINI, M. 2005. Surface motion upregulates superficial zone protein and hyaluronan production in chondrocyte-seeded three-dimensional scaffolds. *Tissue Eng,* 11, 249-56.

GRIMSHAW, M. J. & MASON, R. M. 2000. Bovine articular chondrocyte function in vitro depends upon oxygen tension. *Osteoarthritis Cartilage,* 8, 386-92.

GUILAK, F., RATCLIFFE, A., LANE, N., ROSENWASSER, M. P. & MOW, V. C. 1994. Mechanical and biochemical changes in the superficial zone of articular cartilage in canine experimental osteoarthritis. *J Orthop Res,* 12, 474-84.

GUILLEMETTE, M. D., CUI, B., ROY, E., GAUVIN, R., GIASSON, C. J., ESCH, M. B., CARRIER, P., DESCHAMBEAULT, A., DUMOULIN, M. & TONER, M. 2009. Surface topography induces 3D self-orientation of cells and extracellular matrix resulting in improved tissue function. *Integrative Biology,* 1, 196-204.

HANGODY, L., FECZKO, P., BARTHA, L., BODO, G. & KISH, G. 2001. Mosaicplasty for the treatment of articular defects of the knee and ankle. *Clin Orthop Relat Res*, S328-36.

HAUGH, M. G., MEYER, E. G., THORPE, S. D., VINARDELL, T., DUFFY, G. P. & KELLY, D. J. 2011. Temporal and spatial changes in cartilage-matrix-specific gene expression in mesenchymal stem cells in response to dynamic compression. *Tissue Eng Part A,* 17, 3085-93.

HAYES, A. J., HALL, A., BROWN, L., TUBO, R. & CATERSON, B. 2007. Macromolecular organization and in vitro growth characteristics of scaffold-free neocartilage grafts. *J Histochem Cytochem,* 55, 853-66.

HILAIRE, M. L. 2006. Treatment of Osteoarthritis. *U.S. Pharmacist,* 31, 49-55.

HOLMES, M. H. & MOW, V. C. 1990. The nonlinear characteristics of soft gels and hydrated connective tissues in ultrafiltration. *J Biomech,* 23, 1145-56.

HOMICZ, M. R., SCHUMACHER, B. L., SAH, R. L. & WATSON, D. 2002. Effects of serial expansion of septal chondrocytes on tissue-engineered neocartilage composition. *Otolaryngol Head Neck Surg,* 127, 398-408.

HORTON, W. E., JR., BENNION, P. & YANG, L. 2006. Cellular, molecular, and matrix changes in cartilage during aging and osteoarthritis. *J Musculoskelet Neuronal Interact,* 6, 379-81.

HUANG, A. H., FARRELL, M. J., KIM, M. & MAUCK, R. L. 2010. Long-term dynamic loading improves the mechanical properties of chondrogenic mesenchymal stem cell-laden hydrogel. *Eur Cell Mater,* 19, 72-85.

HUANG, C. Y., REUBEN, P. M. & CHEUNG, H. S. 2005. Temporal expression patterns and corresponding protein inductions of early responsive genes in rabbit bone marrow-derived mesenchymal stem cells under cyclic compressive loading. *Stem Cells,* 23, 1113-21.

HUNZIKER, E. B. 1999. Articular cartilage repair: are the intrinsic biological constraints undermining this process insuperable? *Osteoarthritis Cartilage,* 7, 15-28.

HUNZIKER, E. B. 2002. Articular cartilage repair: basic science and clinical progress. A review of the current status and prospects. *Osteoarthritis Cartilage,* 10, 432-63.

HWANG, N. S., VARGHESE, S., LEE, H. J., THEPRUNGSIRIKUL, P., CANVER, A., SHARMA, B. & ELISSEEFF, J. 2007. Response of zonal chondrocytes to extracellular matrix-hydrogels. *FEBS Lett,* 581, 4172-8.

IGNAT'EVA, N. Y., DANILOV, N. A., AVERKIEV, S. V., OBREZKOVA, M. V., LUNIN, V. V. & SOBOL', E. N. 2007. Determination of hydroxyproline in tissues and the evaluation of the collagen content of the tissues. *Journal of Analytical Chemistry,* 62, 51-57.

JOHNSTONE, B., HERING, T. M., CAPLAN, A. I., GOLDBERG, V. M. & YOO, J. U. 1998. In vitro chondrogenesis of bone marrow-derived mesenchymal progenitor cells. *Exp Cell Res,* 238, 265-72.

KAFIENAH, W., MISTRY, S., DICKINSON, S. C., SIMS, T. J., LEARMONTH, I. & HOLLANDER, A. P. 2007. Three-dimensional cartilage tissue engineering using adult stem cells from osteoarthritis patients. *Arthritis Rheum,* 56, 177-87.

KAFIENAH, W. & SIMS, T. J. 2004. Biochemical methods for the analysis of tissue-engineered cartilage. *Methods Mol Biol,* 238, 217-30.

KANG, H., PENG, J., LU, S., ZHANG, L., HUANG, J., SUI, X., ZHAO, B., WANG, A., XU, W. & LUO, Z. 2012. In vivo cartilage repair using adipose - derived stem cell - loaded decellularized cartilage ECM scaffolds. *Journal of tissue engineering and regenerative medicine*.

KELLY, D. J. & JACOBS, C. R. 2010. The role of mechanical signals in regulating chondrogenesis and osteogenesis of mesenchymal stem cells. *Birth Defects Res C Embryo Today,* 90, 75-85.

KHEIR, E., STAPLETON, T., SHAW, D., JIN, Z., FISHER, J. & INGHAM, E. 2011. Development and characterization of an acellular porcine cartilage bone matrix for use in tissue engineering. *J Biomed Mater Res A,* 99, 283-94.

KHOSHGOFTAR, M., WILSON, W., ITO, K. & VAN DONKELAAR, C. C. 2012. Influence of tissue- and cell-scale extracellular matrix distribution on the mechanical properties of tissue-engineered cartilage. *Biomech Model Mechanobiol.*

KHOSHGOFTAR, M., WILSON, W., ITO, K. & VAN DONKELAAR, R. 2013. The effects of matrix inhomogeneities on the cellular mechanical environment in tissue-engineered cartilage: an in silico investigation. *Tissue Eng Part C Methods.*

KIM, T. K., SHARMA, B., WILLIAMS, C. G., RUFFNER, M. A., MALIK, A., MCFARLAND, E. G. & ELISSEEFF, J. H. 2003. Experimental Model for Cartilage Tissue Engineering to Regenerate the Zonal Organization of Articular Cartilage☆. *Osteoarthritis and Cartilage,* 11, 653-664.

KIM, Y. J., SAH, R. L., DOONG, J. Y. & GRODZINSKY, A. J. 1988. Fluorometric assay of DNA in cartilage explants using Hoechst 33258. *Anal Biochem,* 174, 168-76.

KIRALY, K., HYTTINEN, M., LAPVETELAINEN, T., ELO, M., KIVIRANTA, I., DOBAI, J., MODIS, L., HELMINEN, H. & AROKOSKI, J. 1997. Specimen preparation and quantification of collagen birefringence in unstained sections of articular cartilage using image analysis and polarizing light microscopy. *The Histochemical Journal,* 29, 317-327.

KISIDAY, J. D., FRISBIE, D. D., MCILWRAITH, C. W. & GRODZINSKY, A. J. 2009. Dynamic compression stimulates proteoglycan synthesis by mesenchymal stem cells in the absence of chondrogenic cytokines. *Tissue Eng Part A,* 15, 2817-24.

KISIDAY, J. D., JIN, M., DIMICCO, M. A., KURZ, B. & GRODZINSKY, A. J. 2004. Effects of dynamic compressive loading on chondrocyte biosynthesis in self-assembling peptide scaffolds. *J Biomech,* 37, 595-604.

KLEIN, T. J., CHAUDHRY, M., BAE, W. C. & SAH, R. L. 2007. Depth-dependent biomechanical and biochemical properties of fetal, newborn, and tissue-engineered articular cartilage. *J Biomech,* 40, 182-90.

KLEIN, T. J., MALDA, J., SAH, R. L. & HUTMACHER, D. W. 2009a. Tissue engineering of articular cartilage with biomimetic zones. *Tissue Eng Part B Rev,* 15, 143-57.

KLEIN, T. J., RIZZI, S. C., REICHERT, J. C., GEORGI, N., MALDA, J., SCHUURMAN, W., CRAWFORD, R. W. & HUTMACHER, D. W. 2009b. Strategies for zonal cartilage repair using hydrogels. *Macromol Biosci,* 9, 1049-58.

KLEIN, T. J., SCHUMACHER, B. L., SCHMIDT, T. A., LI, K. W., VOEGTLINE, M. S., MASUDA, K., THONAR, E. J. & SAH, R. L. 2003. Tissue engineering of stratified articular cartilage from chondrocyte subpopulations. *Osteoarthritis and Cartilage,* 11, 595-602.

KORHONEN, R. K., JULKUNEN, P., WILSON, W. & HERZOG, W. 2008. Importance of collagen orientation and depth-dependent fixed charge densities of cartilage on mechanical behavior of chondrocytes. *Journal of biomechanical engineering,* 130, 021003.

LAWRENCE, R. C., FELSON, D. T., HELMICK, C. G., ARNOLD, L. M., CHOI, H., DEYO, R. A., GABRIEL, S., HIRSCH, R., HOCHBERG, M. C., HUNDER, G. G., JORDAN, J. M., KATZ, J. N., KREMERS, H. M. & WOLFE, F. 2008. Estimates of the prevalence of arthritis and other rheumatic conditions in the United States. Part II. *Arthritis Rheum,* 58, 26-35.

LEE, C. R., GRODZINSKY, A. J., HSU, H. P., MARTIN, S. D. & SPECTOR, M. 2000. Effects of harvest and selected cartilage repair procedures on the physical and biochemical properties of articular cartilage in the canine knee. *J Orthop Res,* 18, 790-9.

LEE, J., CUDDIHY, M. J. & KOTOV, N. A. 2008. Three-dimensional cell culture matrices: state of the art. *Tissue Eng Part B Rev,* 14, 61-86.

LEE, R. B. & URBAN, J. P. 1997. Evidence for a negative Pasteur effect in articular cartilage. *Biochem J,* 321 (Pt 1), 95-102.

LENNON, D. P. & CAPLAN, A. I. 2006. Isolation of human marrow-derived mesenchymal stem cells. *Exp Hematol,* 34, 1604-5.

LI, J., ZHAO, Z., YANG, J., LIU, J., WANG, J., LI, X. & LIU, Y. 2009. p38 MAPK mediated in compressive stress-induced chondrogenesis of rat bone marrow MSCs in 3D alginate scaffolds. *J Cell Physiol,* 221, 609-17.

LI, W. J., JIANG, Y. J. & TUAN, R. S. 2006. Chondrocyte phenotype in engineered fibrous matrix is regulated by fiber size. *Tissue Eng,* 12, 1775-85.

LI, Z., KUPCSIK, L., YAO, S. J., ALINI, M. & STODDART, M. J. 2010. Mechanical load modulates chondrogenesis of human mesenchymal stem cells through the TGF-beta pathway. *J Cell Mol Med,* 14, 1338-46.

LIU, Y., BUCKLEY, C. T., DOWNEY, R., MULHALL, K. J. & KELLY, D. J. 2012. The role of environmental factors in regulating the development of cartilaginous grafts engineered using osteoarthritic human infrapatellar fat pad-derived stem cells. *Tissue Eng Part A,* 18, 1531-41.

LIU, Y., BUCKLEY, C. T., MULHALL, K. J. & KELLY, D. J. 2013. Combining BMP-6, TGF-β3 and hydrostatic pressure stimulation enhances the functional development of cartilage tissues engineered using human infrapatellar fat pad derived stem cells. *Biomaterials Science,* 1, 745.

LORENZO, P., BAYLISS, M. T. & HEINEGARD, D. 1998. A novel cartilage protein (CILP) present in the mid-zone of human articular cartilage increases with age. *J Biol Chem,* 273, 23463-8.

MA, J., HE, X. & JABBARI, E. 2011. Osteogenic differentiation of marrow stromal cells on random and aligned electrospun poly (L-lactide) nanofibers. *Annals of biomedical engineering,* 39, 14-25.

MALDA, J., ROUWKEMA, J., MARTENS, D. E., LE COMTE, E. P., KOOY, F. K., TRAMPER, J., VAN BLITTERSWIJK, C. A. & RIESLE, J. 2004a. Oxygen gradients in tissue-engineered PEGT/PBT cartilaginous constructs: measurement and modeling. *Biotechnol Bioeng,* 86, 9-18.

MALDA, J., TEN HOOPE, W., SCHUURMAN, W., VAN OSCH, G. J., VAN WEEREN, P. R. & DHERT, W. J. 2010. Localization of the potential zonal marker clusterin in native cartilage and in tissue-engineered constructs. *Tissue Eng Part A,* 16, 897-904.

MALDA, J., WOODFIELD, T. B., VAN DER VLOODT, F., KOOY, F. K., MARTENS, D. E., TRAMPER, J., VAN BLITTERSWIJK, C. A. & RIESLE, J. 2004b. The effect of PEGT/PBT scaffold architecture on oxygen gradients in tissue engineered cartilaginous constructs. *Biomaterials,* 25, 5773-80.

MANSOUR, J. M. & MOW, V. C. 1976. The permeability of articular cartilage under compressive strain and at high pressures. *J Bone Joint Surg Am,* 58, 509-16.

MAROUDAS, A., BULLOUGH, P., SWANSON, S. & FREEMAN, M. 1968. The permeability of articular cartilage. *Journal of Bone & Joint Surgery, British Volume,* 50, 166-177.

MATSIKO, A., GLEESON, J. P. & O'BRIEN, F. J. 2014. Scaffold mean pore size influences mesenchymal stem cell chondrogenic differentiation and matrix deposition. *Tissue Engineering Part A*.

MAUCK, R. L., BAKER, B. M., NERURKAR, N. L., BURDICK, J. A., LI, W. J., TUAN, R. S. & ELLIOTT, D. M. 2009. Engineering on the straight and narrow: the mechanics of nanofibrous assemblies for fiber-reinforced tissue regeneration. *Tissue Eng Part B Rev,* 15, 171-93.

MAUCK, R. L., BYERS, B. A., YUAN, X. & TUAN, R. S. 2007. Regulation of cartilaginous ECM gene transcription by chondrocytes and MSCs in 3D culture in response to dynamic loading. *Biomech Model Mechanobiol,* 6, 113-25.

MAUCK, R. L., SOLTZ, M. A., WANG, C. C., WONG, D. D., CHAO, P. H., VALHMU, W. B., HUNG, C. T. & ATESHIAN, G. A. 2000. Functional tissue engineering of articular cartilage through dynamic loading of chondrocyte-seeded agarose gels. *J Biomech Eng,* 122, 252-60.

MAUCK, R. L., YUAN, X. & TUAN, R. S. 2006. Chondrogenic differentiation and functional maturation of bovine mesenchymal stem cells in long-term agarose culture. *Osteoarthritis Cartilage,* 14, 179-89.

MCCULLEN, S. D., AUTEFAGE, H., CALLANAN, A., GENTLEMAN, E. & STEVENS, M. M. 2012. Anisotropic fibrous scaffolds for articular cartilage regeneration. *Tissue Eng Part A,* 18, 2073-83.

MESALLATI, T., BUCKLEY, C. T., NAGEL, T. & KELLY, D. J. 2012. Scaffold architecture determines chondrocyte response to externally applied dynamic compression. *Biomech Model Mechanobiol*.

MEYER, E. G., BUCKLEY, C. T., THORPE, S. D. & KELLY, D. J. 2010. Low oxygen tension is a more potent promoter of chondrogenic differentiation than dynamic compression. *J Biomech,* 43, 2516-23.

MIKIC, B., ISENSTEIN, A. L. & CHHABRA, A. 2004. Mechanical modulation of cartilage structure and function during embryogenesis in the chick. *Ann Biomed Eng,* 32, 18-25.

MIKIC, B., JOHNSON, T. L., CHHABRA, A. B., SCHALET, B. J., WONG, M. & HUNZIKER, E. B. 2000. Differential effects of embryonic immobilization on the development of fibrocartilaginous skeletal elements. *J Rehabil Res Dev,* 37, 127-33.

MIRONOV, V., REIS, N. & DERBY, B. 2006. Review: bioprinting: a beginning. *Tissue Eng,* 12, 631-4.

MITROVIC, D., QUINTERO, M., STANKOVIC, A. & RYCKEWAERT, A. 1983. Cell density of adult human femoral condylar articular cartilage. Joints with normal and fibrillated surfaces. *Lab Invest,* 49, 309-16.

MOUTOS, F. T., FREED, L. E. & GUILAK, F. 2007. A biomimetic three-dimensional woven composite scaffold for functional tissue engineering of cartilage. *Nature materials,* 6, 162-167.

MOW, V. C. & GUO, X. E. 2002. Mechano-electrochemical properties of articular cartilage: their inhomogeneities and anisotropies. *Annu Rev Biomed Eng,* 4, 175-209.

MOW, V. C. & WANG, C. C. 1999. Some bioengineering considerations for tissue engineering of articular cartilage. *Clin Orthop Relat Res,* S204-23.

MUIR, H., BULLOUGH, P. & MAROUDAS, A. 1970. The distribution of collagen in human articular cartilage with some of its physiological implications. *J Bone Joint Surg Br,* 52, 554-63.

MURPHY, C. M., HAUGH, M. G. & O'BRIEN, F. J. 2010. The effect of mean pore size on cell attachment, proliferation and migration in collagen–glycosaminoglycan scaffolds for bone tissue engineering. *Biomaterials,* 31, 461-466.

NAGEL, T. & KELLY, D. J. 2012. Apparent behaviour of charged and neutral materials with ellipsoidal fibre distributions and cross-validation of finite element implementations. *Journal of the mechanical behavior of biomedical materials,* 9, 122-129.

NAGEL, T. & KELLY, D. J. 2013. The composition of engineered cartilage at the time of implantation determines the likelihood of regenerating tissue with a normal collagen architecture. *Tissue Eng Part A,* 19, 824-33.

NARMONEVA, D., WANG, J. & SETTON, L. 1999. Nonuniform swelling-induced residual strains in articular cartilage. *Journal of biomechanics,* 32, 401-408.

NEHRER, S., BREINAN, H. A., RAMAPPA, A., YOUNG, G., SHORTKROFF, S., LOUIE, L. K., SLEDGE, C. B., YANNAS, I. V. & SPECTOR, M. 1997. Matrix collagen type and pore size influence behaviour of seeded canine chondrocytes. *Biomaterials,* 18, 769-776.

NG, K. W., ATESHIAN, G. A. & HUNG, C. T. 2009. Zonal chondrocytes seeded in a layered agarose hydrogel create engineered cartilage with depth-dependent cellular and mechanical inhomogeneity. *Tissue Eng Part A,* 15, 2315-24.

NG, K. W., MAUCK, R. L., STATMAN, L. Y., LIN, E. Y., ATESHIAN, G. A. & HUNG, C. T. 2006. Dynamic deformational loading results in selective application of mechanical stimulation in a layered, tissue-engineered cartilage construct. *Biorheology,* 43, 497-507.

NG, K. W., WANG, C. C., MAUCK, R. L., KELLY, T. A., CHAHINE, N. O., COSTA, K. D., ATESHIAN, G. A. & HUNG, C. T. 2005. A layered agarose approach to fabricate depth-dependent inhomogeneity in chondrocyte-seeded constructs. *J Orthop Res,* 23, 134-41.

NGUYEN, L. H., KUDVA, A. K., GUCKERT, N. L., LINSE, K. D. & ROY, K. 2011a. Unique biomaterial compositions direct bone marrow stem cells into specific chondrocytic

phenotypes corresponding to the various zones of articular cartilage. *Biomaterials,* 32, 1327-38.

NGUYEN, L. H., KUDVA, A. K., SAXENA, N. S. & ROY, K. 2011b. Engineering articular cartilage with spatially-varying matrix composition and mechanical properties from a single stem cell population using a multi-layered hydrogel. *Biomaterials,* 32, 6946-52.

NORIEGA, S. E., HASANOVA, G. I., SCHNEIDER, M. J., LARSEN, G. F. & SUBRAMANIAN, A. 2012. Effect of fiber diameter on the spreading, proliferation and differentiation of chondrocytes on electrospun chitosan matrices. *Cells Tissues Organs,* 195, 207-21.

NUGENT-DERFUS, G., TAKARA, T., O'NEILL, J., CAHILL, S., G RTZ, S., PONG, T., INOUE, H., ANELOSKI, N., WANG, W. & VEGA, K. 2007. Continuous passive motion applied to whole joints stimulates chondrocyte biosynthesis of PRG4. *Osteoarthritis and cartilage,* 15, 566-574.

OWEN, J. R. & WAYNE, J. S. 2006. Influence of a superficial tangential zone over repairing cartilage defects: implications for tissue engineering. *Biomech Model Mechanobiol,* 5, 102-10.

OWEN, J. R. & WAYNE, J. S. 2011. Contact models of repaired articular surfaces: influence of loading conditions and the superficial tangential zone. *Biomech Model Mechanobiol,* 10, 461-71.

PAREKH, A., MANTLE, B., BANKS, J., SWARTS, J. D., BADYLAK, S. F., DOHAR, J. E. & HEBDA, P. A. 2009. Repair of the tympanic membrane with urinary bladder matrix. *The Laryngoscope,* 119, 1206-1213.

PEI, M., HE, F., BOYCE, B. M. & KISH, V. L. 2009. Repair of full-thickness femoral condyle cartilage defects using allogeneic synovial cell-engineered tissue constructs. *Osteoarthritis Cartilage,* 17, 714-22.

PEI, M., HE, F. & VUNJAK-NOVAKOVIC, G. 2008. Synovium-derived stem cell-based chondrogenesis. *Differentiation,* 76, 1044-56.

PELTTARI, K., WINTER, A., STECK, E., GOETZKE, K., HENNIG, T., OCHS, B. G., AIGNER, T. & RICHTER, W. 2006. Premature induction of hypertrophy during in vitro chondrogenesis of human mesenchymal stem cells correlates with calcification and vascular invasion after ectopic transplantation in SCID mice. *Arthritis Rheum,* 54, 3254-66.

PITTENGER, M. F., MACKAY, A. M., BECK, S. C., JAISWAL, R. K., DOUGLAS, R., MOSCA, J. D., MOORMAN, M. A., SIMONETTI, D. W., CRAIG, S. & MARSHAK, D. R. 1999. Multilineage potential of adult human mesenchymal stem cells. *Science,* 284, 143-7.

POOLE, A. R. 2001. Cartilage in health and disease *In:* KOOPMAN, W. J. (ed.) *Arthritis and Allied Conditions: A Textbook of Rheumatology.*

QI, W. N. & SCULLY, S. P. 1997. Extracellular collagen modulates the regulation of chondrocytes by transforming growth factor - β 1. *Journal of orthopaedic research,* 15, 483-490.

RIEPPO, J., HYTTINEN, M. M., HALMESMAKI, E., RUOTSALAINEN, H., VASARA, A., KIVIRANTA, I., JURVELIN, J. S. & HELMINEN, H. J. 2009. Changes in spatial collagen content and collagen network architecture in porcine articular cartilage during growth and maturation. *Osteoarthritis Cartilage,* 17, 448-55.

ROTH, V. & MOW, V. C. 1980. The intrinsic tensile behavior of the matrix of bovine articular cartilage and its variation with age. *J Bone Joint Surg Am,* 62, 1102-17.

SCHINAGL, R. M., GURSKIS, D., CHEN, A. C. & SAH, R. L. 1997. Depth-dependent confined compression modulus of full-thickness bovine articular cartilage. *J Orthop Res,* 15, 499-506.

SCHUMACHER, B. L., BLOCK, J. A., SCHMID, T. M., AYDELOTTE, M. B. & KUETTNER, K. E. 1994. A novel proteoglycan synthesized and secreted by chondrocytes of the superficial zone of articular cartilage. *Arch Biochem Biophys,* 311, 144-52.

SCHWARZ, S., ELSAESSER, A. F., KOERBER, L., GOLDBERG - BOCKHORN, E., SEITZ, A. M., BERMUELLER, C., D RSELEN, L., IGNATIUS, A., BREITER, R. & ROTTER, N. 2012a. Processed xenogenic cartilage as innovative biomatrix for cartilage tissue engineering: effects on chondrocyte differentiation and function. *Journal of tissue engineering and regenerative medicine.*

SCHWARZ, S., KOERBER, L., ELSAESSER, A. F., GOLDBERG-BOCKHORN, E., SEITZ, A. M., DURSELEN, L., IGNATIUS, A., WALTHER, P., BREITER, R. & ROTTER, N. 2012b. Decellularized cartilage matrix as a novel biomatrix for cartilage tissue-engineering applications. *Tissue Eng Part A,* 18, 2195-209.

SENGERS, B. G., VAN DONKELAAR, C. C., OOMENS, C. W. & BAAIJENS, F. P. 2005. Computational study of culture conditions and nutrient supply in cartilage tissue engineering. *Biotechnol Prog,* 21, 1252-61.

SHARMA, B., WILLIAMS, C. G., KIM, T. K., SUN, D., MALIK, A., KHAN, M., LEONG, K. & ELISSEEFF, J. H. 2007. Designing zonal organization into tissue-engineered cartilage. *Tissue Eng,* 13, 405-14.

SHEEHY, E. J., BUCKLEY, C. T. & KELLY, D. J. 2012. Oxygen tension regulates the osteogenic, chondrogenic and endochondral phenotype of bone marrow derived mesenchymal stem cells. *Biochem Biophys Res Commun,* 417, 305-10.

SHERIDAN, W., DUFFY, G. P. & MURPHY, B. 2012. Mechanical characterization of a customized decellularized scaffold for vascular tissue engineering. *Journal of the mechanical behavior of biomedical materials,* 8, 58-70.

STEADMAN, J. R., RODKEY, W. G., BRIGGS, K. K. & RODRIGO, J. J. 1999. The microfracture technique to treat full thickness articular cartilage defects of the knee. *Der Orthopäde,* 28, 26-32.

STEADMAN, J. R., RODKEY, W. G. & RODRIGO, J. J. 2001. Microfracture: surgical technique and rehabilitation to treat chondral defects. *Clin Orthop Relat Res,* S362-9.

STEELE, J. A., MCCULLEN, S. D., CALLANAN, A., AUTEFAGE, H., ACCARDI, M. A., DINI, D. & STEVENS, M. M. 2014. Combinatorial scaffold morphologies for zonal articular cartilage engineering. *Acta Biomater,* 10, 2065-75.

STEWARD, A. J., THORPE, S. D., VINARDELL, T., BUCKLEY, C. T., WAGNER, D. R. & KELLY, D. J. 2012. Cell-matrix interactions regulate mesenchymal stem cell response to hydrostatic pressure. *Acta Biomater,* 8, 2153-9.

STEWARD, A. J., WAGNER, D. R. & KELLY, D. J. 2014. Exploring the roles of integrin binding and cytoskeletal reorganization during mesenchymal stem cell mechanotransduction in soft and stiff hydrogels subjected to dynamic compression. *J Mech Behav Biomed Mater,* 38, 174-82.

THORPE, S. D., BUCKLEY, C. T., STEWARD, A. J. & KELLY, D. J. 2012. European Society of Biomechanics S.M. Perren Award 2012: the external mechanical environment can override the influence of local substrate in determining stem cell fate. *J Biomech,* 45, 2483-92.

THORPE, S. D., BUCKLEY, C. T., VINARDELL, T., O'BRIEN, F. J., CAMPBELL, V. A. & KELLY, D. J. 2008. Dynamic compression can inhibit chondrogenesis of mesenchymal stem cells. *Biochem Biophys Res Commun,* 377, 458-62.

THORPE, S. D., BUCKLEY, C. T., VINARDELL, T., O'BRIEN, F. J., CAMPBELL, V. A. & KELLY, D. J. 2010. The response of bone marrow-derived mesenchymal stem cells to dynamic compression following TGF-beta3 induced chondrogenic differentiation. *Ann Biomed Eng,* 38, 2896-909.

THORPE, S. D., NAGEL, T., CARROLL, S. F. & KELLY, D. J. 2013. Modulating gradients in regulatory signals within mesenchymal stem cell seeded hydrogels: a novel strategy to engineer zonal articular cartilage. *PLoS One,* 8, e60764.

TORZILLI, P. A., DETHMERS, D. A., ROSE, D. E. & SCHRYUER, H. F. 1983. Movement of interstitial water through loaded articular cartilage. *J Biomech,* 16, 169-79.

VALENTIN, J. E., TURNER, N. J., GILBERT, T. W. & BADYLAK, S. F. 2010. Functional skeletal muscle formation with a biologic scaffold. *Biomaterials,* 31, 7475-7484.

VEILLEUX, N. H., YANNAS, I. V. & SPECTOR, M. 2004. Effect of passage number and collagen type on the proliferative, biosynthetic, and contractile activity of adult canine articular chondrocytes in type I and II collagen-glycosaminoglycan matrices in vitro. *Tissue Eng,* 10, 119-27.

VINARDELL, T., BUCKLEY, C. T., THORPE, S. D. & KELLY, D. J. 2011. Composition-function relations of cartilaginous tissues engineered from chondrocytes and mesenchymal stem cells isolated from bone marrow and infrapatellar fat pad. *J Tissue Eng Regen Med,* 5, 673-83.

VINARDELL, T., ROLFE, R. A., BUCKLEY, C. T., MEYER, E. G., AHEARNE, M., MURPHY, P. & KELLY, D. J. 2012a. Hydrostatic pressure acts to stabilise a chondrogenic phenotype in porcine joint tissue derived stem cells. *Eur Cell Mater,* 23, 121-32; discussion 133-4.

VINARDELL, T., SHEEHY, E. J., BUCKLEY, C. T. & KELLY, D. J. 2012b. A comparison of the functionality and in vivo phenotypic stability of cartilaginous tissues engineered from different stem cell sources. *Tissue Eng Part A,* 18, 1161-70.

WAKITANI, S., GOTO, T., PINEDA, S. J., YOUNG, R. G., MANSOUR, J. M., CAPLAN, A. I. & GOLDBERG, V. M. 1994. Mesenchymal cell-based repair of large, full-thickness defects of articular cartilage. *J Bone Joint Surg Am,* 76, 579-92.

WANG, C. C., DENG, J. M., ATESHIAN, G. A. & HUNG, C. T. 2002. An automated approach for direct measurement of two-dimensional strain distributions within articular cartilage under unconfined compression. *J Biomech Eng,* 124, 557-67.

WANG, D. W., FERMOR, B., GIMBLE, J. M., AWAD, H. A. & GUILAK, F. 2005. Influence of oxygen on the proliferation and metabolism of adipose derived adult stem cells. *J Cell Physiol,* 204, 184-91.

WICKHAM, M. Q., ERICKSON, G. R., GIMBLE, J. M., VAIL, T. P. & GUILAK, F. 2003. Multipotent Stromal Cells Derived From the Infrapatellar Fat Pad of the Knee. *Clinical*

Orthopaedics and Related Research, 412, 196-212 10.1097/01.blo.0000072467.53786.ca.

WILLIAMSON, A. K., CHEN, A. C., MASUDA, K., THONAR, E. J. & SAH, R. L. 2003. Tensile mechanical properties of bovine articular cartilage: variations with growth and relationships to collagen network components. *J Orthop Res,* 21, 872-80.

WILLIAMSON, A. K., CHEN, A. C. & SAH, R. L. 2001. Compressive properties and function-composition relationships of developing bovine articular cartilage. *J Orthop Res,* 19, 1113-21.

WILSON, W., HUYGHE, J. M. & VAN DONKELAAR, C. C. 2007. Depth-dependent compressive equilibrium properties of articular cartilage explained by its composition. *Biomech Model Mechanobiol,* 6, 43-53.

WISE, J. K., YARIN, A. L., MEGARIDIS, C. M. & CHO, M. 2009. Chondrogenic differentiation of human mesenchymal stem cells on oriented nanofibrous scaffolds: engineering the superficial zone of articular cartilage. *Tissue Eng Part A,* 15, 913-21.

WONG, M. L., LEACH, J. K., ATHANASIOU, K. A. & GRIFFITHS, L. G. 2011. The role of protein solubilization in antigen removal from xenogeneic tissue for heart valve tissue engineering. *Biomaterials,* 32, 8129-8138.

WOODFIELD, T. B., MALDA, J., DE WIJN, J., PETERS, F., RIESLE, J. & VAN BLITTERSWIJK, C. A. 2004. Design of porous scaffolds for cartilage tissue engineering using a three-dimensional fiber-deposition technique. *Biomaterials,* 25, 4149-61.

WOODFIELD, T. B., VAN BLITTERSWIJK, C. A., DE WIJN, J., SIMS, T. J., HOLLANDER, A. P. & RIESLE, J. 2005. Polymer scaffolds fabricated with pore-size gradients as a model for studying the zonal organization within tissue-engineered cartilage constructs. *Tissue Eng,* 11, 1297-311.

XU, C. C., CHAN, R. W., WEINBERGER, D. G., EFUNE, G. & PAWLOWSKI, K. S. 2010. A bovine acellular scaffold for vocal fold reconstruction in a rat model. *Journal of Biomedical Materials Research Part A,* 92, 18-32.

YANG, Q., PENG, J., LU, S.-B., GUO, Q.-Y., ZHAO, B., ZHANG, L., WANG, A., XU, W., XIA, Q. & MA, X. 2011. Evaluation of an extracellular matrix-derived acellular biphasic scaffold/cell construct in the repair of a large articular high-load-bearing osteochondral defect in a canine model. *Chinese Medical Journal-Beijing,* 124, 3930.

YOO, J. U., BARTHEL, T. S., NISHIMURA, K., SOLCHAGA, L., CAPLAN, A. I., GOLDBERG, V. M. & JOHNSTONE, B. 1998. The chondrogenic potential of human bone-marrow-derived mesenchymal progenitor cells. *J Bone Joint Surg Am,* 80, 1745-57.

ZENG, Q. Y., CHEN, R., DARMAWAN, J., XIAO, Z. Y., CHEN, S. B., WIGLEY, R., LE CHEN, S. & ZHANG, N. Z. 2008. Rheumatic diseases in China. *Arthritis Res Ther,* 10, R17.

ZHOU, S., CUI, Z. & URBAN, J. P. 2004. Factors influencing the oxygen concentration gradient from the synovial surface of articular cartilage to the cartilage-bone interface: a modeling study. *Arthritis Rheum,* 50, 3915-24.